NATIONAL TECHNICAL UNIVERSITY OF ATHENS

SCHOOL OF NAVAL ARCHITECTURE & MARINE ENGINEERING

DIVISION OF MARINE ENGINEERING

DIPLOMA THESIS

Elastohydrodynamic analysis of journal bearings with deformable surface

IOANNIS PERVELIS

thesis committee:

Supervisor: C. I. Papadopoulos, Associate Professor, NTUA

Members: K. N. Anyfantis, Assistant Professor, NTUA

G. Papalamprou, Associate Professor, NTUA

Athens, 2023

ΕΘΝΙΚΟ ΜΕΤΣΟΒΙΟ ΠΟΛΥΤΕΧΝΕΙΟ

ΣΧΟΛΗ ΝΑΥΠΗΓΩΝ ΜΗΧΑΝΟΛΟΓΩΝ ΜΗΧΑΝΙΚΩΝ

ΤΟΜΕΑΣ ΝΑΥΤΙΚΗΣ ΜΗΧΑΝΟΛΟΓΙΑΣ

ΔΙΠΛΩΜΑΤΙΚΗ ΕΡΓΑΣΙΑ

Ελαστοϋδροδυναμική μελέτη εδράνων ολίσθησης με παραμορφώσιμη επιφάνεια

ΙΩΑΝΝΗΣ ΠΕΡΒΕΛΗΣ

Εξεταστική Επιτροπή

Επιβλέπων: Χ. Ι. Παπαδόπουλος, Αναπληρωτής Καθηγητής ΕΜΠ

Μέλη: Κ. Ν. Ανυφαντής, Επίκουρος Καθηγητής, ΕΜΠ

Γ. Παπαλάμπρου, Αναπληρωτής Καθηγητής, ΕΜΠ

Αθήνα, 2023

Table Of Contents

Acknowledgements

This work marks not only the end of my undergraduate studies in the school of Naval Architecture and Marine Engineering of NTUA, but also consists of one of the most important tasks throughout those years. I devoted time, effort and passion in order to complete it and I should express my gratitude to all the people that supported my journey.

First and foremost, I am immensely grateful to my supervisor, Prof. Christos Papadopoulos for his unwavering guidance, expertise and patience throughout my research journey. His insightful feedback, constructive criticism, and continuous encouragement have been instrumental in shaping this thesis.

I extend my heartfelt gratitude to Prof. Christos Papadopoulos' team and more specifically to G. Rossopoulos for his valuable advice and ability to help in the most critical steps of this thesis. Furthermore I would like to thank D. Skaltsas and G. Charvalos for their support and help.

I could not forget the contribution from my friends in NTUA, and especially Nikos Simosis for his continuous patience and help, moral support and understanding.

I am indebted to my family and friends for their unwavering love, encouragement, and belief in my abilities.

To all those who have contributed in one way or another, your support has been vital, and I am truly grateful. Thank you for being a part of this meaningful journey!

"The future is not something to be predicted, but to be achieved"

Abstract

Friction is one of the most important causes of energy losses in mechanical systems. In ships, substantial friction losses are present in the propulsion system, both in the engine and in the shaft arrangement. Journal bearings play a critical role in various rotating machinery applications, such as engines, marine shafts, turbines, and industrial equipment. Understanding the behavior of journal bearings under different operational conditions is crucial for optimizing their design and ensuring efficient and reliable performance.

This research project employs a multidisciplinary approach, integrating principles of tribology, solid mechanics, and fluid dynamics. The research methodology involves numerical simulations based on finite element analysis and computational fluid dynamics. The known Reynolds equation for hydrodynamic lubrication is coupled with the Finite Element software CalculiX, in order to perform a fluid-solid interaction. In this way, the elastic displacements of the bearing bush are accounted for, and a more accurate solution is reached.

The thesis aims to achieve several objectives. Firstly, it aims to develop a comprehensive understanding of the elastohydrodynamic lubrication phenomena occurring in journal bearings, including the formation of lubricant films, pressure distribution, and the effects of material deformation. Secondly, it investigates the influence of key parameters, such as bush thickness, load, deformation, misalignment and rotational speed on the bearing's performance and reliability. This analysis is conducted for both oil and water lubricated bearings, and is compared to other EHD numerical techniques like the Winkler method.

Based on the above objectives, conclusions are drawn concerning the EHD analysis, and the user may have a better insight towards selecting the most appropriate method (FEM or Winkler) in order to balance the needed accuracy and computational time. Achieving an optimal trade-off between these two factors is essential to obtain reliable and efficient results, with reasonable computational resources.

Σύνοψη

Η τριβή είναι η συνηθέστερη και πιο σημαντική αιτία ενεργειακών απωλειών σε ένα μηχανικό σύστημα. Στο σύστημα πρόωσης πλοίων, σημαντικές απώλειες λόγω τριβής παρουσιάζονται τόσο στη κύρια μηχανή όσο και στο αξονικό σύστημα. Τα ακτινικά έδρανα παίζουν κρίσιμο ρόλο σε ποικίλες εφαρμογές περιστρεφόμενων μηχανημάτων, όπως σε μηχανές, ναυτικούς άξονες, τουρμπίνες και βιομηχανικό εξοπλισμό. Η κατανόηση της συμπεριφοράς των ακτινικών εδράνων σε διάφορες συνθήκες λειτουργίας είναι κομβική για τη βελτιστοποίηση της σχεδίασης τους, και για τη διασφάλιση της απόδοσης αλλά και της αξιοπιστίας τους.

Η συγκεκριμένη ερευνητική εργασία εμπλέκει πολλούς επιστημονικούς κλάδους, και συνδυάζει βασικές αρχές από την τριβολογία, την μηχανική των στερεών και τη δυναμική ρευστών. Η μεθοδολογία εμπεριέχει αριθμητικές προσομοιώσεις, βασισμένες στην μέθοδο των πεπερασμένων στοιχείων και στην υπολογιστική ρευστοδυναμική. Η γνωστή εξίσωση του Reynolds για την υδροδυναμική λίπανση, συνδυάζεται με ένα πρόγραμμα πεπερασμένων στοιχείων, το CalculiX, ώστε να μελετηθεί η αλληλεπίδραση στερεού με ρευστό. Μέσω αυτού του τρόπου, οι ακτινικές παραμορφώσεις της επιφάνειας του εδράνου λαμβάνονται υπόψη, και μια πιο ακριβής λύση του προβλήματος επιτυγχάνεται.

Η συγκεκριμένη εργασία προσπαθεί να πετύχει αρκετούς στόχους. Αρχικά, προσπαθεί να προσφέρει μια καλή κατανόηση σε διάφορα φαινόμενα που αφορούν την ελαστοϋδροδυναμική λίπανση σε ακτινικά έδρανα ολίσθησης, όπως ο σχηματισμός του φιλμ λιπαντικού, της κατανομής πίεσης και της επίδρασης των παραμορφώσεων του υλικού. Στη συνέχεια διερευνά την επίδραση των σημαντικών παραγόντων όπως του πάχους της επιφάνειας του εδράνου, του φορτίου, της παραμόρφωσης, της απευθυγράμμισης αλλά και της περιστροφικής ταχύτητας του άξονα στην συμπεριφορά και αξιοπιστία του εδράνου. Αυτή η ανάλυση γίνεται τόσο για έδρανα λιπαινόμενα με λάδι όσο και με νερό και συγκρίνεται με άλλες αριθμητικές τεχνικές, όπως η μέθοδος του Winkler.

Με βάση τους παραπάνω στόχους, εξάγονται συμπεράσματα σχετικά με την ελαστοϋδροδυναμική ανάλυση εδράνων και ο χρήστης μπορεί να έχει μια πιο βαθιά γνώση όσον αφορά την επιλογή εργαλείου μεταξύ πεπερασμένων στοιχείων και Winkler ώστε να βρει μια απαραίτητη ισορροπία μεταξύ ακρίβειας και απαιτούμενου χρόνου. Η εύρεση αυτής της ισορροπίας είναι βασική ώστε να βρεθούν αξιόπιστα και ακριβή αποτελέσματα με την βοήθεια λογικού υπολογιστικού κόστους.

Table Of Figures

Nomenclature

B :	Bearing width
C :	Bearing Clearance
D:	Bearing Diameter
EHD:	Elastohydrodynamic
e :	Eccentricity
F :	Friction Force
FEM:	Finite Element Method
HD:	Hydrodynamic
h :	lubricant film thickness
h_d :	displacements
h_{min}:	minimum film thickness
L:	Bearing Length
N:	Shaft rotational speed
O_b,O_s:	bush center, shaft center
P, Pmax :	Pressure, Maximum Pressure
Q_{in}, Q_{leak}:	Inlet flow rate, Leakage flow rate
R:	Bearing radius
S :	Sommerfeld Number
t :	Time
U:	Rotor Linear Velocity
W:	Total hydrodynamic Force
x:	x axis coordinate
y:	y axis coordinate

z:	z axis coordinate
η :	fluid dynamic viscosity
θ:	hydrodynamic film angle
μ :	friction coefficient
ρ :	lubricant density
$\tau_{x,y}$:	shear stress in x, y direction
φ :	attitude angle

1. Introduction

Tribology is a multidisciplinary field that deals with the study of interacting surfaces in relative motion, including friction, wear, and lubrication. The field encompasses a broad range of applications, including automotive, marine and aerospace engineering, machinery design, and biomedical devices, among others. One of the key areas of research in tribology is the study of journal bearings, which are widely used in rotating machinery to support the shafts and provide a low-friction interface between the shaft and the bearing.

Journal bearings are one of the most commonly used types of bearings in rotating machinery, including engines, marine shafts, turbines, compressors, and pumps. They consist of a shaft that rotates within a cylindrical or conical bearing surface, supported by a thin film of lubricant that separates the shaft and the bearing surface. The lubricant film serves multiple purposes, including reducing friction and wear, dissipating heat, and providing a damping effect that can help reduce vibration and noise.

The design and performance of journal bearings are critical factors in the efficiency and reliability of rotating machinery. Poorly designed or improperly maintained bearings can lead to excessive wear and damage to the shaft, bearing, and other components, as well as increased energy consumption and reduced operating lifespan. Therefore, there is a great need for research and development in the field of journal bearings to improve their performance, reduce their environmental impact, and extend their service life.

The study of journal bearings is a complex and challenging area of tribology, due to the complex interaction between the rotating shaft, bearing surface, and lubricant film. The behavior of the lubricant film is affected by a range of factors, including the viscosity and temperature of the lubricant, the load on the bearing, the speed of rotation, the surface roughness of the shaft and bearing and the elastic deformation of the bearing's bush. Additionally, the lubricant film can undergo various forms of instability, including hydrodynamic instability, boundary lubrication, and mixed lubrication, which can have significant effects on the performance and lifespan of the bearing.

Given the importance of journal bearings in rotating machinery, there is a great need for research in this field to improve their performance and extend their service life. The development of new materials, lubricants, and design techniques can help achieve these goals, as can the use of advanced computational tools and experimental methods to study the complex interaction between the rotating shaft, bearing surface, and lubricant film. By improving our understanding of journal bearings and their behavior, we can create more efficient and reliable rotating machinery that can help reduce energy consumption and environmental impact, while improving the reliability and safety of these critical components.

1.1 Literature Overview

There were three men who within a few years and independent of each other discovered and formulated the mechanism of hydrodynamic lubrication and laid its foundation as a branch of engineering science. They were a Russian, N. P. Petrov (1836-1920), and two British, B. Tower (1845-1904) and O. Reynolds (1842-1912). What all three had in common was that they perceived the process of lubrication as being due not to the mechanical interaction of two solid surfaces but to the dynamics of a fluid film separating them. This is the fundamental aspect of hydrodynamic lubrication and within three years, 1883-1886, both its theoretical and experimental foundations were firmly established.

The crystallization of the concept started with Nicolai Petrov[2] whose main interest was in the area of friction. He postulated two cardinal things: first, that the important fluid property with regard to friction is not its density, as was assumed by his contemporaries, but viscosity; and second, that the nature of friction in a bearing is not the result of the rubbing of two solid surfaces but stems from the viscous shearing of an intervening fluid film.

Beauchamp Tower, an engineer, an inventor, and a research assistant, conducted a famous series of experiments which was to lead to the discovery of the presence of hydrodynamic pressures in the fluid film in 1883-1884[3]. When the journal started to rotate, Tower noticed that oil was being pumped out of the bearing. In order to stop the leakage, first a cork and then a wooden plug were inserted, but both were ejected from the hole. With his keen insight Tower realized what was happening: a fluid film was separating the journal from the bearing and the fluid was under high pressure. Tower went on to modify his bearing geometry in the direction of what we now know to be the correct way of supplying lubricant, namely a set of axial grooves. Tower then installed a set of pressure gauges over the bearing surface. He obtained a map of hydrodynamic pressures which when integrated over the bearing surface equaled the applied load.

Both Petrov and Tower arrived at their concepts via experimentation and all that was needed to give the edifice a solid scientific ground was a theoretical basis for the experimental observations. This was achieved by Osborne Reynolds almost simultaneously with the two others. As a result, Petrov, Tower, and Reynolds can be considered the founding fathers of the concept of hydrodynamic lubrication.

The concept of elastohydrodynamic lubrication (EHL) was first developed by two independent researchers in the 1940s: Professor Grubin in the Soviet Union and Dr. H.P. Lundberg in the United States. In 1949, Professor Grubin published a paper [4], which presented a theoretical analysis of the elastic deformation of a rolling body in contact with a plane under the influence of a lubricant. He showed that the elastic deformation of the contacting bodies could significantly affect the lubricant film thickness and pressure distribution, and proposed the term "elastohydrodynamic lubrication" to describe this phenomenon. Dr. H.P. Lundberg published [5] in 1952.

Some of the most well-known and highly-regarded books on the subject of Elastohydrodynamic lubrication (EHL) are [6] and [7].

1.2 Goals Of The Present Study

The main purpose of the present thesis is to couple the known Reynolds equation for hydrodynamic lubrication with a FEM solver (CalculiX) in order to obtain a solution that takes into consideration the elastic deformation of the bearing's bush, caused by the hydrodynamic pressures that are generated. The elastic deformations alter the film thickness distribution of the initial rigid bearing geometry leading to different results of the critical bearing parameters like pressure distribution, minimum film thickness,eccentricity ratio, friction losses and load capacity.

In chapter 2, the basics of journal bearing geometry and materials are discussed for oil and water lubricated bearings. The main differences of oil and water properties are mentioned in order to understand their different behavior. Then, the well-known Reynolds equation is derived, by pointing and explaining all the necessary assumptions along with the physical meaning of each term.

In chapter 3, the steps and flowcharts of each solver as well as their couple are shown. The coupled solver consists of a c++ solver that solves Reynolds equation with finite difference method (hydrodynamic solution) and then calls CALCULIX FEM tool to solve the structural problem, obtaining the displacements by an iterative scheme.

In chapter 4, the validation of the proposed model is presented by comparing the results with the corresponding available literature findings. It also includes simulations of oil and water lubricated bearings when elasticity of bush is taken into account.

In Chapter 5 and 6, the main results of the present work are summarized, and conclusions and future work are drawn.

2. Journal Bearings

2.1 Introduction

Journal bearings are a type of hydrodynamic bearing used to support rotating machinery such as shafts, propellers, and turbines. They work by creating a thin film of lubricant between the rotating and stationary surfaces, which reduces friction and wear. Journal bearings are commonly used in ships to support the weight of propellers and transmit torque from the engine. Proper maintenance and lubrication is crucial to their effective function and failure to do so can result in increased friction and wear, leading to premature failure of the machinery and potentially hazardous situations for the ship and its crew.
Journal bearings are typically cylindrical in shape and consist of a journal (the rotating component) and a bearing (the stationary component). The bearing is typically made of a softer material, such as bronze or babbitt, and is designed to conform to the shape of the journal. The clearance between the journal and bearing is critical, as it determines the thickness of the lubricating film and the amount of load the bearing can support.

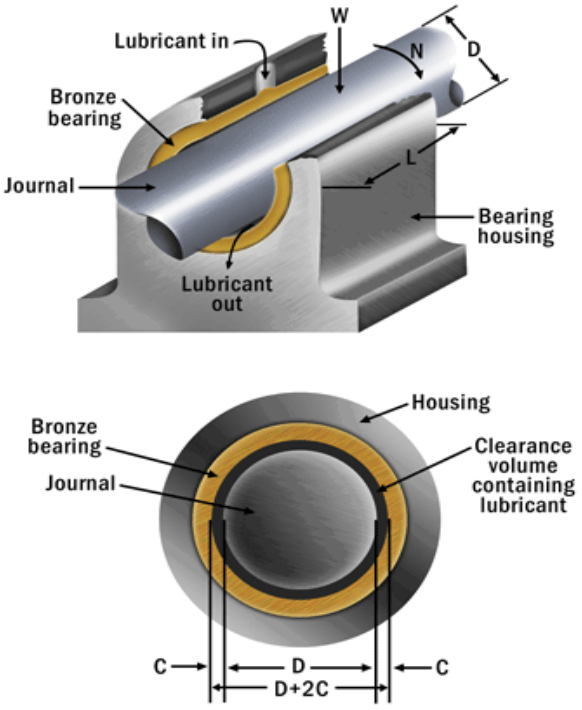

Figure 2.1 : typical journal bearing [8]

According to [7], there are 4 main types of lubrication:

1. *hydrodynamic lubrication* : hydrodynamic lubrication is generally characterized by conformal surfaces. A positive pressure develops in a hydrodynamically lubricated journal or thrust bearing because the bearing surfaces converge and the relative motion and the viscosity of the fluid separate the surfaces. In hydrodynamic lubrication the films are generally thick so that opposing solid surfaces are prevented from coming into contact. This condition is often referred to as "the ideal form of lubrication," since it provides low friction and high resistance to wear. The lubrication of the solid surfaces is governed by the bulk physical properties of the lubricant, notably the viscosity, and the frictional characteristics arise purely from the shearing of the viscous lubricant.
2. *elastohydrodynamic lubrication* : Elastohydrodynamic lubrication (EHL) is a form of hydrodynamic lubrication where elastic deformation of the lubricated surfaces becomes significant. There are two kinds of EHL:
    - Hard EHL : Hard EHL relates to materials of high elastic modulus such as metals. In this form of lubrication the elastic deformation and the pressure viscosity effects are equally important.
    - Soft EHL : Soft EHL relates to materials of low elastic modulus such as rubber. The maximum pressure in soft EHL is usually some MPa in contrast to Hard EHL that is some GPa. This low pressure has a negligible effect on the viscosity variation throughout the conjunction.
3. *boundary lubrication* : Because in boundary lubrication the solids are not separated by the lubricant, fluid film effects are negligible and there is considerable asperity contact. The contact lubrication mechanism is governed by the physical and chemical properties of thin surface films of molecular proportions. The properties of the bulk lubricant are of minor importance, and the friction coefficient is essentially independent of fluid viscosity.
4. *Partial or Mixed Lubrication* : If the pressures in elastohydrodynamically lubricated machine elements are too high or the running speeds are too low, the lubricant film will be penetrated. Some contact will take place between the asperities, and partial lubrication (sometimes referred to as "mixed lubrication") will occur. The behavior of the conjunction in a partial lubrication regime is governed by a combination of boundary and fluid film effects.

2.2 Effect Of Lubricant Properties On Hydrodynamic Bearings

Most hydrodynamic journal bearings in ships are typically lubricated with oil, as oil provides good lubrication and can withstand the high loads and temperatures generated by the stern tube assembly. The oil used for lubrication is usually a mineral oil or a synthetic oil that is specially formulated for marine applications and is designed to provide good lubrication and protect against wear and corrosion.
In addition to the oil lubrication system, some modern ships also use water-lubricated stern tube bearings. These bearings rely on a flow of seawater to provide lubrication and cooling, which can reduce the risk of pollution from oil leaks and reduce the need for oil changes and maintenance.
The most important differences of oil and water as lubricants are presented below [10]:

- **viscosity** : The largest difference between water and oil lies in their viscosities. At a temperature of 20oC water has a viscosity 1 cP while a mineral oil 65 cP. The relatively low viscosity of water has 3 results.
    1. The bearing load capacity is greatly reduced when compared to oil for the same eccentricity ratio or film thickness.
    2. The frictional drag in the bearing, for the same film thickness as an oil lubricated bearing is very much lower provided the bearing is operating in the laminar flow regime.
    3. The Reynolds number for a given speed of rotation is high and hence the bearing flow changes to non-laminar much earlier than in an oil lubricated bearing . This will result in the frictional drag being increased but it will still be less than in a comparable oil lubricated bearing.

  In addition, the viscosity of water is virtually independent of pressure. For instance, at 20oC an increase of pressure from atmospheric to 350 bar increases the viscosity by about 2% and the same pressure rise at 100 oC increases the viscosity by about 1%.

- **density and specific heat** : The density and specific heat of water are higher than those for oils, the latter by a factor of more than 2. Compared with an oil, a given lubricant volume flow will therefore remove more than twice as much heat from a bearing for the same temperature. However since the frictional drag in water lubricated bearings is low, the heat generated is also low and the temperature rise of a given volume of lubricant is also low. The water leaving a hydrodynamically lubricated bearing is often within 1oC or 2oC of the inlet temperature and thus isoviscous conditions are justified.

- **flash point** : Water has no flash point in contrast to oil. In applications where high pressures have to be used close to hot components there is a risk of fire if there is a leak of a conventional oil. The risk is eliminated by using water rather than oil.

2.3 Bearing Materials

2.3.1 Oil Lubricated Bearings Materials

Typically, there are used metallic materials that are based on powder – metallurgy and are made of white metal (tin and lead based), copper or aluminum based bronzes, porous metals and coated metals. They are relatively economical, suitable for high production rates and can be manufactured to precision tolerances.

The Babbitts are among the most widely used materials for hydrodynamically lubricated bearings. Babbitts are either tin- or lead-base alloys having excellent embeddability and conformability characteristics. They are unsurpassed in compatibility and thus prevent shaft scoring. Tin- and lead-base babbitts have relatively low load-carrying capacity. This capacity is increased by metallurgically bonding these alloys to stronger backing materials such as steel, cast iron, or bronze. Babbitt linings are either still cast or centrifugally cast onto the backing material. Fatigue strength is increased by decreasing the thickness of the babbitt lining.

The advantages of tin-based white metals in comparison to their lead-based counterparts include higher thermal conductivity, higher compression strength, higher fatigue and impact strength, and higher corrosion resistance. On the other hand, lead-based white metals exhibit a lower friction coefficient, better bonding to the shells, and better properties for casting. However, the increase in use of lead-based white metal is attributed mostly to its lower cost. For ice-class, navy vessels or environmental regulations tin-based white metal lining is recommended.

2.3.2 Water Lubricated Bearings Materials

In water lubricated bearings non – metallic materials are used such as polymers, elastomers, ceramics and composites. Some significant characteristics of non-metallic materials are they are characterized by low wear rates, relatively high performance rating and the ability to conform under load.

Some materials that have proven to be effective in water-lubricated bearings and are commonly used in marine applications are presented :

- Rubber : Rubber is a common material used in water-lubricated stern tube bearings. It is resistant to corrosion, can absorb shock and vibration, and has good sealing properties.
- Composite materials: Composite materials such as synthetic fiber reinforced plastics (FRP) and carbon fiber reinforced plastics (CFRP) are lightweight, corrosion-resistant, and can be designed to minimize wear and noise.
- Ceramics: Ceramics such as silicon nitride, zirconia, and alumina offer excellent wear resistance, hardness, and can withstand high temperatures.

2.4 Journal Bearing Geometry

In the following figure the geometry of a typical journal bearing is illustrated. R_1 is the radius of the bush, R_2 is the radius of the shaft, O_b is the center of the bush and O_s is the center of the shaft. The distance of the two center O_bO_s is called eccentricity e. The angle between axis yy' and the line connecting the two centers is called the attitude angle φ. In this particular angle the minimum and maximum film thickness can be calculated.

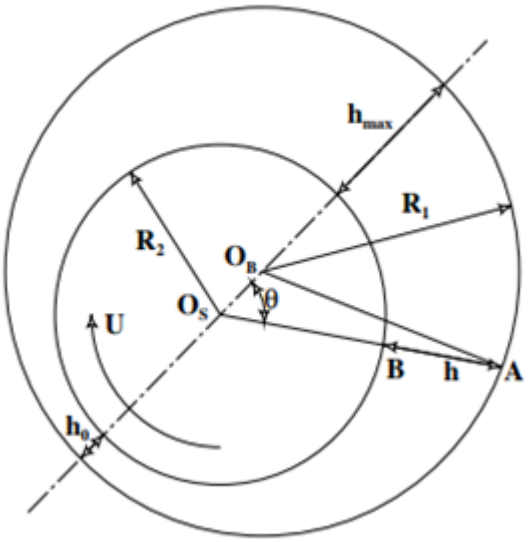

Figure 2.2: typical journal bearing geometry[10]

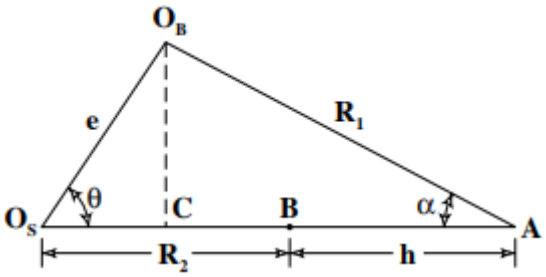

Figure 2.3: geometrical evaluation of film thickness shape[10]

We observe the triangle O_bO_sA. The angle 'α' can be considered really small. From observation of the above triangle we can write:

$$O_sA = O_sC + CA = O_sB + BA \ or$$

$$O_sA = e \cdot \cos\theta + R_1 \cdot \cos(a) = R_2 + h, \ thus$$

$$h = e \cdot \cos\theta + R_1 \cdot \cos(a) - R_2$$

applying the sine rule, it becomes:

$$\frac{e}{\sin(\alpha)} = \frac{R_1}{\sin(\theta)} \Rightarrow \sin(\alpha) = \frac{e}{R_1} \cdot \sin(\theta)$$

We use the known formula:

$$\sin(\alpha)^2 + \cos(\alpha)^2 = 1$$

and substituting for sin(α) we get:

$$\cos(\alpha) = \sqrt{1 - \sin^2(\alpha)} = \sqrt{1 - \left(\frac{e}{R_1}\right)^2 \cdot \sin^2\theta}$$

since e/R_1<< 1 then :

cos(α) ≃ 1

so we get by substituting :

$$h = e \cdot \cos\theta + R_1 - R_2 = e \cdot \cos\theta + c$$

where c is called clearance and is the difference of the two radius (bush and shaft) meaning

$$c = R_1 - R_2$$

or

$$h = c \cdot (1 + \varepsilon \cdot \cos\theta) \qquad (1)$$

where "ε" is called eccentricity ratio and is equal to $\frac{e}{c}$.

The above equation for the film thickness gives a good description of the film shape in journal bearings to within 0.1 % accuracy.

2.5 Hydrodynamic Lubrication

All hydrodynamic lubrication can be expressed mathematically in the form of an equation which was originally derived by Reynolds and is commonly known throughout the literature as the 'Reynolds equation'. There are several ways of deriving this equation. Since it is a simplification of the Navier-Stokes momentum and continuity equation it can be derived from this basis. It is, however, more often derived by considering the equilibrium of an element of liquid subjected to viscous shear and applying the continuity of flow principle. In this thesis the full equations of motion will be used and simplified based on the difference in order of magnitude of specific terms.
There are two conditions for the occurrence of hydrodynamic lubrication:

- two surfaces must move relatively to each other with sufficient velocity for a load carrying lubricating film to be generated and,
- surfaces must be inclined at some angle to each other, i.e. if the surfaces are parallel a pressure field will not form in the lubricating film to support the required load.

There are two exceptions to this last rule: hydrodynamic pressure can be generated between parallel stepped surfaces or the surfaces can move towards each other. The principle of hydrodynamic pressure generation between moving non-parallel surfaces is schematically illustrated in Figure 2.4 .

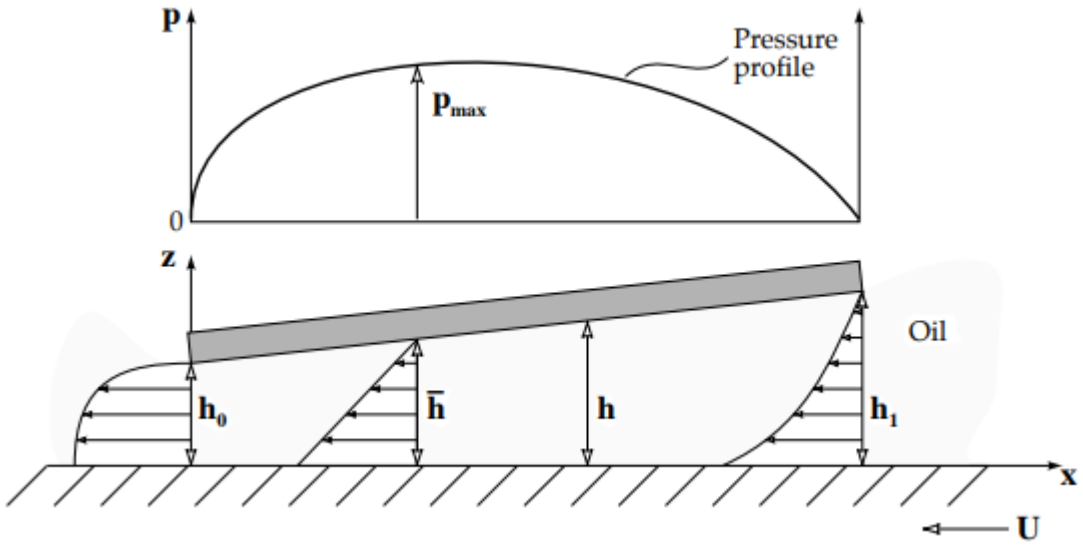

Figure 2.4 : hydrodynamic pressure generation between non-parallel surfaces[10].

It can be assumed that the bottom surface, sometimes called the 'runner', is covered with lubricant and moves with a certain velocity. The top surface is inclined at a certain angle to the bottom surface. As the bottom surface moves it drags the lubricant along it into the converging wedge. A pressure field is generated as otherwise there would be more lubricant entering the wedge than leaving it. Thus at the beginning of the wedge the increasing pressure restricts the entry flow and at the exit there is a decrease in pressure boosting the exit flow. The pressure gradient therefore causes the fluid velocity profile to

bend inwards at the entrance to the wedge and bend outwards at the exit, as shown in Figure 2.4. The generated pressure separates the two surfaces and is also able to support a certain load. It is also possible for the wedge to be curved or wrapped around a shaft to form a journal bearing. If the wedge remains planar then a pad bearing is obtained. The entire process of hydrodynamic pressure generation can be described mathematically to enable accurate prediction of bearing characteristics.

2.5.1 Reynolds Equation Derivation

The necessary assumptions will be mentioned at each stage of the analysis rather than being mentioned in the beginning, in order to keep the analysis general at each step.

The first reasonable assumption is that the effective radius of curvature of bearing components is generally very large compared with the film thickness. This observation enables the analysis to consider an equivalent curved surface near a plane; all effects due to curvature of the fluid film being neglected.

The second assumption is that the lubricant is Newtonian, meaning that the viscous shear stress is at all times proportional to the rate of shear. There is some evidence of non-Newtonian behavior in elasto-hydrodynamic films, particularly where friction force measurements are concerned, but the theoretical analysis will be limited to Newtonian fluids.

The Reynolds equation is derived by applying the basic equations of motion and continuity to the lubricant. The full equations of motion for a Newtonian fluid in cartesian coordinates have been derived, for example, by Pai (1956)[9]. The equations can be written in the following form :

$$\rho \cdot \frac{Du}{Dt} = \rho \cdot X - \frac{\partial P}{\partial x} + \frac{2}{3} \cdot \frac{\partial}{\partial x}\left[\eta \cdot \left(\frac{\partial u}{\partial x} - \frac{\partial v}{\partial y} \right) \right] + \frac{2}{3} \cdot \frac{\partial}{\partial x}\left[\eta \cdot \left(\frac{\partial u}{\partial x} - \frac{\partial w}{\partial z} \right) \right]$$
$$+ \frac{\partial}{\partial z}\left[\eta \cdot \left(\frac{\partial u}{\partial z} - \frac{\partial w}{\partial x} \right) \right] + \frac{\partial}{\partial y}\left[\eta \cdot \left(\frac{\partial v}{\partial x} - \frac{\partial u}{\partial y} \right) \right] \qquad (2)$$

This equation refers to the xx' axis. In a similar manner the equations in yy' and zz' are found in a circular replacement way.

The terms on the left-hand side represent inertia effects and on the right-hand side are the body force, pressure and viscous terms in that order.

For representative lubricating films, the inertia and body forces can be shown to be negligible compared with the viscous and pressure forces. If the inertia and body force terms are neglected, the reduced equations of motion imply that the pressure and viscous forces acting on the fluid are in equilibrium. When the first equation of motion is reduced in this way it takes the form:

$$\frac{\partial P}{\partial x}=\frac{2}{3}\cdot\frac{\partial}{\partial x}\left[\eta\cdot\left(\frac{\partial u}{\partial x}-\frac{\partial v}{\partial y}\right)\right]+\frac{2}{3}\cdot\frac{\partial}{\partial x}\left[\eta\cdot\left(\frac{\partial u}{\partial x}-\frac{\partial w}{\partial z}\right)\right]+\frac{\partial}{\partial z}\left[\eta\cdot\left(\frac{\partial u}{\partial z}-\frac{\partial w}{\partial x}\right)\right]$$
$$+\frac{\partial}{\partial y}\left[\eta\cdot\left(\frac{\partial v}{\partial x}-\frac{\partial u}{\partial y}\right)\right] \qquad (3)$$

Similar expressions are obtained for the y- and z-directions. Owing to the minute thickness of the fluid film in relation to other dimensions in a lubricated contact, the derivatives of the velocity components u and v with respect to z are large compared with all other velocity gradients. Furthermore, if l is a representative length of the contact or bearing, the pressure gradient across the film (i.e. in the z direction), can be shown to be of order (h/l) times the pressure gradients along the film. Since h<<l the variation of pressure across the film is normally quite insignificant. These observations permit the second equation of motion to be neglected. The remaining equations of motion become:

$$\frac{\partial P}{\partial x}=\frac{\partial}{\partial z}\left(\eta\cdot\frac{\partial u}{\partial z}\right)$$
$$\frac{\partial P}{\partial y}=\frac{\partial}{\partial z}\left(\eta\cdot\frac{\partial v}{\partial z}\right) \qquad (4)$$

It should be noted that the analysis has not been restricted to an isoviscous fluid. Furthermore, since an equation of state has not yet been introduced, the equations apply to compressible and incompressible fluids.

As stated above, pressure can be considered to be a function of x,y only, because of the thin film approximation.
Thus, equations (4) can be integrated directly to give general expressions for the velocity gradients:

$$\frac{\partial u}{\partial z}=\frac{z}{\eta}\cdot\frac{\partial p}{\partial x}+\frac{A}{\eta}$$

$$\frac{\partial v}{\partial z}=\frac{z}{\eta}\cdot\frac{\partial p}{\partial y}+\frac{C}{\eta} \qquad (5)$$

where A and C are integration constants.
The viscosity of the lubricant may change considerably across the thin film (z direction) as a result of temperature variations that arise in some bearing problems.
An approach that is satisfactory in most fluid film applications is to treat η as the average value of the viscosity across the film. Note that this does not restrict the variation of viscosity in the x and y directions. This approach is pursued in this thesis.

With η representing an average value of viscosity across the film, integrating equations (5) gives the velocity components as:

$$u = \frac{z^2}{2 \cdot \eta} \cdot \frac{\partial p}{\partial x} + A \cdot \frac{z}{\eta} + B$$

$$v = \frac{z^2}{2 \cdot \eta} \cdot \frac{\partial p}{\partial y} + C \cdot \frac{z}{\eta} + D \qquad (6)$$

In order to calculate the constants we need some boundary values for velocity. The next assumption is that there is no slip in the fluid-solid interface. These boundary values are:

- z=0 , u= u_b , v= v_b
- z=h , u=u_a , v= v_a

The subscripts a and b refer to conditions on the upper (curved) and lower (plane) surfaces, respectively. Therefore,u_a, v_a and w_a refer to the velocity components of the upper surface in the x, y, and z directions, respectively, and u_b, v_b, and w_b refer to the velocity components of the lower surface in the same directions. With the boundary conditions applied to equations (6) the velocity gradients and velocity components are:

$$\frac{\partial u}{\partial z} = \left(\frac{2z - h}{2\eta} \right) \cdot \frac{\partial p}{\partial x} - \frac{u_b - u_a}{h}$$

$$\frac{\partial v}{\partial z} = \left(\frac{2z - h}{2\eta} \right) \cdot \frac{\partial p}{\partial y} - \frac{v_b - v_a}{h}$$

$$u = -z \cdot \left(\frac{h - z}{2\eta} \right) \cdot \frac{\partial p}{\partial x} + u_b \cdot \left(\frac{h - z}{h} \right) + u_a \cdot \frac{z}{h}$$

$$v = -z \cdot \left(\frac{h - z}{2\eta} \right) \cdot \frac{\partial p}{\partial y} + v_b \cdot \left(\frac{h - z}{h} \right) + v_a \cdot \frac{z}{h} \qquad (7)$$

The viscous shear stresses acting on the solids can be expressed as:

$$\tau_{zx} = \eta \cdot \left(\frac{\partial w}{\partial x} + \frac{\partial u}{\partial z} \right)$$

$$\tau_{zy} = \eta \cdot \left(\frac{\partial w}{\partial y} + \frac{\partial v}{\partial z} \right) \qquad (8)$$

In the order-of-magnitude evaluation $\partial w/\partial x$ and $\partial w/\partial y$ are much smaller than $\partial u/\partial z$ and $\partial v/\partial z$. Therefore,

$$\tau_{zx} = \eta \cdot \frac{\partial u}{\partial z}$$

$$\tau_{zy} = \eta \cdot \frac{\partial v}{\partial z} \qquad (9)$$

and the viscous shear stresses acting on the solid surfaces can be expressed:

$$\left(\tau_{zx}\right)_{z=0} = \left(\eta \cdot \frac{\partial u}{\partial z}\right)_{z=0} = -\frac{h}{2} \cdot \frac{\partial p}{\partial x} - \frac{\eta \cdot \left(u_b - u_a\right)}{h}$$

$$\left(-\tau_{zx}\right)_{z=h} = -\left(\eta \cdot \frac{\partial u}{\partial z}\right)_{z=h} = -\frac{h}{2} \cdot \frac{\partial p}{\partial x} + \frac{\eta \cdot \left(u_b - u_a\right)}{h}$$

$$\left(\tau_{zy}\right)_{z=0} = \left(\eta \cdot \frac{\partial v}{\partial z}\right)_{z=0} = -\frac{h}{2} \cdot \frac{\partial p}{\partial y} - \frac{\eta \cdot \left(v_{b-} v_a\right)}{h}$$

$$\left(-\tau_{zy}\right)_{z=h} = -\eta \cdot \left(\frac{\partial v}{\partial z}\right)_{z=h} = -\frac{h}{2} \cdot \frac{\partial p}{\partial y} + \frac{\eta \cdot \left(v_b - v_a\right)}{h} \qquad (10)$$

The negative signs on the viscous shear stress indicate that it acts opposite to the direction of motion.
The volume flow rates per unit width in the x and y directions are defined as:

$$q'_x = \int_0^h u \, \mathrm{d}z$$

$$q'_y = \int_0^h v \, \mathrm{d}z \qquad (11)$$

Substituting equations (7) in these equations gives:

$$q'_x = -\frac{h^3}{12\eta} \cdot \frac{\partial p}{\partial x} + \frac{\left(u_a + u_b\right) \cdot h}{2}$$

$$q'_y = -\frac{h^3}{12\eta} \cdot \frac{\partial p}{\partial y} + \frac{\left(v_a + v_b\right) \cdot h}{2} \qquad (12)$$

By the form of the above, we can observe that the terms on the right hand side of these equations are Poiseuille (pressure) flow and Couette flow correspondingly.

The next step is to express the continuity equation in integral form for convenience:

$$\int_0^h \left[\frac{\partial \rho}{\partial t} + \frac{\partial(\rho \cdot u)}{\partial x} + \frac{\partial(\rho \cdot v)}{\partial y} + \frac{\partial(\rho \cdot w)}{\partial z} \right] \mathrm{d}z = 0 \qquad (13)$$

We use Leibniz rule of integration which is:

$$\int_0^h \frac{\partial\left[f(x,y,z)\right]}{\partial x} \mathrm{d}z = -f(x,y,h) \cdot \frac{\partial h}{\partial x} + \frac{\partial\left[\int_0^h f(x,y,z)\,\mathrm{d}z\right]}{\partial x}$$

if ρ is assumed to be the mean force density across the film (as was done earlier for the viscosity across the film), the u component term in the integrated continuity equation is:

$$\int_0^h \frac{\partial(\rho \cdot u)}{\partial x} \mathrm{d}z = -(\rho \cdot u)_{z=h} \cdot \frac{\partial h}{\partial x} + \frac{\partial\left(\int_0^h \rho \cdot u\,\mathrm{d}z\right)}{\partial x} =$$

$$-\rho \cdot u_a \cdot \frac{\partial h}{\partial x} + \frac{\partial\left(\int_0^h \rho \cdot u\,\mathrm{d}z\right)}{\partial x} \qquad (14)$$

Similarly, for the v component:

$$-\rho \cdot v_a \cdot \frac{\partial h}{\partial y} + \frac{\partial}{\partial y}\left(\rho \cdot \int_0^h v\,\mathrm{d}z\right) \qquad (15)$$

As far as the w component is concerned we can integrate directly:

$$\int_0^h \frac{\partial(\rho \cdot w)}{\partial z} \mathrm{d}z = \rho \cdot \left(w_a - w_b\right) \qquad (16)$$

Therefore, the integrated continuity equation becomes:

$$h\cdot\frac{\partial\rho}{\partial t}-\rho\cdot u_a\cdot\frac{\partial h}{\partial x}+\frac{\partial\left(\rho\cdot\int_0^h u\,dz\right)}{\partial x}-\rho\cdot v_a\cdot\frac{\partial h}{\partial y}+\frac{\partial\left(\rho\cdot\int_0^h v\,dz\right)}{\partial y}+\rho\cdot\left(w_a-w_b\right)=0 \tag{17}$$

The integrals in this equation represent the volume flow rates per unit width (q'_x and q'_y) described in equations (12). Introducing these flow rate expressions into the integrated continuity equation yields the general Reynolds equation:

$$0=\frac{\partial}{\partial x}\left(-\frac{\rho\cdot h^3}{12\eta}\cdot\frac{\partial p}{\partial x}\right)+\frac{\partial}{\partial y}\left(-\frac{\rho\cdot h^3}{12\eta}\cdot\frac{\partial p}{\partial y}\right)+\frac{\partial}{\partial x}\left[\frac{\rho\cdot h\cdot\left(u_a+u_b\right)}{2}\right]$$

$$+\frac{\partial}{\partial y}\left[\frac{\rho\cdot h\cdot\left(v_a+v_b\right)}{2}\right]+\rho\cdot\left(w_a-w_b\right)-\rho\cdot u_a\cdot\frac{\partial h}{\partial x}-\rho\cdot v_a\cdot\frac{\partial h}{\partial y}+h\cdot\frac{\partial\rho}{\partial t} \tag{18}$$

we can write the above equation in the following form:

$$\frac{\partial}{\partial x}\left(\frac{\rho\cdot h^3}{12\eta}\cdot\frac{\partial p}{\partial x}\right)+\frac{\partial}{\partial y}\left(\frac{\rho\cdot h^3}{12\eta}\cdot\frac{\partial p}{\partial y}\right)=$$

$$\frac{\partial}{\partial x}\left[\frac{\rho\cdot h\left(u_a+u_b\right)}{2}\right]+\frac{\partial}{\partial y}\left[\frac{\rho\cdot h\left(v_a+v_b\right)}{2}\right]+\frac{\partial(\rho\cdot h)}{\partial t} \tag{19}$$

We will show that the above equations are equivalent:

First, observe that the film thickness h is a function of x, y, and t.

$$h=f(x,y,t)$$

From the definition of a total derivative:

$$Dh=\frac{\partial h}{\partial t}\cdot dt+\frac{\partial h}{\partial x}\cdot dx+\frac{\partial h}{\partial y}\cdot dy \tag{20}$$

or

$$\frac{Dh}{Dt} = \frac{\partial h}{\partial t} + \frac{\partial h}{\partial x} \cdot \frac{dx}{dt} + \frac{\partial h}{\partial y} \cdot \frac{dy}{dt}$$

But,

$$u_a = \frac{dx}{dt} \ , \ v_a = \frac{dy}{dt}, \frac{Dh}{Dt} = w_a - w_b \ , \ so$$

$$w_a - w_b = \frac{\partial h}{\partial t} + u_a \cdot \frac{\partial h}{\partial x} + v_a \cdot \frac{\partial h}{\partial y} \quad or$$

$$\frac{\partial h}{\partial t} = w_a - w_b - u_a \cdot \frac{\partial h}{\partial x} - v_a \cdot \frac{\partial h}{\partial y} \qquad (21)$$

so the two equations are equivalent.

2.5.2 Physical Meaning Of Terms In Reynolds Equation

Except for the mathematical proof of Reynolds equation, it is vital to look into the physical significance of each term so that the pressure generation mechanisms can be observed.

In equation (18), The first two terms are the Poiseuille terms and describe the net flow rates due to pressure gradients within the lubricated area. The third and fourth terms describe the known Couette flow or shear-driven flow and builds up due to the surface velocities. The fifth to seventh terms are known as the squeeze effect and the last term stands for local expansion.

- ***density wedge term*** $\left[\left(u_a + u_b \right) \cdot \frac{h}{2} \right] \cdot \frac{\partial \rho}{\partial x}$

The density wedge action is concerned with the rate at which lubricant density changes in the sliding direction as shown in figure (2.5). If the lubricant density changes in the sliding direction, the Couette mass flow for each of the three distinct actions at entry differs from the flow out for the same action. For continuity of mass flow this discrepancy must be eliminated by generating a balancing Poiseuille flow.

The density wedge (sometimes called the thermal wedge) mechanism is not important in most bearings, but may have a more significant impact in parallel surface thrust bearings where the other pressure build up mechanisms are missing.

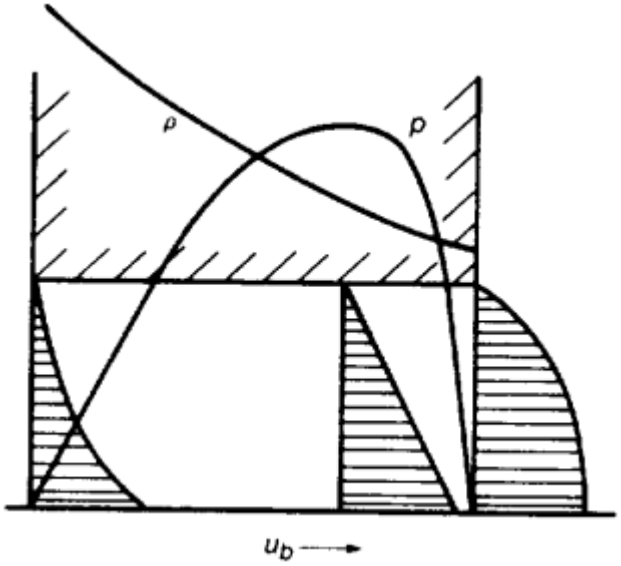

Figure 2.5: density wedge mechanism[7]

- ***stretch term*** $\left(\rho \cdot \frac{h}{2}\right) \cdot \left[\frac{\partial\left(u_a + u_b\right)}{\partial x}\right]$

The stretching term considers the rate at which the surface velocity changes in the sliding direction. This is not about conventional bearings.
Figure (2.6) shows the stretching mechanism:

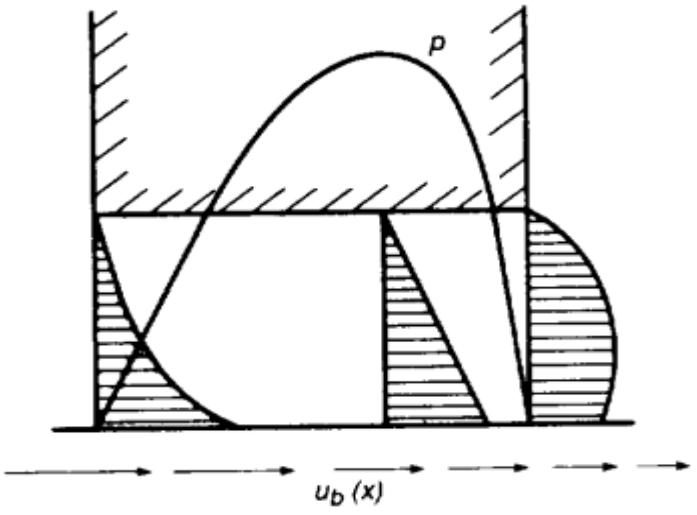

Figure 2.6 : stretch mechanism[7]

- ***normal squeeze term*** $\rho \cdot \left(w_a - w_b \right)$

Normal squeeze action comes up if the surface of the shaft and bearing tend to be pressed towards each other. Positive pressure generation is observed when the film thickness diminishes, meaning that the normal velocity difference of the boundaries is wb>wa , so the film thickness is decreasing. The mechanism is illustrated in Figure (2.7). Normal squeeze action along with physical wedge are the major pressure build up devices in hydrodynamic journal bearings.

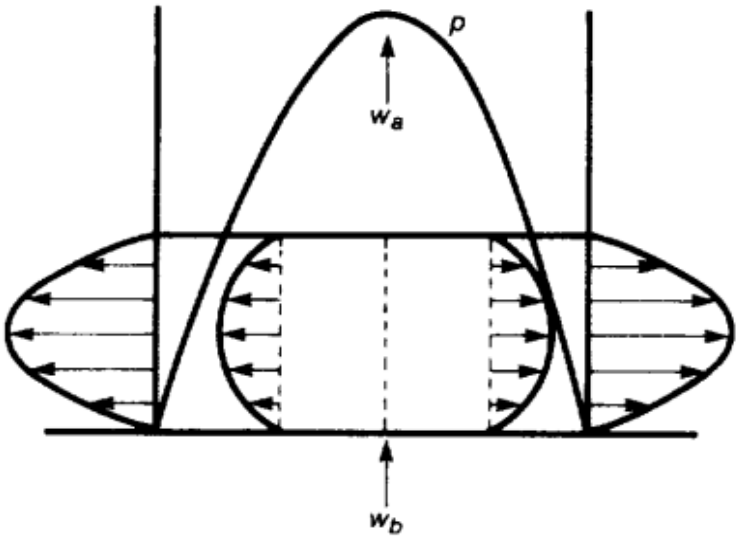

Figure 2.7: normal squeeze mechanism[7]

- ***Physical wedge term*** $\left[\rho \cdot \frac{\left(u_a + u_b \right)}{2} \right] \cdot \left(\frac{\partial h}{\partial x} \right)$

The physical wedge action is extremely important and is the best known device for pressure generation. This action is illustrated for the case of a plane slider and a stationary bearing pad in figure (2.8). At each of the three sections considered, the Couette volume flow rate is proportional to the area of the triangle of height h and base u. Since h varies along the bearing, there is a different Couette flow rate at each section, and flow continuity can be achieved only if a balancing Poiseuille flow is superimposed. For a positive load-carrying capacity the thickness of the lubricant film must decrease in the sliding direction.

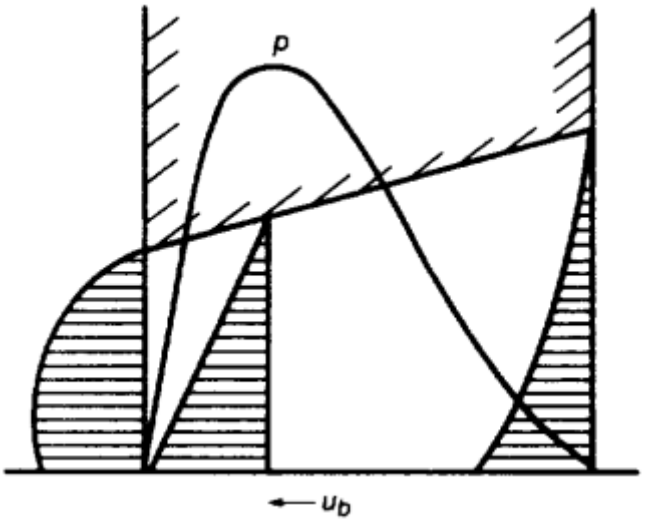

Figure 2.8: Physical wedge mechanism[7]

- ***Translation squeeze term*** $-u_a \cdot \left(\frac{\partial h}{\partial x}\right)$

The translation squeeze action is a result from the translation of the inclined surfaces. By that, the local film thickness can be squeezed by the sliding of the bearing inclined surface. In this case the pressure profile is moving over the space covered by the fixed coordinate system, the pressure at any fixed point being a function of time.

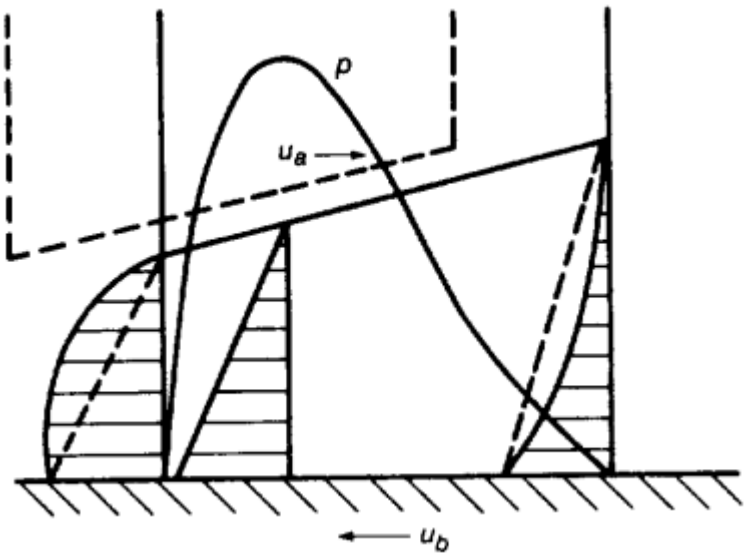

Figure 2.9 : Translation squeeze action[7]

- ***Local expansion term*** $h \cdot \left(\frac{\partial \rho}{\partial t} \right)$

Local expansion term is related to the time rate of change of density. If the lubricant is supplied by heat, it will expand and with the absence of surface velocities a Poiseuille flow will develop. To have a positive load capacity the volume of a given mass of lubricant has to increase so its density must decrease. In bearing analysis local expansion is of no importance.

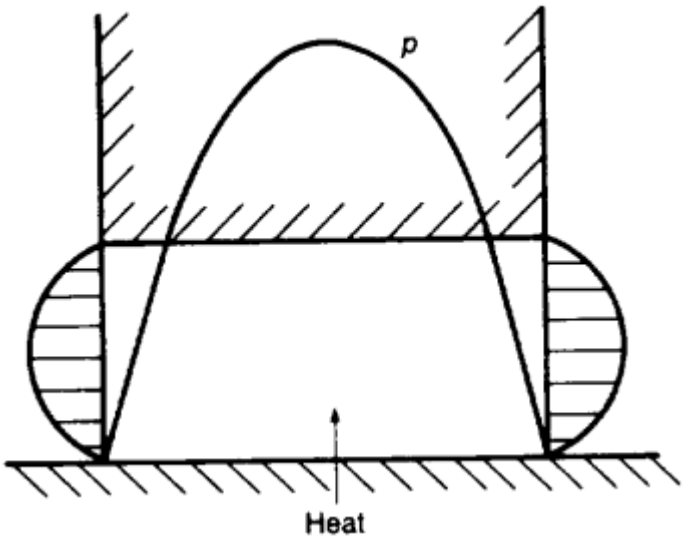

Figure 2.10 : Local expansion[7]

2.5.3 Reduced Form Of Reynolds Equation

In the general form Reynolds equation is quite complex to work with. In this case some simplifications are required in order to reach the reduced equation that will be used in this thesis.

1. As stated above, the two major pressure build up mechanisms are the physical wedge and the normal squeeze action. In this thesis the squeeze action will not be considered, so we either delete the last term in equation (19) , or in equation (18) we assume only tangential motion where :

(22) $$w_a = u_a \cdot \frac{\partial h}{\partial x} + v_a \cdot \frac{\partial h}{\partial y} \; and \; w_b = 0$$

2. The surface velocities are considered to be constant so no stretch term is taken into account as it is reasonable for conventional bearings.

3. Only one surface is moving, the shaft, so there is only one surface velocity u.

The reduced Reynolds equation becomes:

$$\frac{\partial}{\partial x}\left(\frac{\rho \cdot h^3}{\eta} \cdot \frac{\partial p}{\partial x}\right) + \frac{\partial}{\partial y}\left(\frac{\rho \cdot h^3}{\eta} \cdot \frac{\partial p}{\partial y}\right) = 6 \cdot u \cdot \frac{\partial(\rho \cdot h)}{\partial x} + 6 \cdot v \cdot \frac{\partial(\rho \cdot h)}{\partial y} \qquad (23)$$

4. For hydrodynamic lubrication there is pure sliding so v can be assumed as zero.

5. Conventional hydrodynamic bearing lubricants can generally be assumed to be incompressible for most practical purposes. This assumption is based on the fact that the density of the lubricant is relatively constant under typical operating conditions and does not significantly change in response to variations in pressure. When the oil lubricant is compressed its density increases. This increase is usually noticed at pressure > 0.1 GPa. That is why it is reasonable to assume the lubricant is incompressible. If the lubricant is water this assumption is even more valid as mentioned in chapter 2.2. Incompressible fluids do not exist in the real world due to special relativity (can not have infinite speed of sound). For water under standard temperature and pressure the bulk modulus of elasticity divided by density is equal : $\frac{K_s}{\rho} = 2.2 \cdot 10^6 m^2/s^2$.

For lubricating oils the value of bulk modulus is typically $1 - 2 \cdot 10^9 Pa$. According to the literature we can assume a flow to be incompressible without introducing unacceptable error when the Mach number is less than 0.3 which is typically valid.

The Mach number is defined as : $M = V/V_{sound} = V\sqrt{\rho/K_s}$.

6. Another assumption that is used in this thesis is that the viscosity is constant over the lubricant film or as it is common in literature “isoviscous conditions”. This implies that the thermal effects on viscosity are not taken into consideration.

Thus, the final form of Reynolds equation is:

$$\frac{\partial}{\partial x}\left(h^3 \cdot \frac{\partial p}{\partial x}\right) + \frac{\partial}{\partial y}\left(h^3 \cdot \frac{\partial p}{\partial y}\right) = 6 \cdot u \cdot \eta \cdot \frac{\partial h}{\partial x} \qquad (24)$$

2.5.4 Boundary Conditions for Reynolds Equation

In order to obtain a solution for the Reynolds equation, it is essential to use appropriate boundary conditions for the pressure distribution as in every partial differential equation. The following boundary conditions are the most popular[12]:

- ***Full Sommerfeld Boundary Condition***, where the pressure is set as zero at the edges of the wedge. Although it seems as a reasonable boundary condition, two problems occur; At first, the large negative pressures that come up are unrealistic and can not be applied to real fluids. Normal fluids can not stand large and continuous negative pressures without rupturing. Secondly, due to the mirror image of the pressure distribution, the final load capacity is predicted as zero, which is unreasonable.

- ***Half Sommerfeld Boundary Condition***, which is exactly the same with the full Sommerfeld condition, with the only difference being that the predicted negative pressures are set equal to zero. As a condition it is very simple to be applied and gives relatively good results but this sudden pressure change to zero at θ=0 leads to discontinuity of the flow, which is erroneous. However it is still preferred because of the simplicity of its use.

- ***Reynolds Boundary Condition*** , which was proposed by Reynolds[10], who stated that negative pressures can not exist and in the boundary of zero and non-zero pressures the condition:

$$p = \frac{dp}{dx} = 0 \tag{25}$$

should apply.

The following figure represents the pressure distribution of all the three boundary conditions. In this thesis, the Reynolds boundary condition is used.

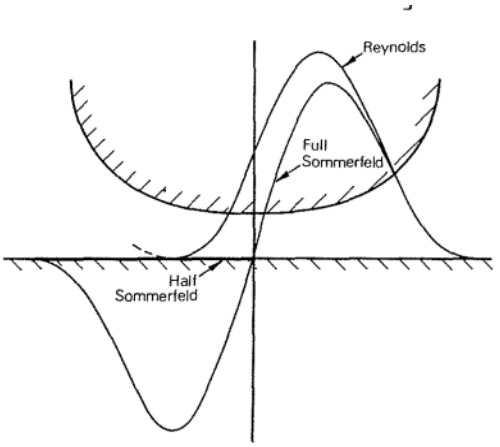

Figure 2.11 : Boundary conditions of Reynolds equation[12]

2.5.5 Design and Performance Parameters

- ***Load Capacity***

In order to calculate the total load that a journal bearing can carry, we have to integrate the pressure over the bearing area. Two vertical load components will be calculated and their vector sum is the total load that the bearing will support.

The first component W_1 is acting along the line that connects the bush's and shaft's centers while the second component W_2 is acting in a direction perpendicular to the first. In this way we also calculate the angle between the line of centers and the load line, known as "attitude angle". This angle gives information about the location of minimum and maximum film thickness.

If we consider a small angle dθ, according to the following figure we can express the two load components as:

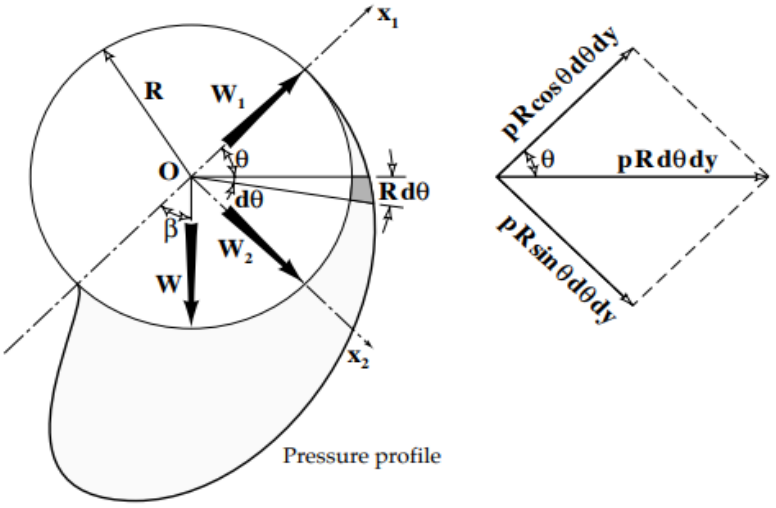

Figure 2.12 : Load components in a journal bearing[10]

$$W_1 = \int_0^{2\pi} \int_0^{L} p \cdot R \cdot \cos\theta \cdot \mathrm{d}\theta \mathrm{d}y$$

$$W_2 = \int_0^{2\pi} \int_0^{L} p \cdot R \cdot \sin\theta \cdot \mathrm{d}\theta \mathrm{d}y \qquad (26)$$

The total load that the bearing will support is the resultant of the two components:

$$W = \sqrt{{W_1}^2 + {W_2}^2} \qquad (27)$$

❖ ***Sommerfeld Number***

Sommerfeld Number is a non-dimensional quantity which is used quite often in hydrodynamic bearings analysis. It is a means of similarity for journal bearings and connects both design and operational parameters. Its formula is:

$$S = \frac{\eta \cdot N \cdot D \cdot L}{W} \cdot \left(\frac{R}{c}\right)^2 \quad (28)$$

where:

- η is the lubricant viscosity
- N is the shaft angular velocity
- D is bearing diameter
- L is the bearing length
- W is the total load applied
- R is bearing radius
- c is the radial clearance between bearing and shaft

❖ ***Friction Force***

The total amount of Friction Force is calculated by integrating the shear stress over the bearing area. With use of equations (7) and (9) we get:

$$F = \int_0^L \int_0^{2\pi R} \tau_{zx} \cdot \mathrm{d}x\,\mathrm{d}y = \int_0^L \int_0^{2\pi R} \eta \cdot \frac{du}{dz}\,\mathrm{d}x\,\mathrm{d}y \longrightarrow$$

$$F = \int_0^L \int_0^{2\pi R} \left(\frac{2z-h}{2} \cdot \frac{\partial p}{\partial x} + \frac{U}{h}\right)\mathrm{d}x\,\mathrm{d}y \quad (29)$$

❖ ***Friction Coefficient***

Friction Coefficient can be expressed by the following fraction, where F stands for total friction force and W stands for total Load :

(30)
$$\mu = \frac{F}{W}$$

❖ ***Inlet and Outlet Flow rates***

The inlet and outlet flow rates per unit length and width have been calculated as (12).

Thus lubricant inflow can be calculated at the bearing entrance by:

$$Q_{in} = \int_0^L q_x \big| x=0 \mathrm{d}y = \int_0^L \left(-\frac{h^3}{12\eta} \cdot \frac{\partial p}{\partial x} + U \cdot \frac{h}{2} \right) \big| x=0 \ \mathrm{d}y \quad (31)$$

The lubricant side leakage can be calculated by:

$$Q_{leak} = \int_0^{2\pi R} q_y \big| y=0 \ \mathrm{d}x + \int_0^{2\pi R} q_y \big| y=L \ \mathrm{d}x =$$

$$\int_0^{2\pi R} \left(-\frac{h^3}{12\eta} \cdot \frac{\partial p}{\partial y} \right) \big| y=0 \ \ \mathrm{d}x + \int_0^{2\pi R} \left(-\frac{h^3}{12\eta} \cdot \frac{\partial p}{\partial y} \right) \big| y=L \ \ \mathrm{d}x \quad (32)$$

For normal bearing operation, lubricant must be supplied to the bearing at the same rate as that of the lubricant leakage; otherwise lubricant starvation will occur, which will generally lead to smaller values of minimum film thickness and higher values of oil temperature.

❖ ***Power Loss***

Power loss is a result of friction and can be expressed as:

$$P_{loss} = F \cdot U = \mu \cdot \ W \cdot \omega \cdot R \quad (33)$$

where:

- F is the total friction force
- μ is friction coefficient
- W is the total bearing Load
- ω is angular speed of the shaft
- R is bearing Radius

3. Numerical Solution

3.1 Film thickness geometry

The clearance between the shaft and the bearing is filled with lubricant. Its shape can be geometrically modeled with appropriate parameters. These parameters can be either constant, as bearing/shaft radius, or variable depending on every step of the problem, as eccentricity and attitude angle. The last two parameters change at every iteration during the solution of the problem as will be explained later. As a result, film thickness shape is also a variable that has to be modeled carefully. In the present thesis, the general film thickness shape is given by:

(34) $$h(\theta,z) = h_{rigid}(\theta) + h_{elastic}(\theta) + h_{thermal}(\theta) + h_{misalignment}(\theta,z)$$

- The first term refers to the rigid bearing geometry which is:

$$h_{rigid}(\theta) = c + e\cdot\cos\theta$$

- The second term is the main task of this thesis and refers to elastic deformations in the bearing's bush due to the hydrodynamic pressures. Deformations are calculated using a Finite Element Method software, CalculiX.

- The third term refers to the thermal expansion of the shaft and to the deformation due to bearing housing dilatation, which in this thesis are not taken into account.

- The last term refers to misalignment, the case that the shaft and bearing centerlines are not parallel. According to [13], misalignment angle can be resolved into two perpendicular angles, similar to the external load angles, one about each axis of the coordinate system. Thus, lateral misalignment angles describe shaft rotations about the vertical y axis, and vertical misalignment angles describe rotations about the horizontal z axis.

(35) $$h_{misalignment}(\theta,z) = z\cdot\left[\psi_y\cdot\cos\left(\theta+\varphi_0\right) + \psi_x\cdot\sin\left(\theta+\varphi_0\right)\right]$$

3.2 Finite Difference Method

The finite difference method is a numerical technique used to approximate solutions to differential equations. The basic idea is to replace the differential equation with a set of algebraic equations that can be solved using standard techniques. The finite difference method works by approximating the derivatives in the differential equation using finite difference approximations. In this method, the solution domain is divided into a grid of points, and the differential equation is approximated at each point using a finite difference formula. These formulas involve evaluating the function at neighboring points and using their values to approximate the derivative. The resulting system of algebraic equations can be solved using various numerical techniques, such as matrix inversion, iterative methods, or relaxation methods. The accuracy of the finite difference method depends on the choice of grid spacing, the order of the finite difference formula used, and the smoothness of the solution. Higher-order finite difference formulas and smaller grid spacing typically yield more accurate solutions, but at the cost of increased computational complexity.

The journal bearing geometry is studied in the unwrapped domain. This unwrapped bearing domain is discretized by a finite element grid of 'Ldiv' points at the y-axis and 'Ddiv' points at the x-axis. In this work a uniform spacing in the x- and y- direction is assumed, therefore 'Ldiv' represent the number of divisions along the length of the bearing and 'Ddiv' represent the number of divisions along the circumference of the bearing. Each point is identified by i, j indices and has four neighboring nodes (except for the boundary nodes). The unwrapped journal bearing grid is presented in Figure (3.1).

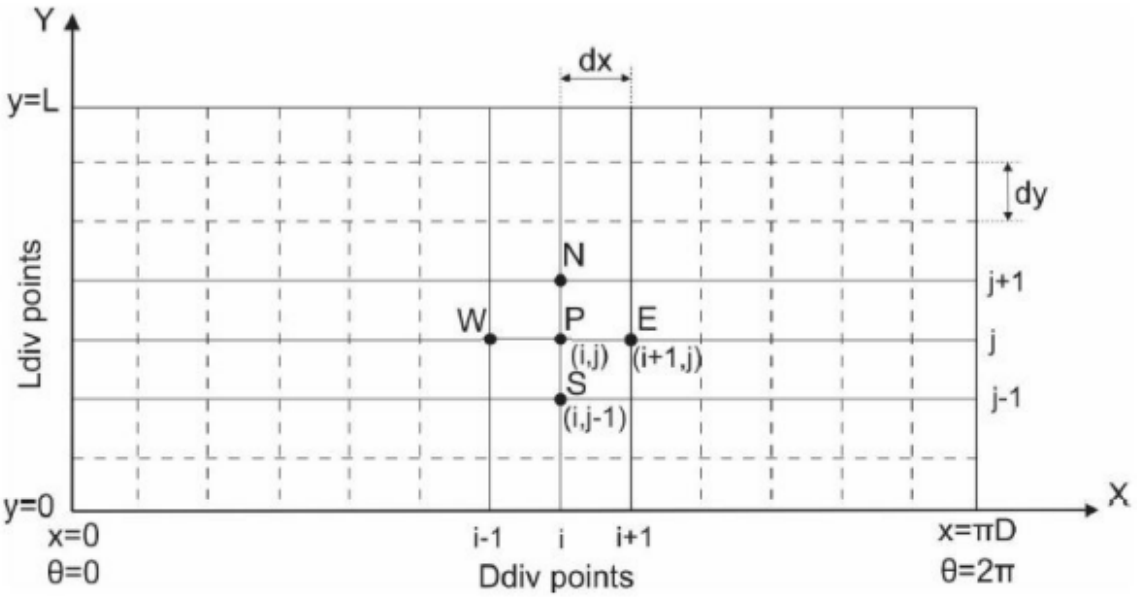

Figure 3.1 : Unwrapped journal bearing geometry

The finite difference method for the solution of elliptic partial differential equations such as equation (24) is well known. The solution is obtained by replacing the derivatives with the appropriate finite difference expression based on the Taylor series expansion.

Some proposed formulations from the literature are [14]:

$$\frac{\partial p}{\partial x} = \frac{p(i+1,j) - p(i-1,j)}{2 \cdot dx}$$

$$\frac{\partial^2 p}{\partial x^2} = \frac{p(i+1,j) - 2 \cdot p(i,j) + p(i-1,j)}{dx^2} \tag{36}$$

and

$$\frac{\partial p}{\partial x} = \frac{-p(i+2,j) + 8 \cdot p(i+1,j) - 8 \cdot p(i-1,j) + p(i-2,j)}{12 \cdot dx} \tag{37}$$

$$\frac{\partial^2 p}{\partial x^2} = \frac{-p(i+2,j) + 16 \cdot p(i+1,j) - 30 \cdot p(i,j) + 16 \cdot p(i-1,j) + p(i-2,j)}{12 \cdot dx^2}$$

where $$dx = \frac{\pi \cdot D}{(Ddiv - 1)}$$

Although the above relationships are given for the x derivatives, the corresponding relationships for the y derivatives are numerically identical. There is no requirement for dy to be equal to dx. The first formulations are the most popular and have a truncation error proportional to dx^2. The second formulations are higher order formulae, having an error proportional to dx^4. Although they are more accurate, they require greater solution time and cannot be applied to the grid nodes nearest the boundary and so another type of approximation must be used at these nodes. In this thesis, the first formulations are used. These finite difference formulae are also used to evaluate the derivatives of the film thickness h, so h must be specified at the nodes.

3.3 Hydrodynamic Solution Algorithm

The first step for an elastohydrodynamic analysis of a journal bearing is to separately solve the hydrodynamic problem , where the bearing is considered as rigid. For that purpose, it is essential to solve Reynolds equation (24) using the finite difference method in order to get the pressure distribution. Several algorithms have been developed to solve problems concerning hydrodynamic lubrication. In this current approach, we will solve the Reynolds Equation using an in-house algorithm developed in the section of Marine Engineering of NTUA, first introduced by Raptis[15].

In the beginning, this in-house solver, written in c++, requires an input file from the user. In this input file all the necessary design and operational data are collected such as bearing length and diameter, radial clearance, rotational speed, misalignment angles, applied loads P_x and P_z in the bearing and oil viscosity. This input file also gives the user the option to choose between other solver parameters such as solver type, convergence criteria, grid points,relaxation factors etc. The last step of the preprocessing is to make an assumption about eccentricity and attitude angle as in most iterative methods.

After reading the initial parameters, the algorithm discretizes the bearing in its unwrapped form into small divisions. Then, the film thickness geometry is calculated using equation (34), without the elastic and thermal terms. The Reynolds Equation is solved numerically according to the Gauss - Seidel iterative method, and the pressure field is calculated. The hydrodynamic force components are then calculated, by integrating the pressure field on the bearing surface. If the initial assumptions of eccentricity and attitude angle are correct, then the equilibrium is attained and the algorithm ends. If not, new eccentricity and attitude angle values are estimated, using a Newton - Raphson method for two variables. At the end of the whole process, the bearing operational parameters are calculated and printed out on an output file.

The flowchart of the previous solver is illustrated in the following Figure 3.2.

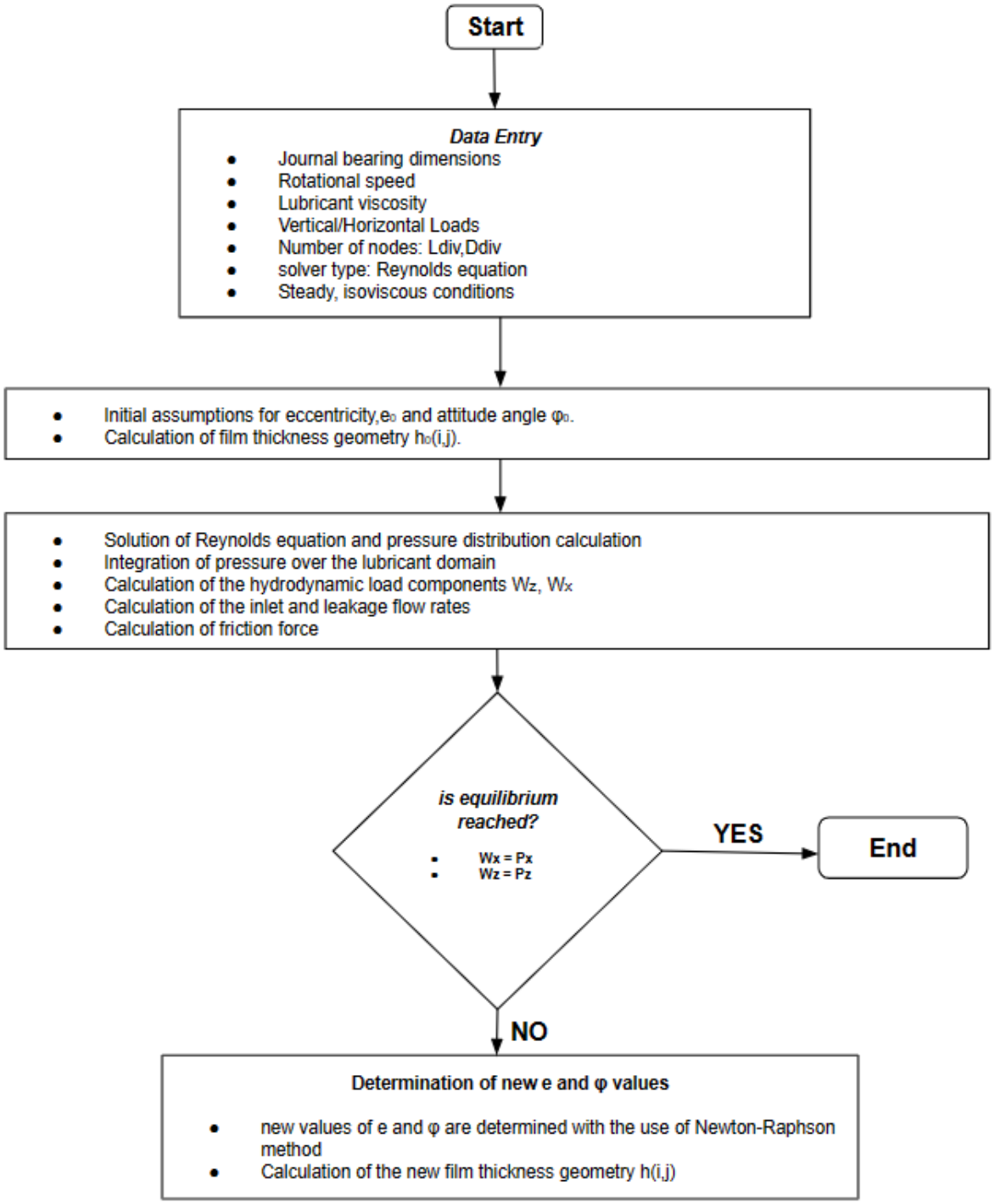

Figure 3.2 : Reynolds equation solution algorithm

3.4 Elastic Foundation Model (Winkler model)

The Winkler Foundation model is a theoretical model used in the field of mechanics to study the behavior of elastic materials, such as beams, plates, and shells, under external loading. In the Winkler Foundation model, an elastic material is treated as a continuous medium that is divided into many small, independent elements, each of which behaves like an independent spring. The model further assumes that the stiffness of each spring is constant and that the springs do not interact with each other. The Winkler Foundation model is also widely used in the field of mechanical engineering to study the behavior of journal bearings.

Due to the fact that the shearing action between two neighboring elastic bars is neglected, the actual deformation at a point is only dependent on the contact pressure at that point, the material and geometric parameters of contact bodies.

The elastic deformation can be therefore expressed as :

$$d_{winkler} = \frac{P_i \cdot T_b}{E'} \tag{38}$$

where T_b is the thickness of the elastic layer (bearing bush), and E' is a combined elastic modulus of the contact bodies. When only one contact body is regarded as elastic body, E' can be represented as:

$$E' = \frac{(1-v)}{(1+v)\cdot(1-2v)} \cdot E \tag{39}$$

where E is Young's modulus of the deformable body, and v is its Poisson's ratio.

Winkler model is a fast technique to estimate the bush deflections. It does not take into account the interaction between the strings so it is preferred when the load, speed and deformations are relatively low and when the bearing bush is thin. In chapter 4 we will see that the winkler model has a satisfying accuracy compared to FEM when the previous requirements are met.

In the following Figure (3.3), winkler model is illustrated:

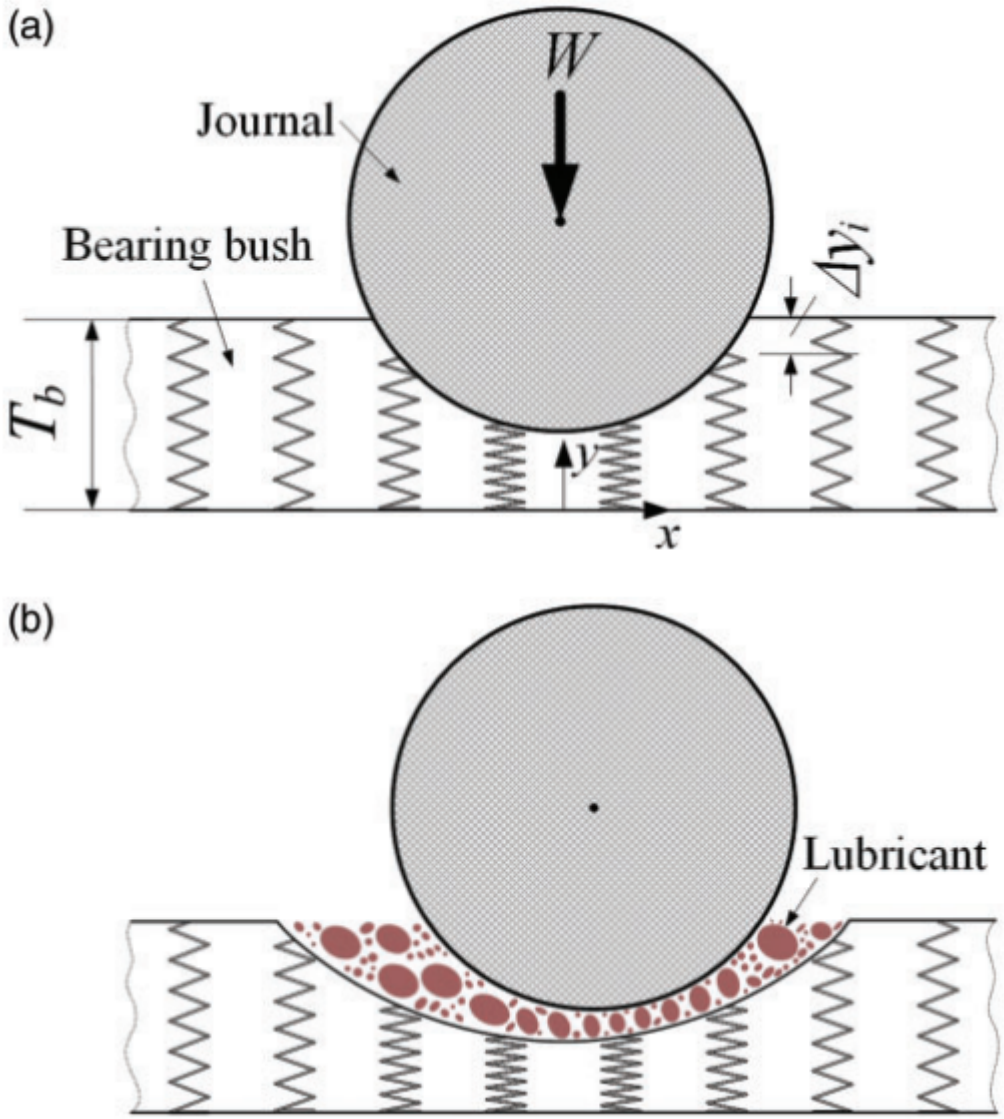

Figure 3.3 : Winkler Elastic Foundation Model [17]

3.5 Finite Element Method

3.5.1 Introduction to Finite Element Analysis

The Finite Element Method (FEM) is a numerical technique used to solve a variety of problems in engineering and physics. It involves dividing a complex domain into smaller, simpler regions called finite elements, which are interconnected through a set of mathematical equations. These equations are then solved using computer algorithms to obtain approximate solutions to the original problem. The FEM has a wide range of applications, from structural analysis and heat transfer to fluid dynamics and electromagnetics. It is particularly useful in situations where analytical solutions are not available or too complex to obtain, or where experimental testing is not feasible or too expensive.

The basic steps to solve a problem using Finite Element method are:

1. *Discretization*: The domain is divided into smaller, simpler regions called finite elements. These elements can be of various shapes, such as triangles, rectangles, or hexagons, depending on the complexity of the problem.
2. *Approximation*: Within each element, the unknown quantities (such as displacement, temperature, or pressure) are represented by a set of interpolation functions. These functions are usually polynomial functions of the coordinates that vary within the element.
3. *Assembly*: The equations governing the behavior of the system are derived by combining the equations for each element. These equations are typically expressed in terms of the nodal values of the unknowns.
4. *Solution*: The resulting set of equations is solved using numerical methods, such as matrix inversion, iterative methods, or direct solvers. The solution provides an approximation of the unknowns throughout the domain.
5. *Post-processing*: The numerical solution is visualized and analyzed to evaluate the accuracy of the results and to extract useful information, such as stresses, strains, or heat fluxes.

We can see a general procedure for Finite Element Analysis in Figure(3.4).

One of the advantages of the FEM is its flexibility in handling complex geometries and boundary conditions. By dividing the domain into smaller elements, the FEM can accommodate irregular shapes and curved boundaries that are difficult to handle analytically. The method can also handle a wide range of boundary conditions, including prescribed displacements, forces, temperatures, or fluxes. One of the main challenges is the choice of element type and size. The accuracy and convergence of the solution depend on the quality of the elements and their distribution throughout the domain. Choosing the wrong type or size of element can lead to inaccurate or unstable solutions.

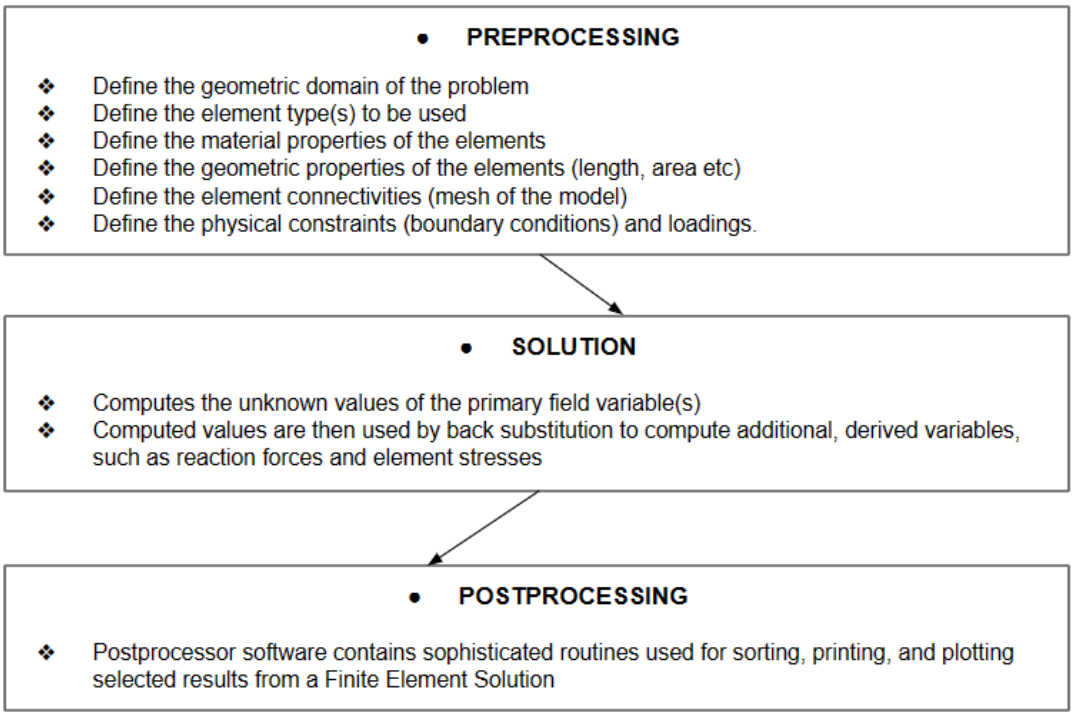

Figure 3.4 : Procedure for FEA

3.5.2 CALCULIX And Fluid-Solid Interaction

CalculiX is an open-source finite element analysis software package that allows users to perform linear and non-linear structural analyses. It is primarily used for mechanical engineering applications such as static and dynamic analyses of structures, heat transfer, and fluid dynamics simulations. The software can handle complex geometries and material properties, and has a wide range of elements and solvers available. It can also perform multiphysics simulations, allowing for the coupling of different physics phenomena such as fluid-structure interaction and thermal stress analysis.

In order to perform an elastohydrodynamic study of a journal bearing we need to couple Reynolds hydrodynamic solution with the structural model of the bearing bush. When elastic radial displacements are taken into account, they modify the film thickness and consequently the pressure distribution. So an iterative scheme is needed until equilibrium is reached.

The film thickness equation is modified to:

(40)
$$h = c + e \cdot \cos\theta + h_d$$

where h_d stands for radial displacements, calculated by CALCULIX software. When journal misalignment is taken into account, the corresponding term for misalignment is superimposed to the above equation (chapter 3.1).

In order to calculate the radial displacements of the bearing bush we solve the bearing pad elasticity problem with CALCULIX. In the present work, the bearing pad is considered elastic, and is housed inside a rigid bearing shell. The deformable bearing pad is modeled with C3D8 hexahedral elements, featuring 8 nodes per element. An example of the bearing mesh is figured below:

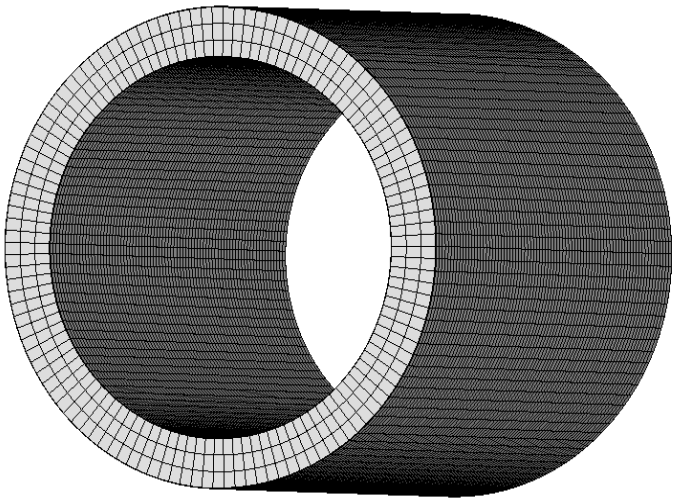

Figure 3.5 : Journal bearing hex mesh

A c++ code was added to the in-house software, which makes the input file (nodes, mesh, boundary and loading conditions) for CALCULIX. Then, the solver runs CALCULIX externally, obtaining the radial displacements of the bush. This is continued for a couple of iterations until the equilibrium is established. The corresponding flowchart of the EHD solution is presented below:

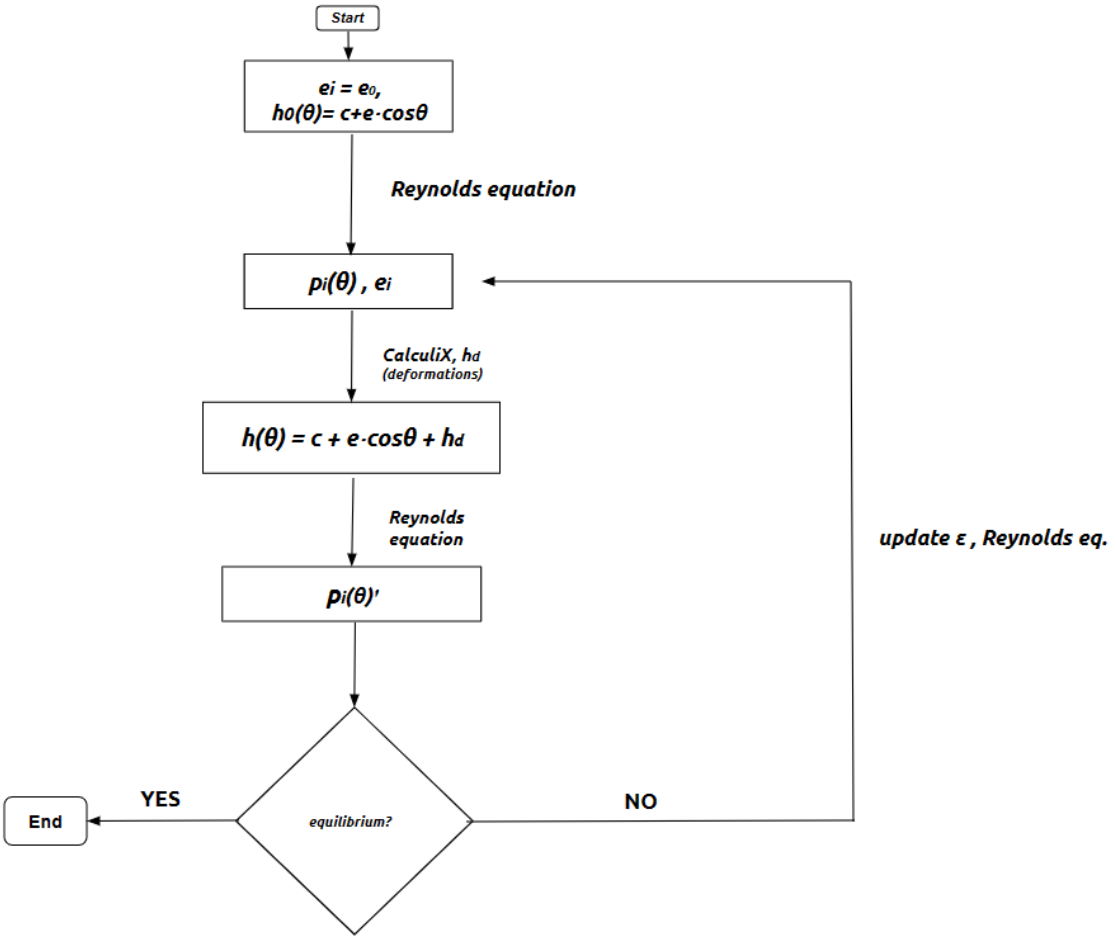

Figure 3.6 : EHD analysis flowchart

At first, similarly with the HD study, the user guesses eccentricity and attitude angle. Then Reynolds equation is solved by FDM and Gauss-Seidel method, obtaining pressure distribution at fluid film nodes. Then, the pressures at nodes are used in the CalculiX input file to obtain the elastic deformations of the bearing. The film thickness formula takes feedback from CalculiX with the deformations, leading via Reynolds equation solution to new pressure distribution. There is a check for equilibrium and if not, Newton- Raphson method is used to predict new eccentricity and attitude angle values. The whole process is repeated until the equilibrium is established.

One of the most important issues that Finite Element Analysis has is the mesh independence and its relation to simulation time. The chosen mesh is vital to lead to accurate results, which is the main purpose of using FEM over other numerical techniques such as winkler foundation. In order to find balance between accuracy and computational costs a proper mesh study has been conducted for the test cases that will be presented in chapter 4. Figure (3.7) shows the deformation contour of a journal bearing using CalculiX.

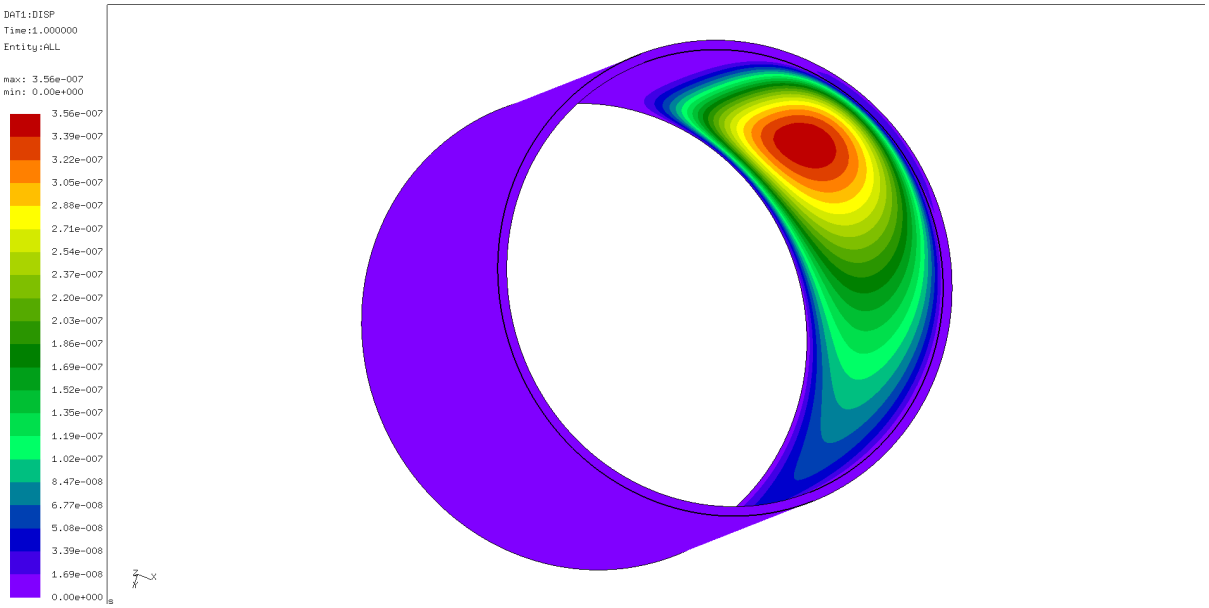

Figure 3.7 : CalculiX displacements contour

4. Validation And Numerical Simulations

4.1 Validation Of The Proposed Model

The proposed Elastohydrodynamic Analysis will be validated against the results published in literature, and more specifically with [16] "The analysis of elastohydrodynamic lubrication in the textured journal bearing, by Rufei Yu, Wei Chen and Pei Li" and with [25] "Analysis of elasto-hydrodynamic lubrication of journal bearing based on different numerical methods, by Fanming Meng and Yuanpei Chen".

In [16], the influences of flexibility and surface texture on the performances of a finite-long journal bearing have been investigated theoretically. The Winkler foundation model has been used to calculate the elastic deformation of the bearing bush, while the steady-state characteristics of a lubricated finite-long journal bearing are studied in the textured and untextured bearing surface, respectively.

The validation will include the untextured bearing geometry only. At first there will be a validation using the Winkler Foundation model, as in the paper and then the proposed coupled model using FEM will be compared.

The basic geometric and operating parameters are the same as in [16] and are listed below:

- ***Bearing Diameter*** ***D = 60.1 mm***
- ***Bearing Length*** ***L = 50 mm***
- ***Radial Clearance*** ***C = 0.05 mm***
- ***Rotational Speed*** ***N = 3000 rpm***
- ***Modulus of Elasticity*** ***E = 80000 MPa***
- ***Poisson's Ratio*** ***v = 0.3***
- ***Lubricant viscosity*** ***η = 0.02 Pa x s***
- ***Bush Thickness*** ***t = 1 mm***
- ***Grid*** ***141(Circumference) x 91(Length) x 3(thickness)***

4.1.1 Validation Of The Winkler Model

The validation process includes comparing the eccentricity and attitude angle values of the EHD simulations from the two models with Load varying from 1 KN to 51 KN. The results are presented in the following plots:

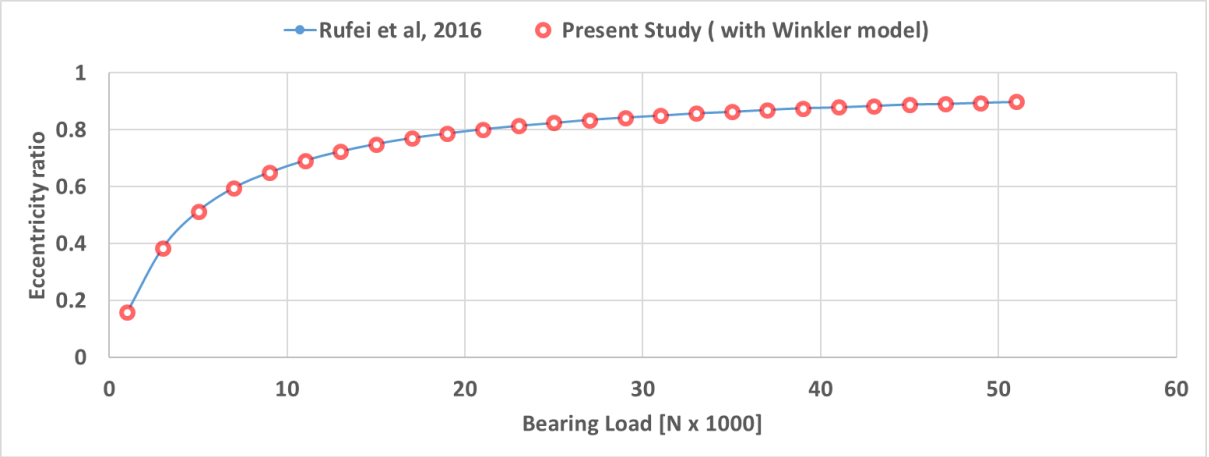

Figure 4.1 : Eccentricity-Load with Winkler Model

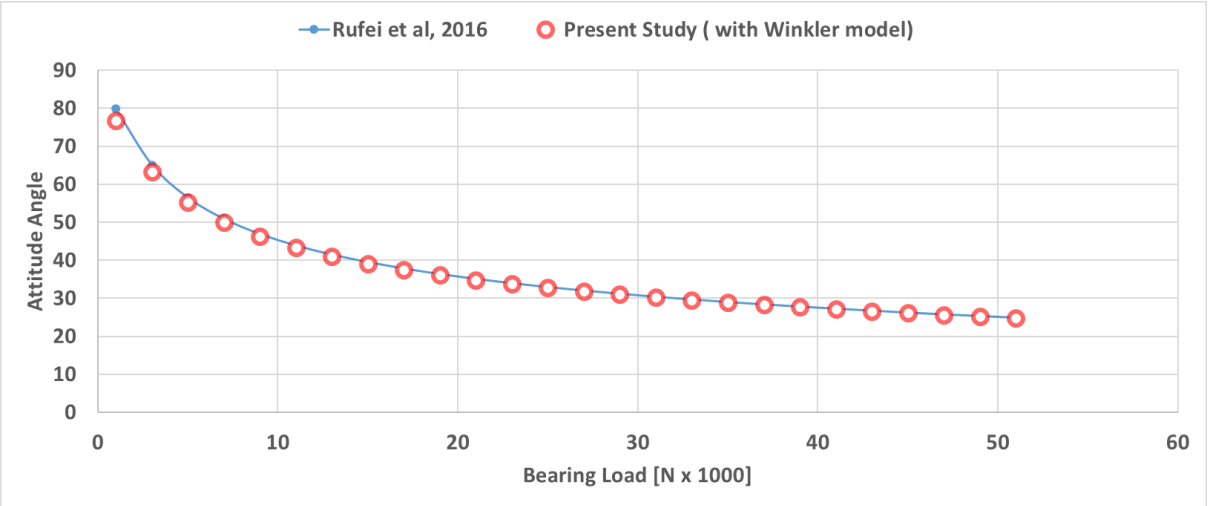

Figure 4.2 : Attitude Angle - Load with Winkler Model

The maximum deviation of the two models is 0.433% between the eccentricity values and 3.979% between the attitude angle values.

4.1.2 Validation Of The FEM Coupled Model

As shown in the next plots the EHD model with CalculiX is in full agreement with the corresponding Winkler Model:

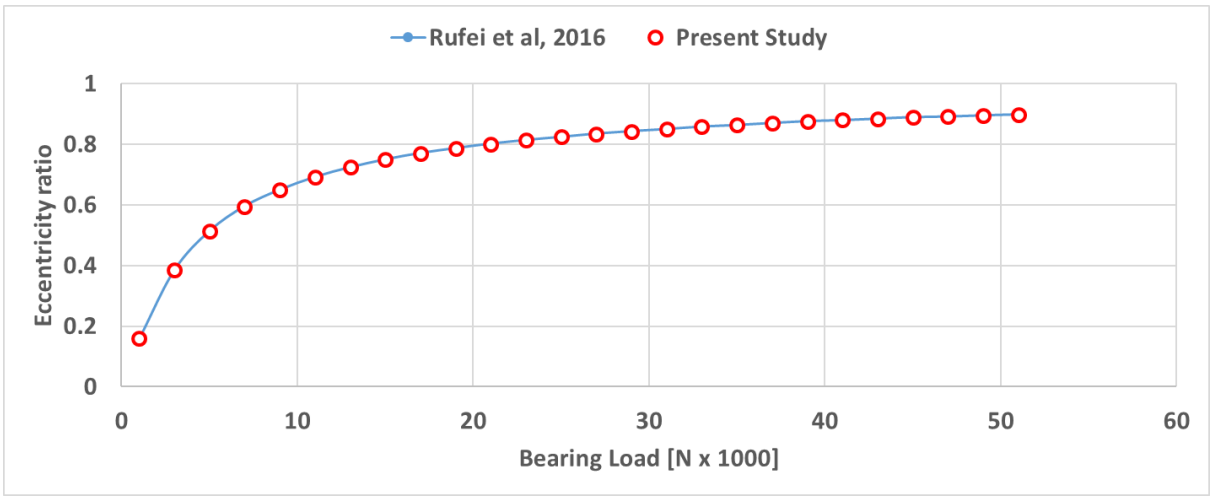

Figure 4.3 : Eccentricity - Load with FEM model

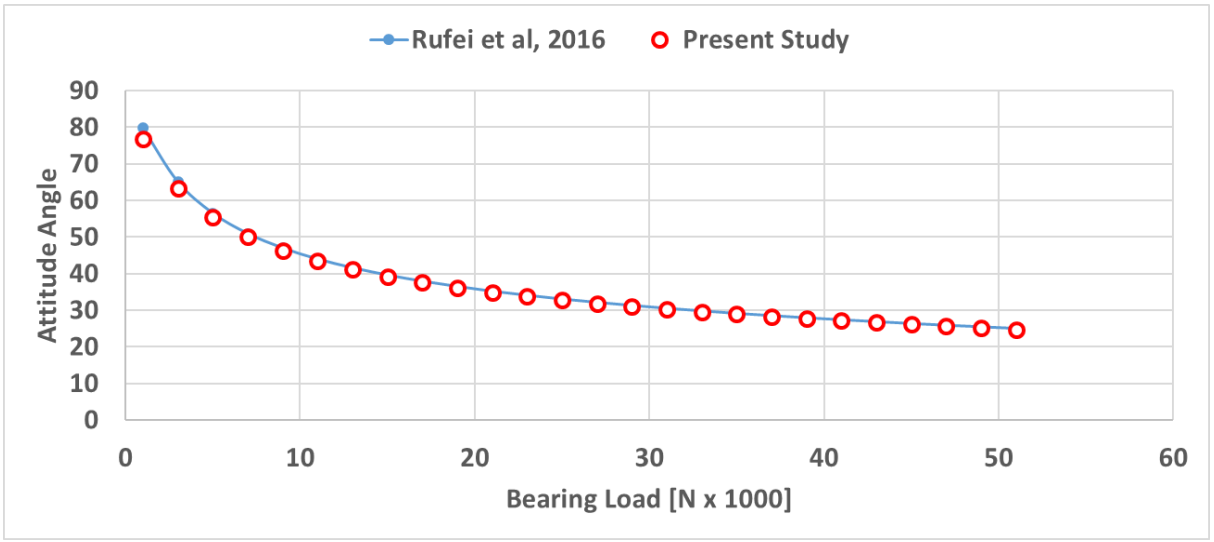

Figure 4.4 : Attitude Angle - Load with FEM Model

In [25], an elasto-hydrodynamic lubrication (EHL) model of journal bearings is established, with the oil film pressure obtained by the finite difference method, and the deformation of bearing calculated by four different numerical methods, i.e. the direct finite element method (DFEM), influence coefficient method (ICM), fast-Fourier transform method (FFTM) and direct Boussinesq method (DBM). In the following figures, we can see the comparison of the proposed EHL model with the corresponding EHL model of the paper based on DFEM. The first plots show the variation of maximum fluid film pressure, minimum film thickness and maximum displacement with eccentricity ratio. The next plots are based on a fixed eccentricity ratio equal to 0.5 and the above parameters are calculated for varying rotational speed, L/D ratios and lubricant viscosity. We observe that there is a good agreement between the proposed model and [25].

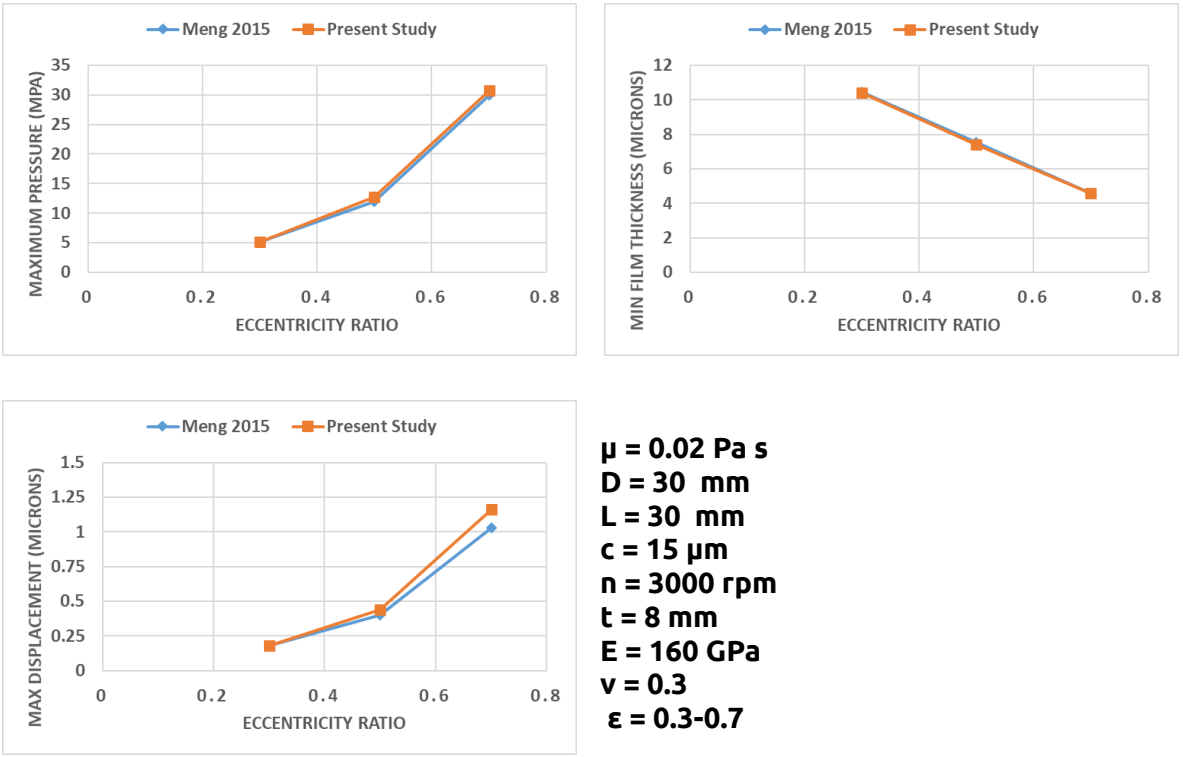

Figure 4.5 : Operational Parameters - Eccentricity ratio

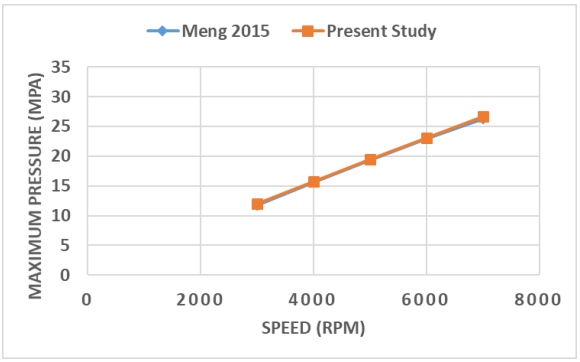

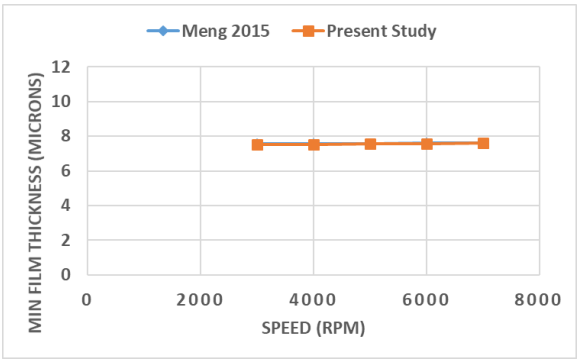

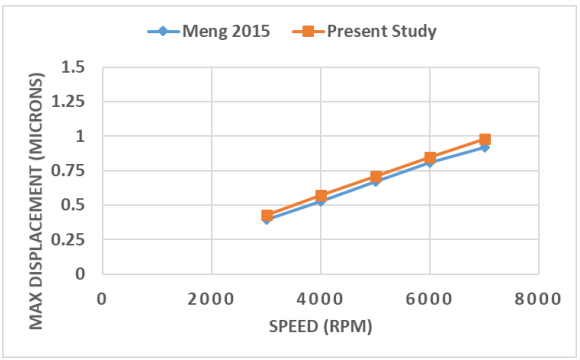

μ = 0.02 Pa s
D = 30 mm
L = 30 mm
c = 15 μm
n = 3000 - 7000 rpm
t = 8 mm
E = 160 GPa
v = 0.3
ε = 0.5

Figure 4.6 : Operational Parameters - speed

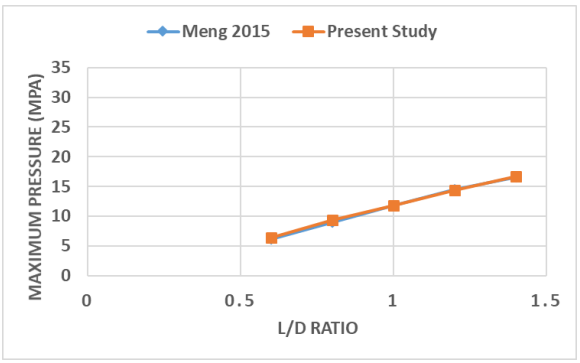

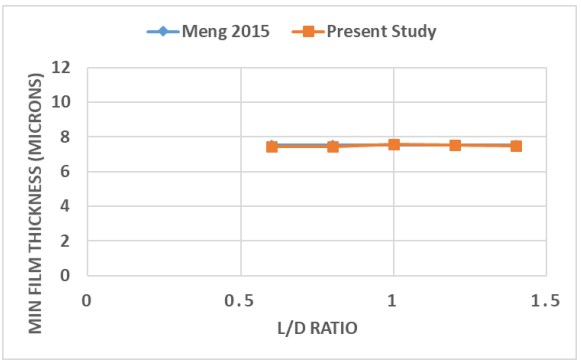

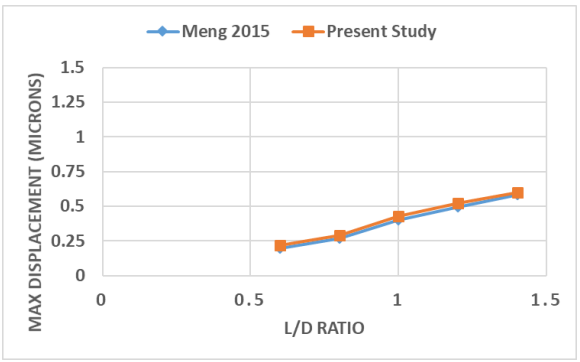

μ = 0.02 Pa s
L/D = 0.6 - 1.4
c = 15 μm
n = 3000 rpm
t = 8 mm
E = 160 GPa
v = 0.3
ε = 0.5

Figure 4.7 : Operational Parameters - L/D ratio

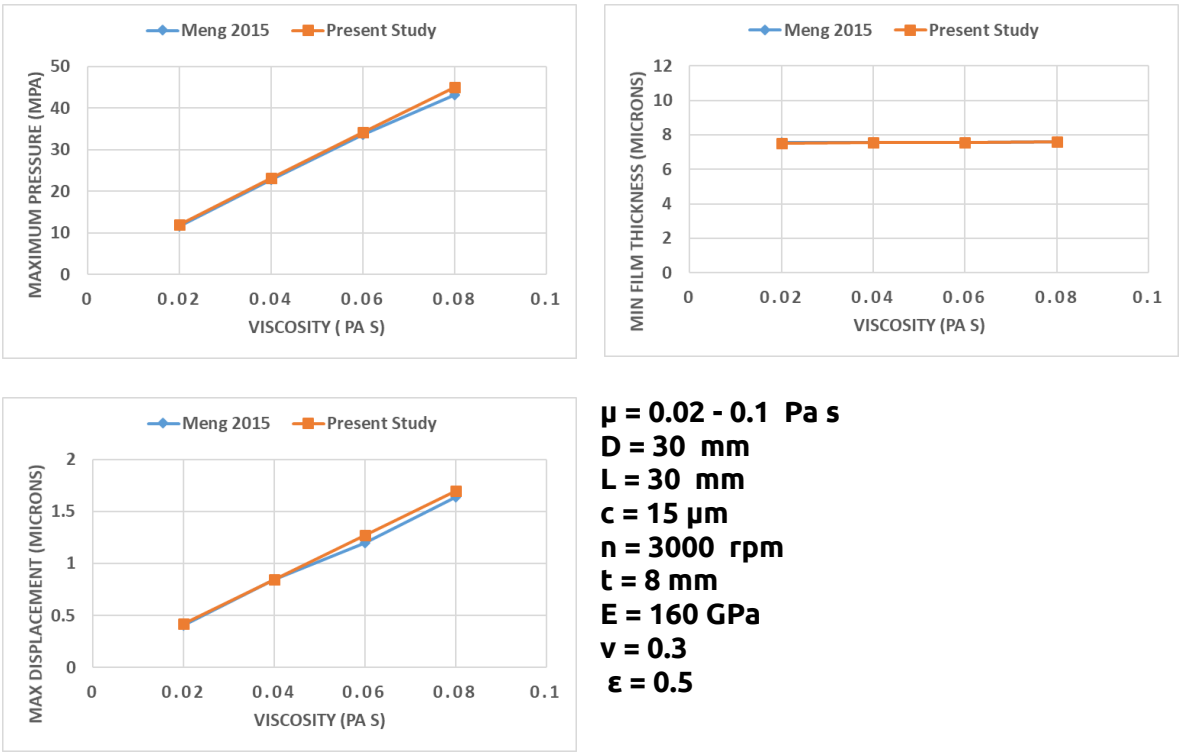

Figure 4.8 : Operational Parameters - viscosity

The present model is also in agreement with [38].

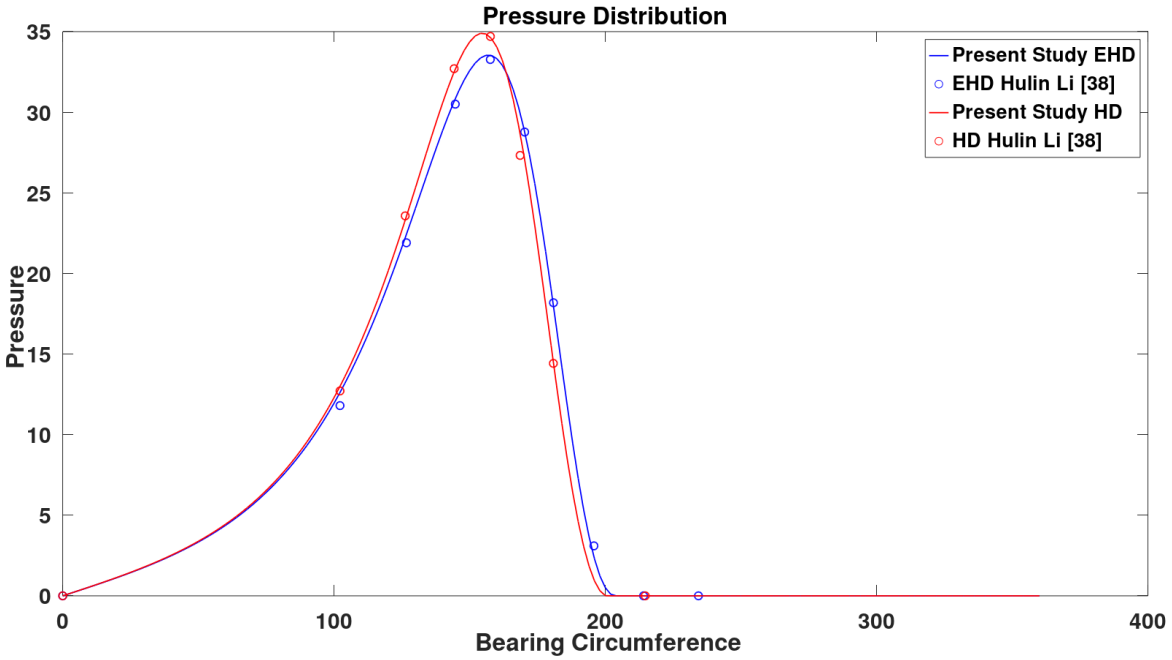

Figure 4.9 : Pressure distribution with the present model and with [38]

4.2 Influence Of Bush Depth

In this Chapter, the influence of the bearing's bush thickness on the accuracy of the predicted elastic deformations is investigated for the two models (Winkler and FEM model).
The geometric and operating parameters are the same as in chapter 4.1 and bush depth takes values for 1 mm, 3 mm and 5 mm. The following plots show the deviation of maximum displacement between the Winkler and FEM model as the bush depth increases.

4.2.1 Oil lubricated bearing

For bush thickness 1 mm:

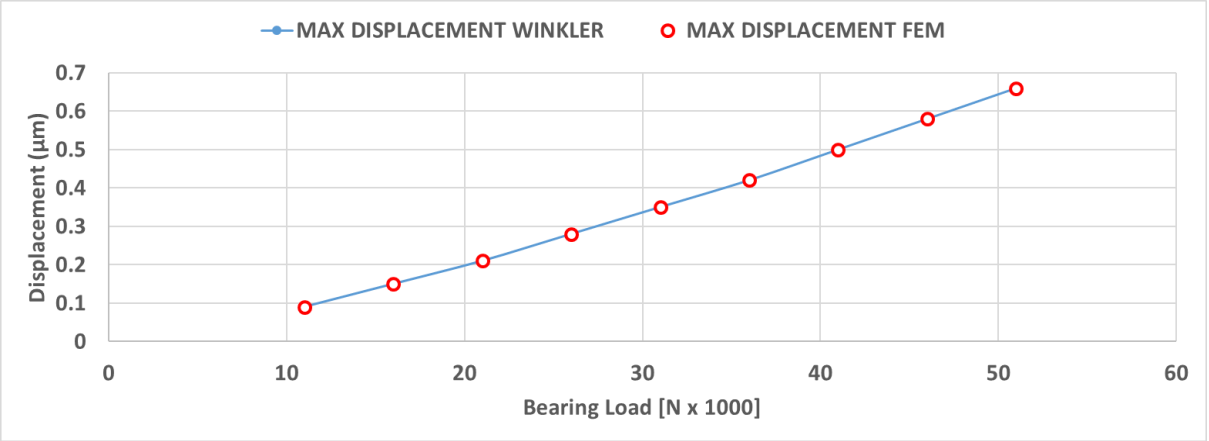

Figure 4.10 : Max displacement - Load for bush thickness 1mm

We can observe that for bush depth 1 mm the two models are in perfect agreement.

For bush thickness 3 mm:

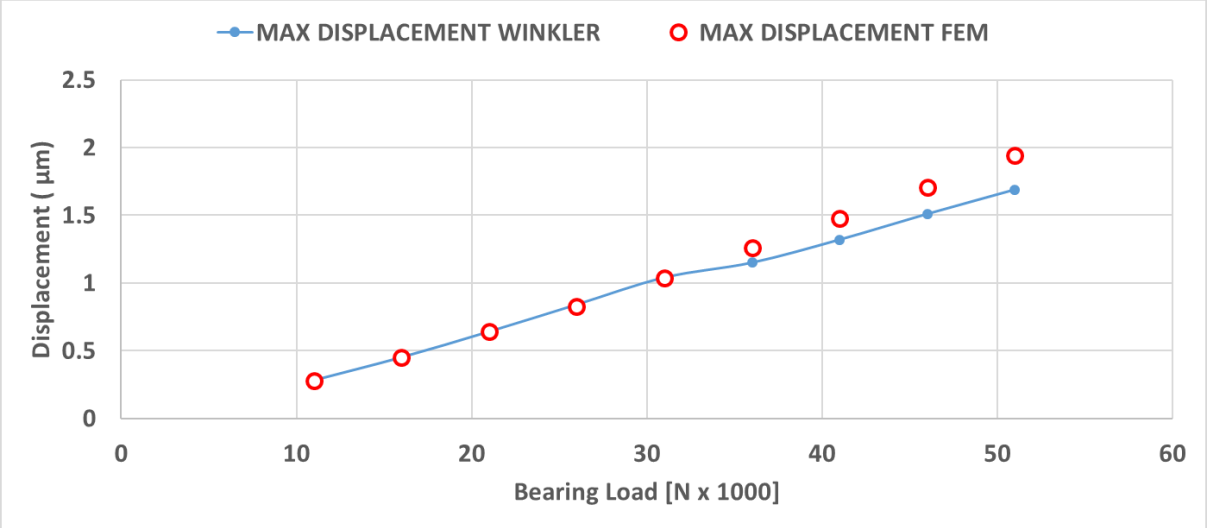

Figure 4.11 : Max displacement - Load for bush thickness 3mm

We can observe that there is a good agreement for the lower loads as in the previous case, but as the load increases there is a deviation between the two models with max error being 14.8%. The Winkler model starts to underestimate the elastic displacements.

For bush thickness 5mm:

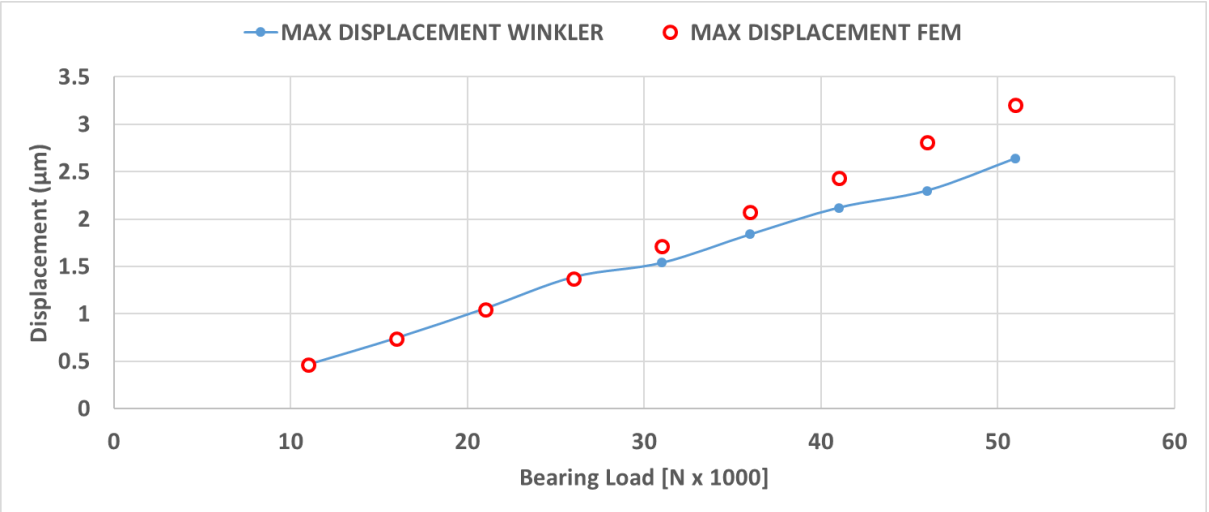

Figure 4.12 : Max displacement - Load for bush thickness 5 mm

We can observe that the deviation between Winkler and FEM is clearly more significant when the bush thickness increases. In the last Figure , for low loads the error is 1-2 % but as the load increases it becomes 22%.

4.2.2 Water Lubricated Bearing

Water lubricated bearings are usually made of polymers, so they are quite more flexible than the previous bearing, meaning that they have a much lower modulus of elasticity. In the present analysis we use the geometric parameters from [18].

- ***Bearing Diameter*** ***D = 446.02 mm***
- ***Bearing Length*** ***L = 890 mm***
- ***Radial Clearance*** ***C = 0.5 mm***
- ***Rotational Speed*** ***N = 100 rpm***
- ***Modulus of Elasticity*** ***E = 600 MPa***
- ***Poisson's Ratio*** ***v = 0.45***
- ***Lubricant viscosity*** ***$\eta = 0.001\ Pa \times s$***
- ***Bush Thickness*** ***t =30,40,50 mm***
- ***Grid*** ***151(Circumference) x 81(Length) x 8(thickness)***

The Load will vary from 5KN to 30KN with the increment of 5 KN. The next plots contain the max displacement predicted by each model in the y axis and the bearing load in the x axis.

<u>For bush thickness 30mm:</u>

Figure 4.13 : Max displacement - Load for bush thickness 30 mm

We can see that in this case where the bush is flexible and the deformations larger than the previous cases, the Winkler model loses its accuracy and as the Load increases this phenomenon is more evident with the error increasing, reaching its maximum value 48.25% at the highest load 30KN.

For bush thickness 40mm:

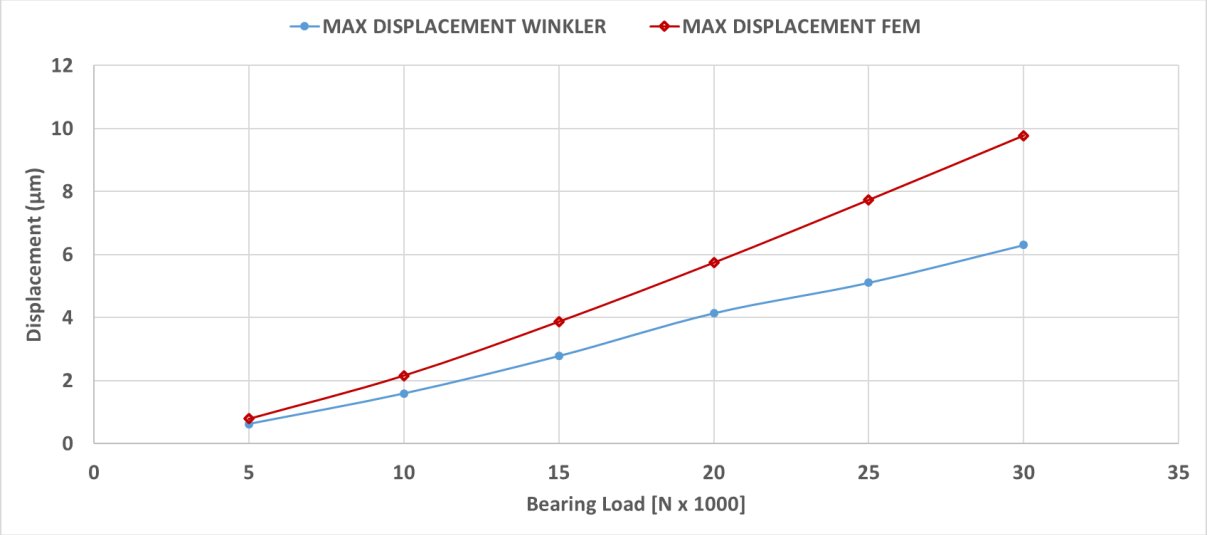

Figure 4.14 : Max displacement - Load for bush thickness 40 mm

For bush thickness 50mm:

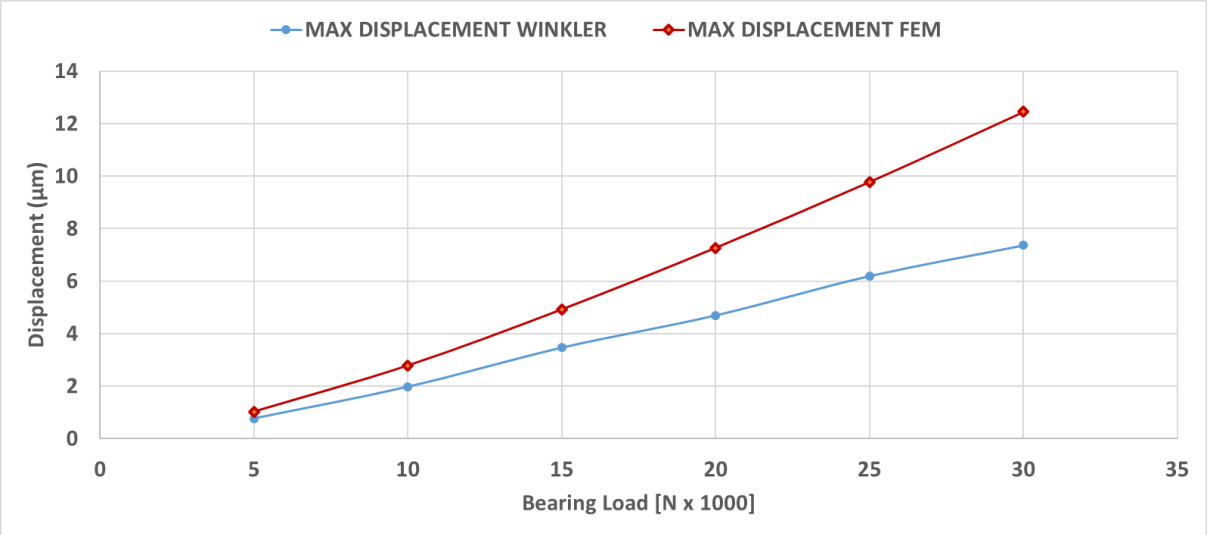

Figure 4.15 : Max displacement - Load for bush thickness 50 mm

In the last plots, we can conclude that the bigger the deflections, the less the accuracy of the Winkler model. The same applies for the increase of bush thickness. For thickness 30 mm the maximum error is 48.25%, for 40 mm is 54.83% and for 50 mm the maximum error becomes 68.93%.

Depending on the above comparison between the two models, it is essential to investigate the causes of the presented error. The Finite Element Method is a reliable method with

great accuracy providing a good mesh and pre-processing. So primarily the investigation is related to Winkler Foundation assumptions, which is a simplified model.

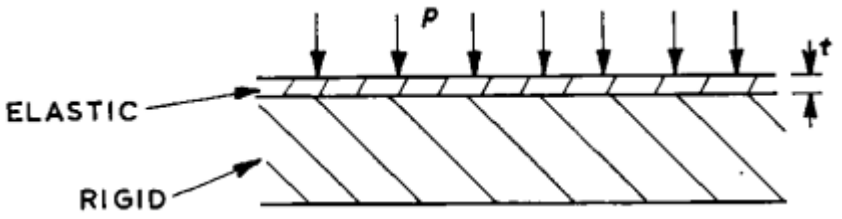

Figure 4.16 : Thin elastic layer inside a rigid housing with uniform pressure[30]

In the problem illustrated in the figure above we will adjust the assumptions for deriving the Winkler Foundation formula just like in [30]. The thickness of the layer is assumed to be thin enough compared to the bearing's dimensions (Length, Radius). With this assumption, the strain components in the axial direction of the bearing vanish. The elastic problem of the thin liner subjected to hydrodynamic pressure can be approximated by a two dimensional plane strain problem. The problem simplifies further because the outer surface of the bearing liner is bonded in a rigid housing and so not allowed to move - making circumferential strain at a point negligible with respect to the radial strain. The radial component of the deformation of the liner at a point can thus be estimated as being proportional to the pressure at that point. With these assumptions it is clear that the model assumes the stresses across the thickness not to vary. If the liner is thick we have a variation of stresses across this direction and we can not ignore the strains across the other two directions (circumferential and axial). In the FEM model the elements of the first layer are not constrained to move in any direction; They are surrounded by the neighboring elements. So if the thickness of the liner is increased or the loads are high, the elements are deformed in all directions. That means that the resistance to vertical displacement is reduced. That explains why the FEM model in this case predicts higher radial displacements.

If we look in equation (39) we can see that the term with the poisson ratio, for typical values of poisson ratio (0.3 - 0.46), is 0.743 - 0.216, which means that this model overestimates stiffness of the liner in the radial directions(due to plain strain conditions). If we take into consideration all the above we can explain why in thick liners or high loads Winkler underestimates the deflections, which is in agreement with [36] and [37].

Another important feature about the thin liner model or Winkler model is its sensitivity to poisson ratio which is also stated in [30], [35] and [37]. As we deduced from the figures of the water lubricated bearing case, the deviation in maximum displacement between the two models is intense. Except for their higher thickness and flexibility, it is attributed to the high poisson ratio that this kind of materials have. As we will see later, as the poisson ratio increases, the Winkler model predicts not only inaccurate results, but is also unable to capture a specific behavior that almost incompressible materials present.

4.3 EHD Analysis Of An Oil Lubricated Bearing

The results of an EHD study of the journal bearing from chapter 4.1 are presented below for Load 51KN.

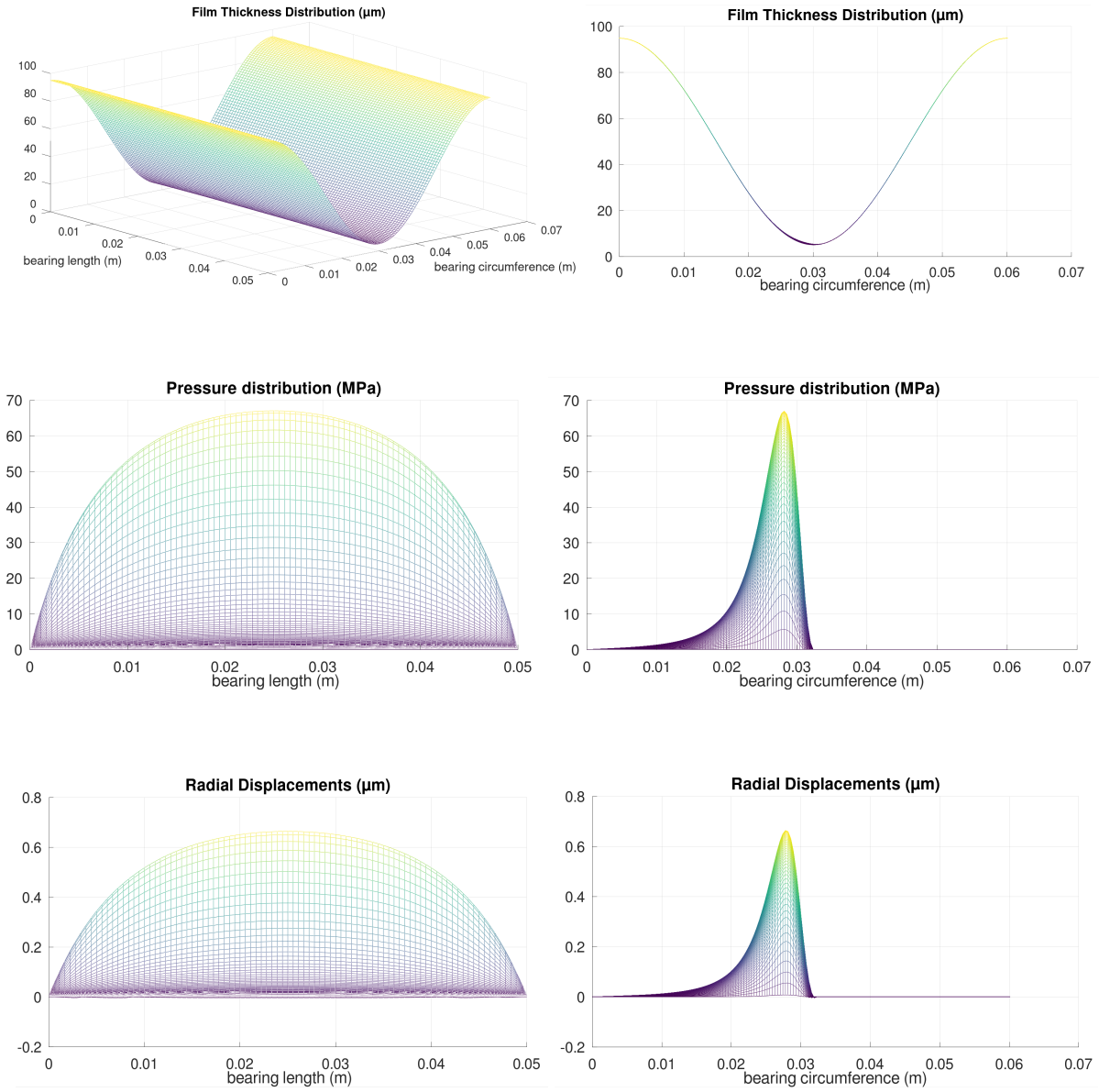

Figure 4.17 : EHD study of a journal bearing

The first two figures refer to film thickness distribution in μm, the middle ones to pressure distribution in MPa and the last two to the elastic deformations of the bearing in μm. The basic simulation results are presented below:

Sommerfeld number = **0.0212825**
Eccentricity Ratio = ***0.89834***
Attitude Angle = ***24.7435 deg***
Maximum Pressure = ***66.89 MPa***
Minimum Film Thickness= ***5.09 μm***
Inlet Flow Rate = ***1.1498 lt/min***
Side Flow Rate = ***1.063 lt/min***
Power Loss = ***0.9 KW***
Friction Torque = ***0.00287 KNm***

As expected, in the EHD study the maximum pressure decreases to 66.89 from 71.36 MPa (HD study) and the minimum film thickness increases to 5.09 μm from 5.06 μm (HD study). The differences are minor because in the present study the deformations are low (max deformation 0.67 μm).

It is vital to compare the displacement field of the present model to the corresponding field of the Winkler Model to note any deviations.

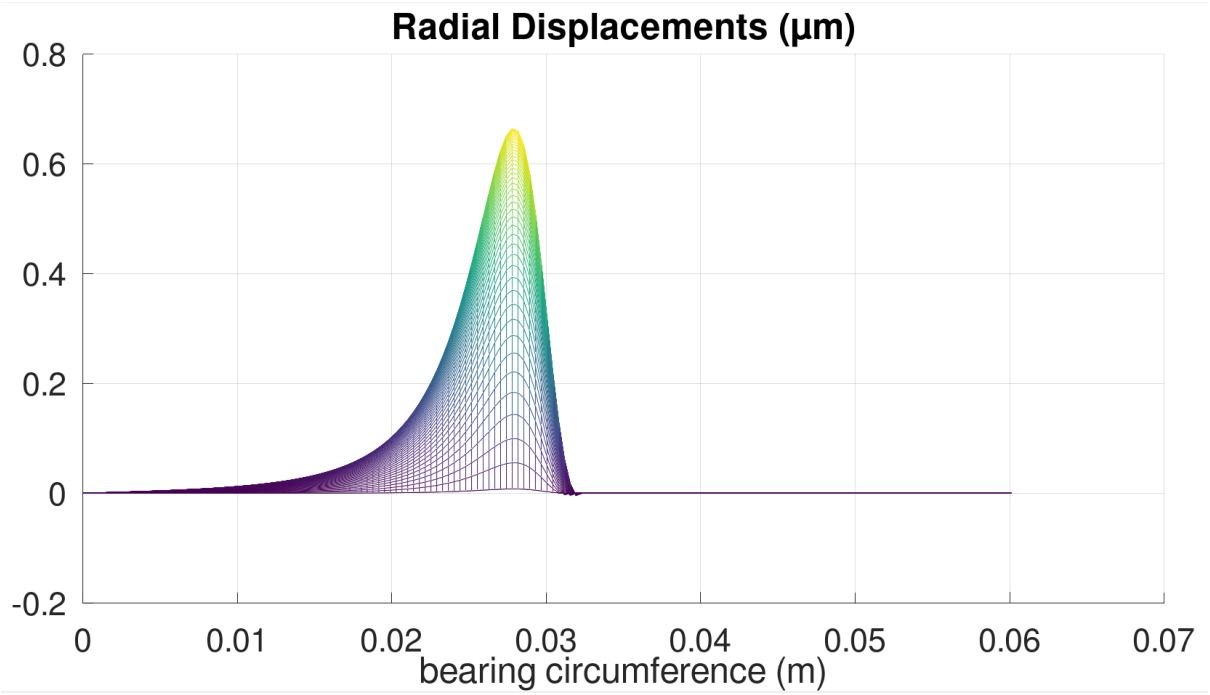

Figure 4.18 : Deformation calculated with FEM Model

In the Winkler Model it is reasonable that the deformation shape is exactly similar to the pressure distribution shape due to their linear relationship. In the coupled FEM model though, there is a "lift" of deformation in the bearing ends. The Winkler Model can not predict this lift because there are no nodal forces there, while FEM can capture the interaction between nodes due to the stress field and can give a more accurate result.

4.4 EHD Analysis Of A Water Lubricated Bearing

The results of the EHD study of the journal bearing from chapter 4.2.2 is presented below, for Load 30 KN and bush thickness 40 mm.

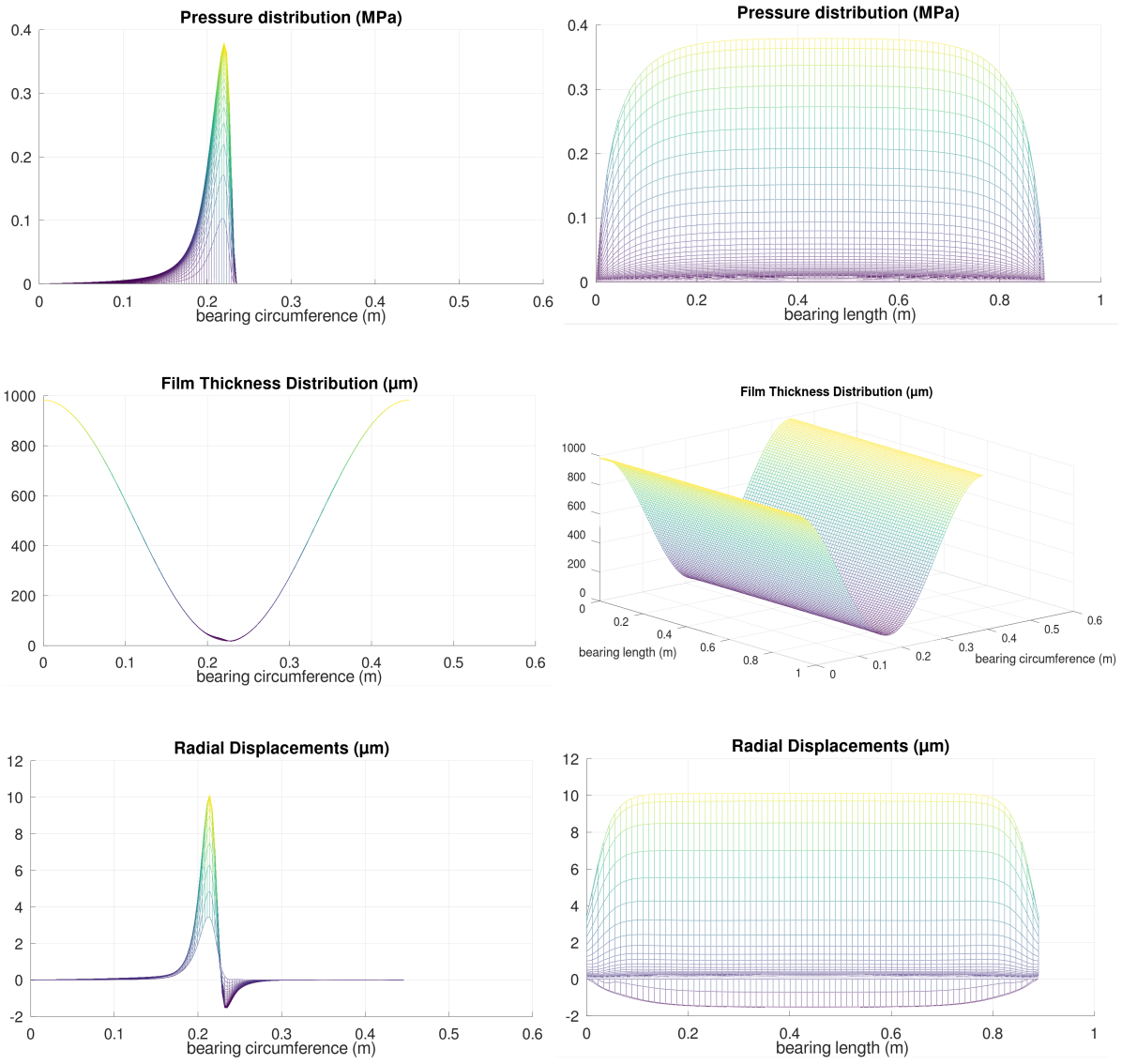

Figure 4.19 : EHD analysis of a water lubricated bearing

The first two figures refer to pressure distribution in MPa, the middle ones to film thickness distribution in μm, and the last two to the elastic deformations of the bearing in μm. The basic simulation results are presented below:

Sommerfeld number =	***0.00438713***
Eccentricity Ratio =	***0.9662***
Attitude Angle =	***14.8475 deg***
Maximum Pressure =	***0.37 MPa***
Minimum Film Thickness=	***17.88 μm***
Inlet Flow Rate =	***29.036 lt/min***
Side Flow Rate =	***27.5799 lt/min***
Power Loss =	***0.0698297 kW***
Friction Torque =	***0.006667 kNm***

4.4.1 Comparison With HD Study

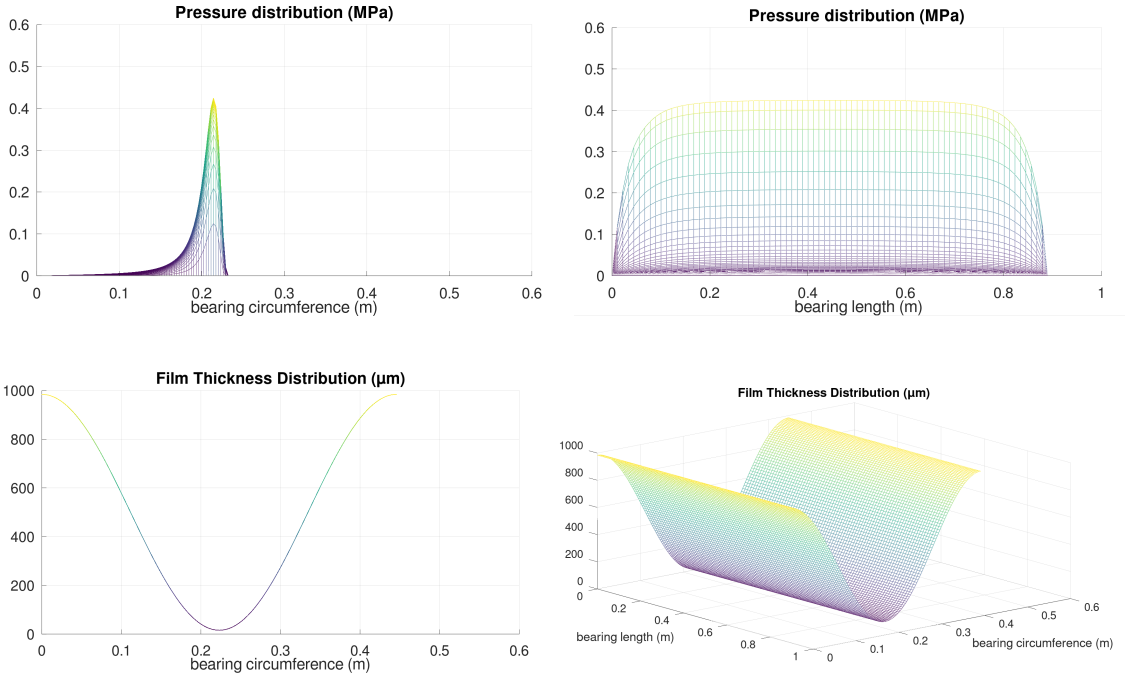

Figure 4.20 : HD study of a water lubricated bearing for comparison

The basic differences between the EHD and HD analysis is observed in the pressure and film thickness. The maximum pressure in EHD study is decreased from 0.42 MPa to 0.37 MPa, while the minimum film thickness increases to 17.88 μm from 15.5 μm. As stated in [34], this was anticipated since elastic deformation creates more pressurized space for the lubricant at the loaded side of the bearing. This in terms causes the pressure to be more evenly distributed and therefore to have a lower maximum value.

Another interesting feature is that the radial displacements in EHD study can be negative especially after the positive pressure zone, or cavitation zone as mentioned in [32]. As stated in chapter 4.2.2, this is a special behavior that is observed for nearly incompressible materials. In [35], Lahmar stated that the thin liner model should be used for thin liners and for liners that are compressible with a poisson ratio close to 0.3. For elastomers that exhibit high poisson ratios (close to 0.5) this model can not take into account the incompressibility of these materials which can be observed by the negative values of displacement in the divergent area of the film (when pressure drops). This behavior is valid for incompressible materials because when they are compressed by pressure, they tend to expand laterally, redistributing their volume to other directions. This explains why the displacements can be in the opposite direction of the lubricant film force. In the following figures this phenomenon will be presented for different values of poisson ratio of the bearing of chapter 4.2.2:

For Load 25KN and bush thickness 30mm the poisson ratio will take values 0.3, 0.35, 0.4 and 0.45:

For poisson ratio 0.3:

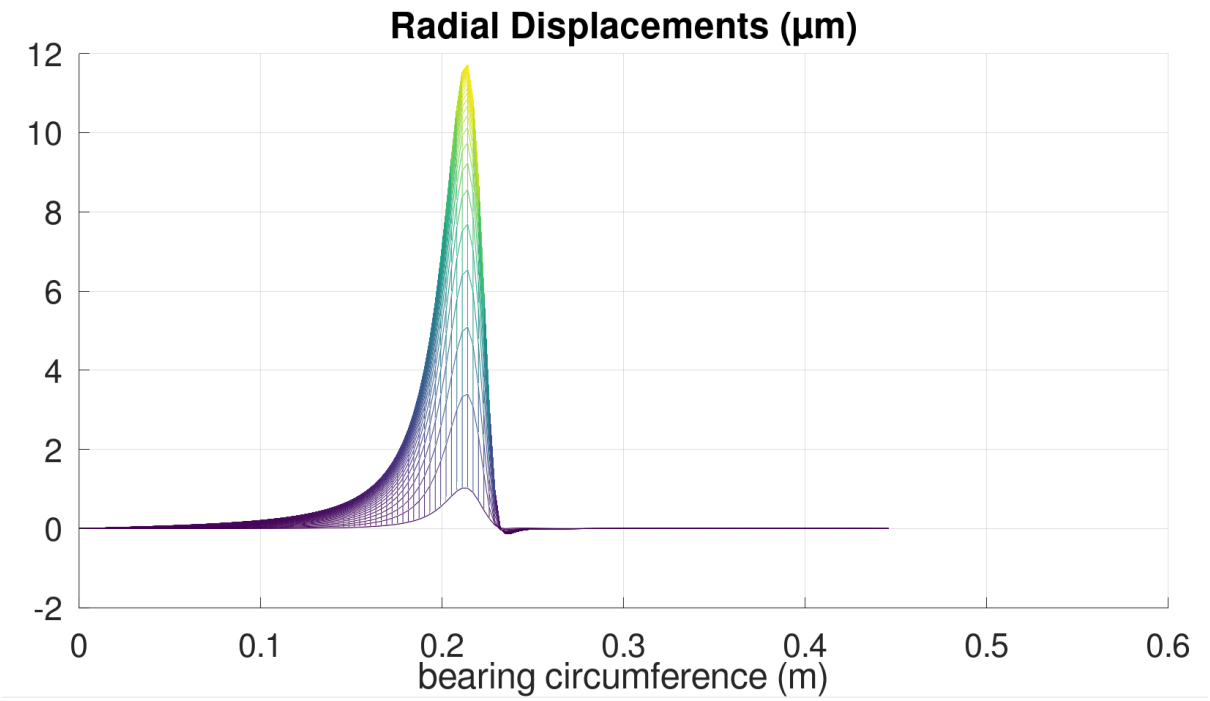

Figure 4.21 : Radial displacements for poisson ratio 0.3

For poisson ratio 0.35:

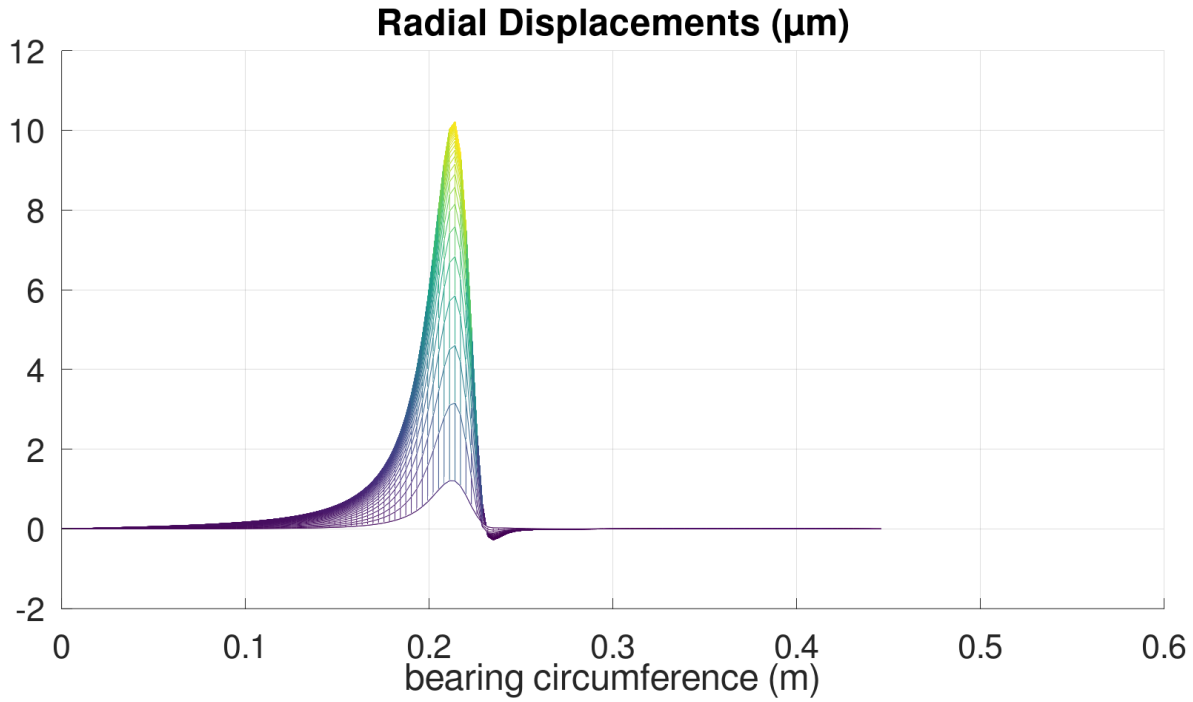

Figure 4.22 : Radial displacements for poisson ratio 0.35

For poisson ratio 0.4:

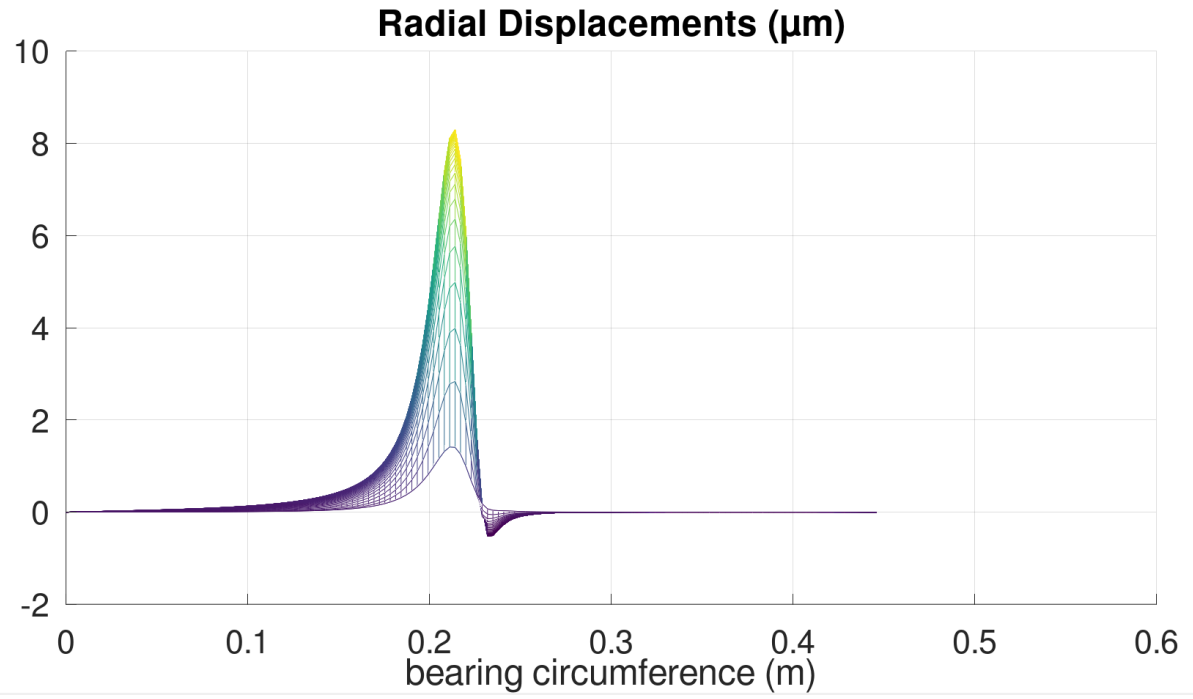

Figure 4.23 : Radial displacements for poisson ratio 0.4

For poisson ratio 0.45:

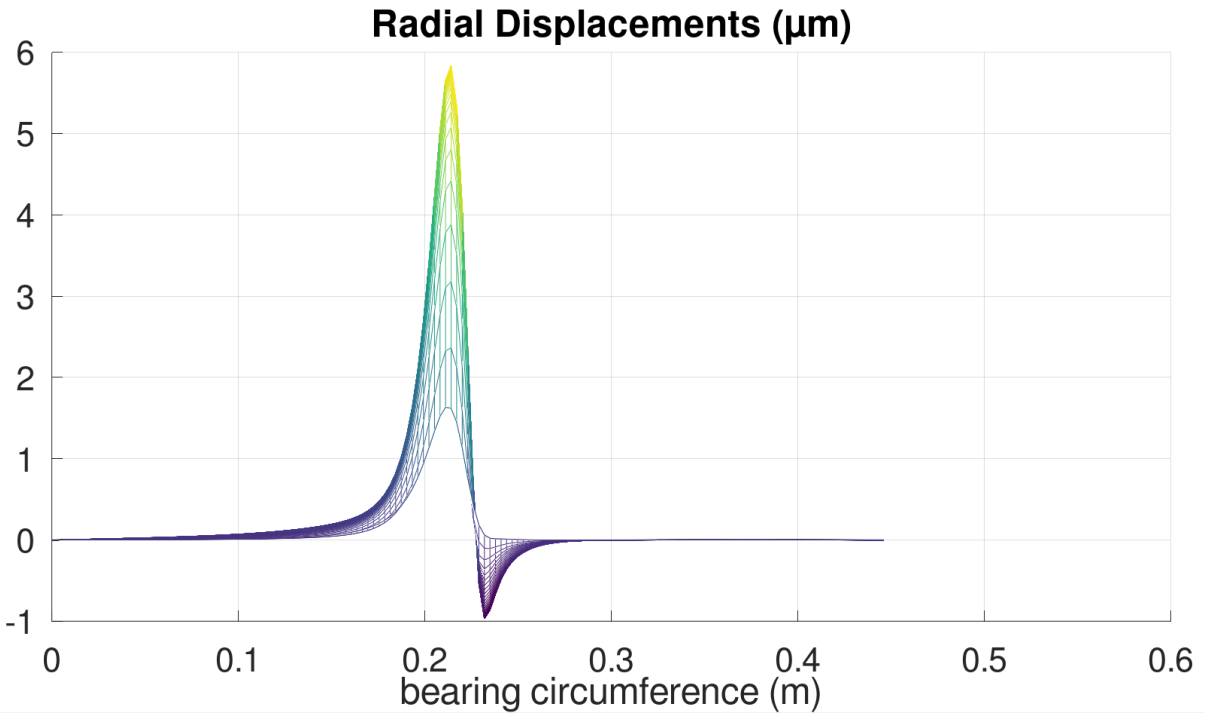

Figure 4.24 : Radial displacements for poisson ratio 0.45

4.5 Effect Of Modulus Of Elasticity

In the present chapter the effect of Elasticity Modulus on journal bearing performance is going to be investigated for the case of an oil and a water lubricated bearing.

4.5.1 Oil Lubricated Bearing

The oil lubricated bearing from chapter 4.1 will be studied under Load 51 KN and Elasticity Modulus varying from 40000 MPa to 80000 MPa. The following figures present the effect of Elasticity Modulus on Maximum pressure, displacement and Minimum film thickness :

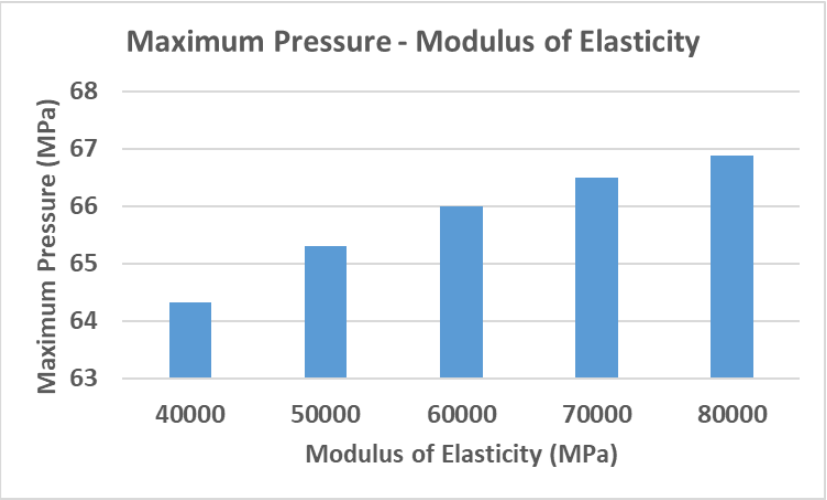

Figure 4.25 : Maximum Pressure - Modulus Of Elasticity

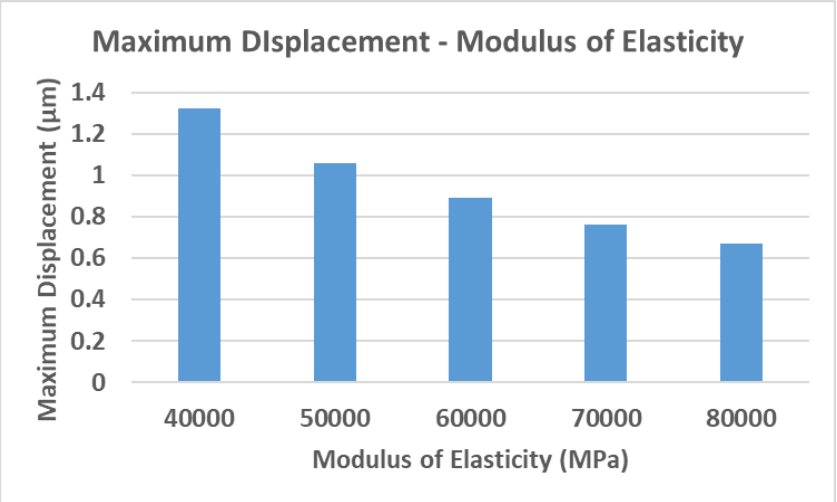

Figure 4.26 : Maximum Displacement - Modulus Of Elasticity

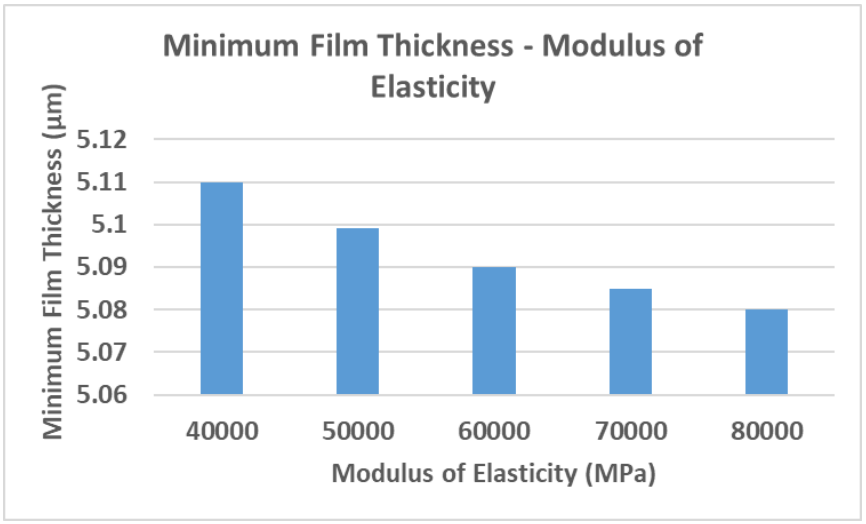

Figure 4.27 : Minimum Film Thickness - Modulus of Elasticity

4.5.2 Water Lubricated Bearing

The water lubricated bearing from chapter 4.2.2 will be studied under Load 20 KN bush thickness 40 mm and Elasticity Modulus varying from 600 MPa to 1400 MPa. The following figures present the effect of Elasticity Modulus on Maximum pressure, displacement and Minimum film thickness :

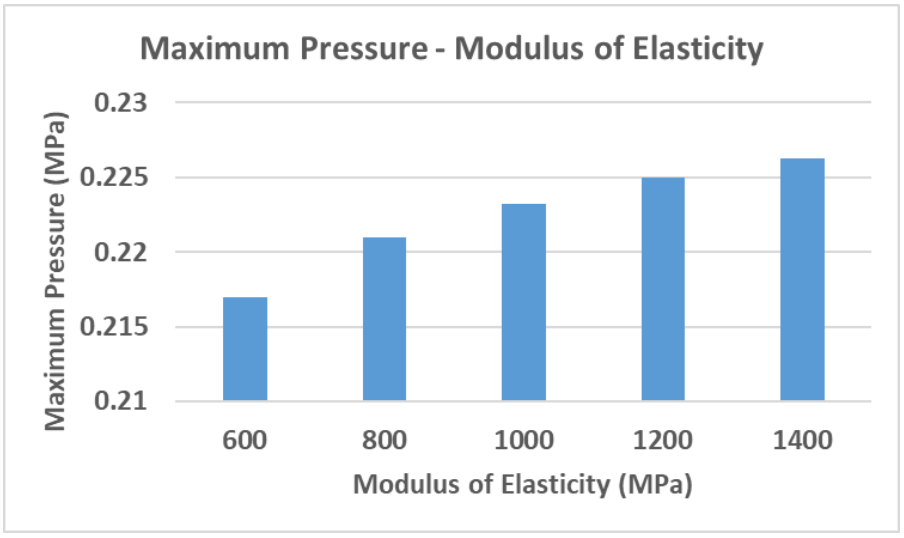

Figure 4.28 : Maximum Pressure - Modulus Of Elasticity

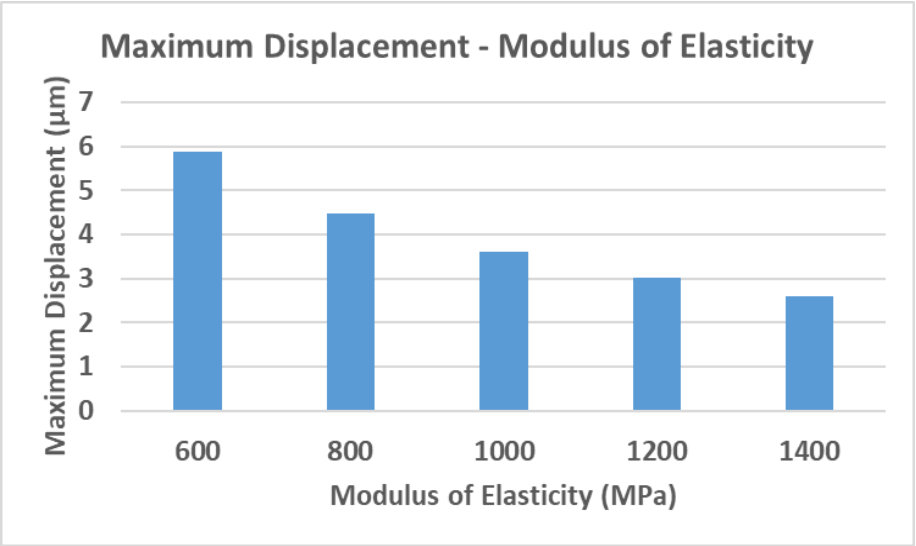

Figure 4.29 : Maximum Displacement - Modulus Of Elasticity

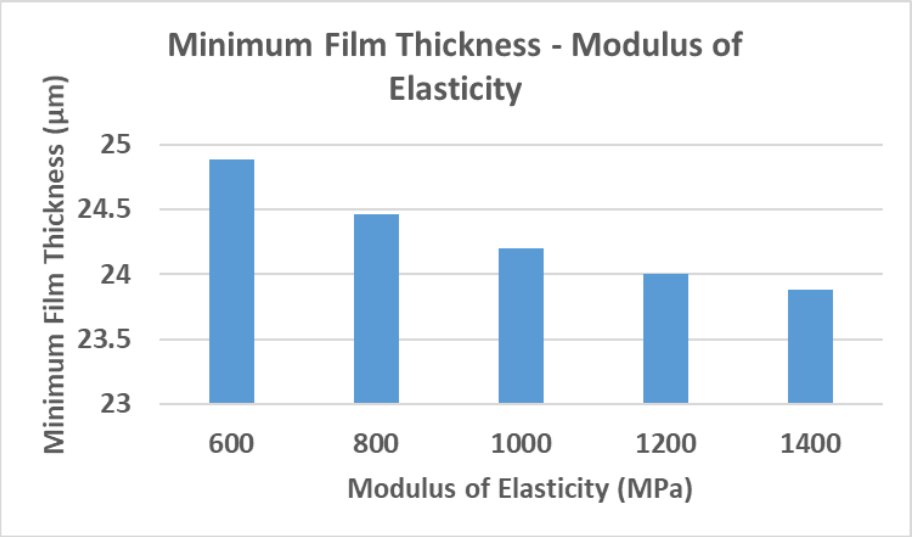

Figure 4.30 : Minimum Film Thickness - Modulus of Elasticity

As expected, in both cases the increase of elasticity modulus increases the stiffness of the bearing bush, so the displacements decrease. This has an impact on minimum film thickness which decreases and consequently the maximum pressure increases.

4.6 EHD Of Misaligned Journal Bearings

The geometric and operational characteristics of the oil lubricated bearing are the same as in chapter 4.1 for Load 21 KN and misalignment angles ψx = 0.1 and 0.2. The water lubricated bearing is the same as 4.2.2 with bush thickness 40 mm and load 5 KN.

4.6.1 Case For ψx = 0.1 (Oil Lubricated Bearing)

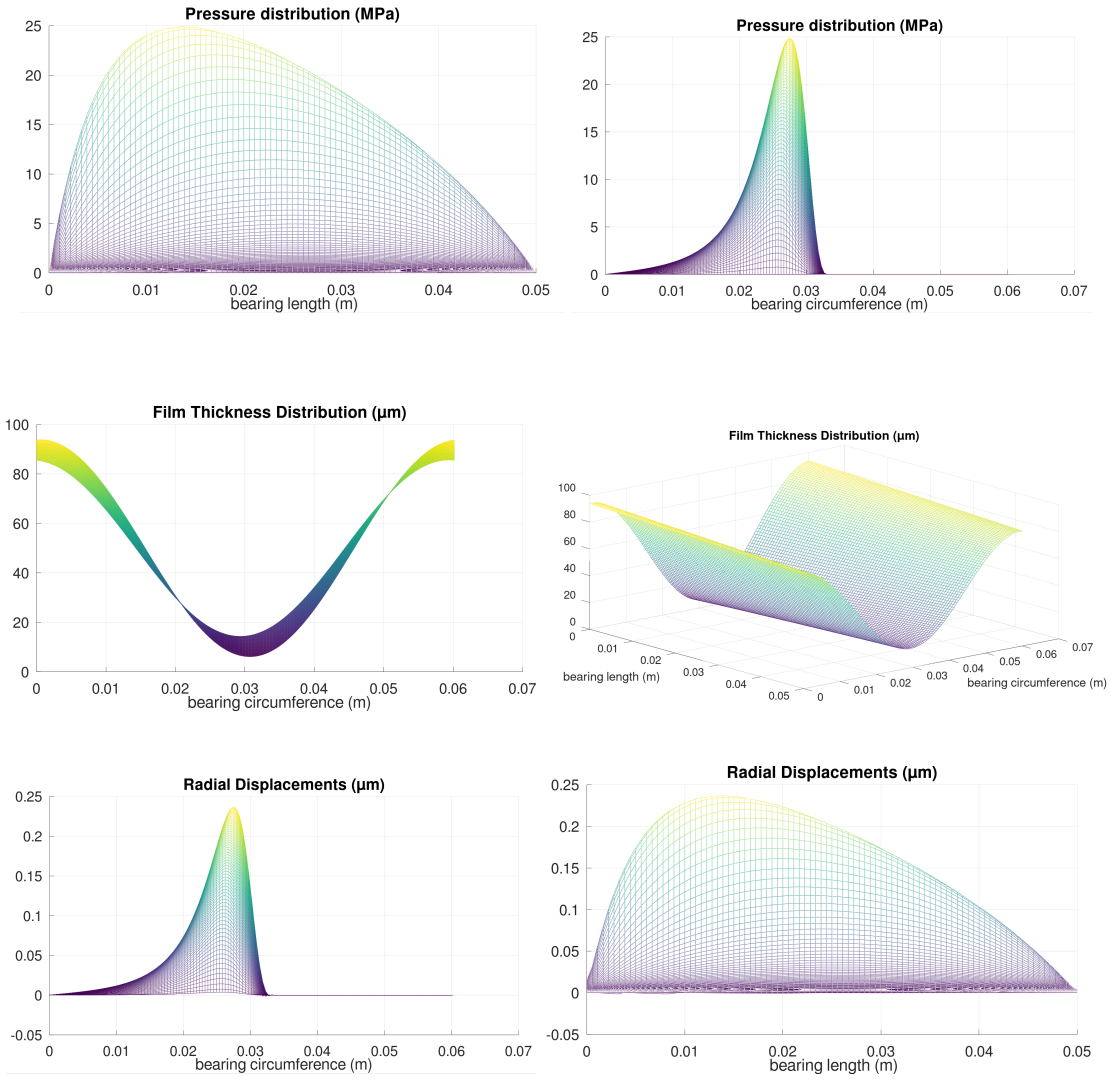

Figure 4.31 : EHD study with misalignment ψx= 0.1 (oil)

The first two figures refer to pressure distribution in MPa, the middle ones to film thickness distribution in μm and the last two to the elastic deformations of the bearing in μm. The basic simulation results are presented below:

Sommerfeld number =	***0.0516861***
Eccentricity Ratio =	***0.79237***
Attitude Angle =	***34.1241 deg***
Maximum Pressure =	***24.65 MPa***
Minimum Film Thickness=	***6.1 µm***
Inlet Flow Rate =	***1.10672 lt/min***
Side Flow Rate =	***0.941205 lt/min***
Power Loss =	***0.638162 kW***
Friction Torque =	***0.00203133 kNm***

4.6.2 Case For ψx = 0.2 (Oil Lubricated Bearing)

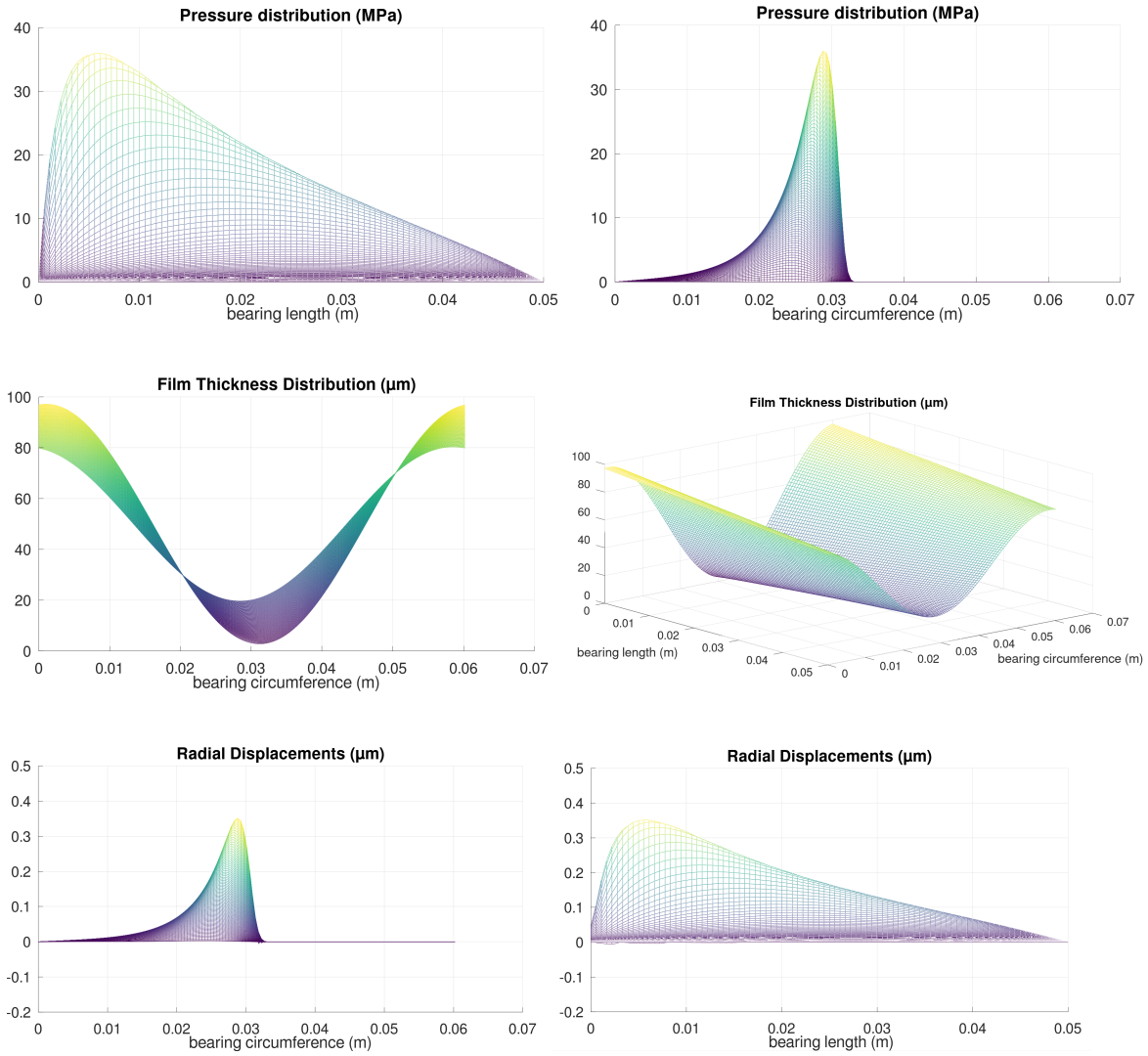

Figure 4.32 : EHD study with misalignment ψx= 0.2 (oil)

The first two figures refer to pressure distribution in MPa,the middle ones to film thickness distribution in μm, and the last two to the elastic deformations of the bearing in μm. The basic simulation results are presented below:

Sommerfeld number = ***0.0516861***
Eccentricity Ratio = ***0.7674***
Attitude Angle = ***31.65 deg***
Maximum Pressure = ***35.43 MPa***
Minimum Film Thickness= ***2.85 μm***
Inlet Flow Rate = ***1.09572 lt/min***
Side Flow Rate = ***0.910636 lt/min***
Power Loss = ***0.642648 kW***
Friction Torque = ***0.002 kNm***

We observe that as misalignment angle increases, it significantly affects the maximum pressure value (increase from 24.65 MPa to 35.43 MPa), while eccentricity ratio and minimum film thickness decrease as expected. An increase in misalignment angle affects the deformation field greatly as well, with maximum displacement increasing from 0.24 μm to 0.35 μm.

4.6.3 Case For ψx = 0.1 (Water Lubricated Bearing)

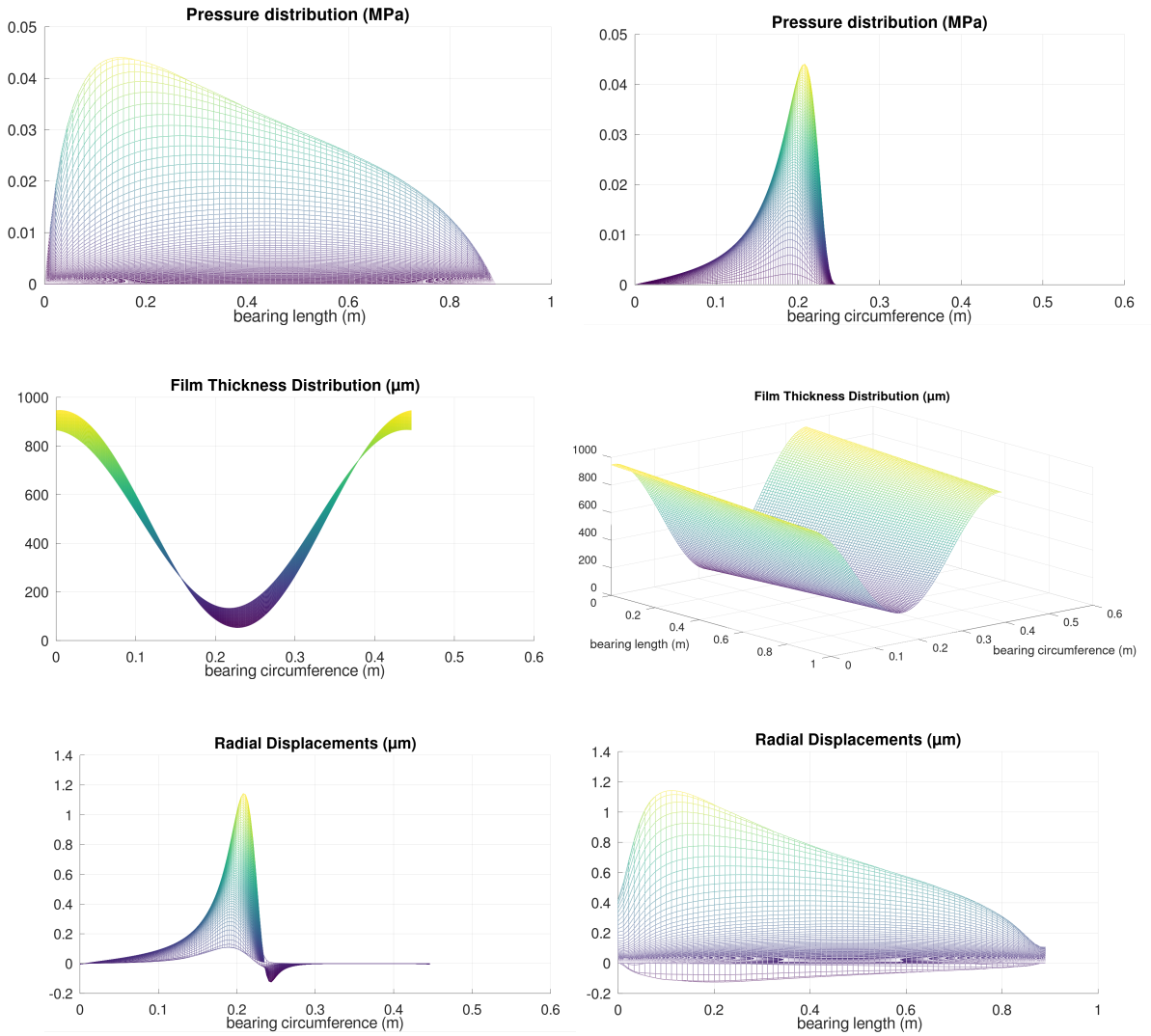

Figure 4.33 : EHD study with misalignment ψx= 0.1 (water)

The first two figures refer to pressure distribution in MPa,the middle ones to film thickness distribution in μm, and the last two to the elastic deformations of the bearing in μm. The basic simulation results are presented below:

Sommerfeld number =	***0.0263228***
Eccentricity Ratio =	***0.812488***
Attitude Angle =	***36.531 deg***
Maximum Pressure =	***0.0441 MPa***
Minimum Film Thickness=	***53.17 µm***
Inlet Flow Rate =	***30.816 lt/min***
Side Flow Rate =	***23.8743 lt/min***
Power Loss =	***0.03 kW***
Friction Torque =	***0.002896 kNm***

4.6.4 Case For ψx = 0.2 (Water Lubricated Bearing)

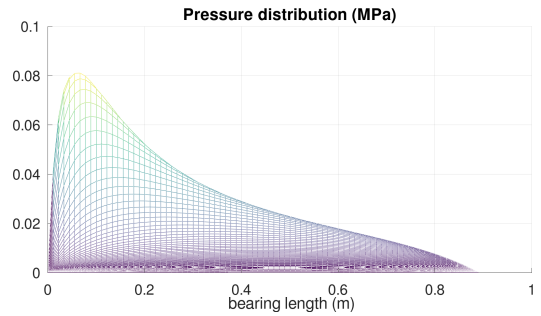

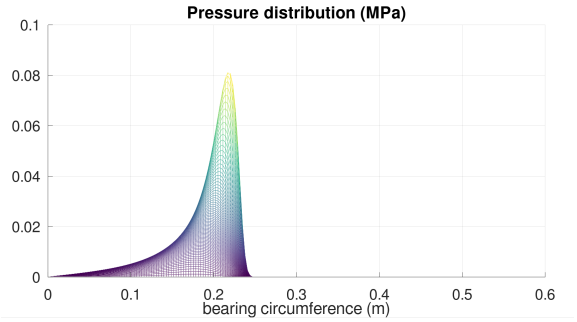

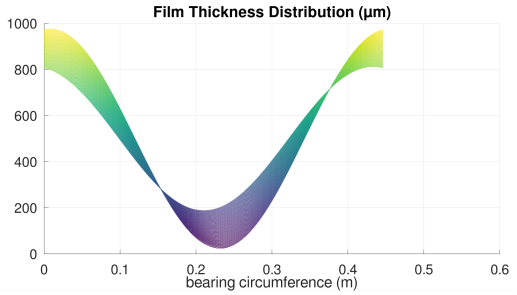

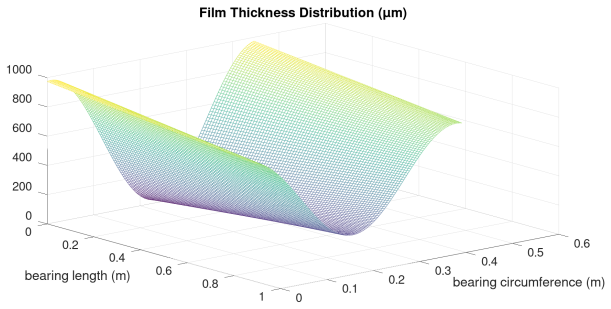

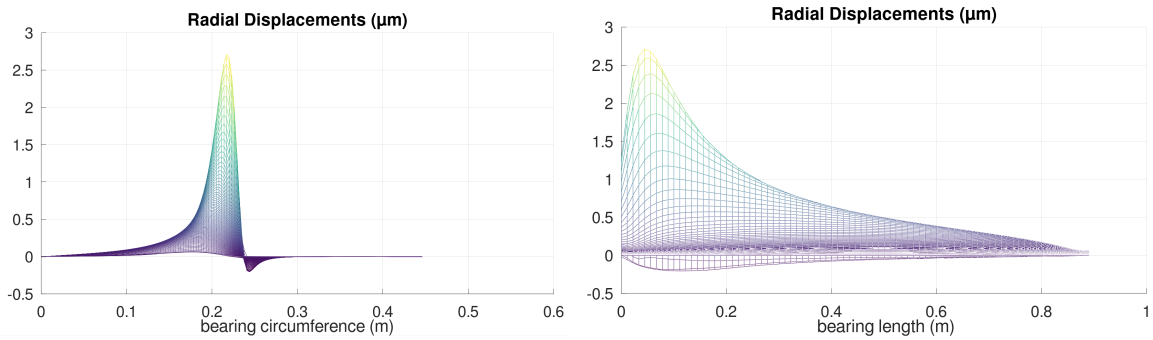

Figure 4.34 : EHD study with misalignment ψx= 0.2 (water)

The first two figures refer to pressure distribution in MPa,the middle ones to film thickness distribution in μm, and the last two to the elastic deformations of the bearing in μm. The basic simulation results are presented below:

Sommerfeld number* = *0.0263228
Eccentricity Ratio* = *0.781
Attitude Angle* = *33.8401 deg
Maximum Pressure* = *0.081 MPa
Minimum Film Thickness*= *23.62 μm
Inlet Flow Rate* = *31.1764 lt/min
Side Flow Rate* = *23.1097 lt/min
Power Loss* = *0.03 kW
Friction Torque* = *0.00287 kNm

It is clear that the effects of the increase of misalignment angle are the same as in the case of the oil lubricated bearing.

4.7 Effect Of Angular Velocity On EHD Study

The effect of angular velocity on Elastohydrodynamic analysis of the bearing in chapter 4.1 is investigated. The performance of the bearing is tested at 1000-6000 RPM and the effect of angular velocity is presented on Eccentricity Ratio, Maximum Pressure, Minimum Film Thickness, Maximum Displacement and Power Loss in the following figures:

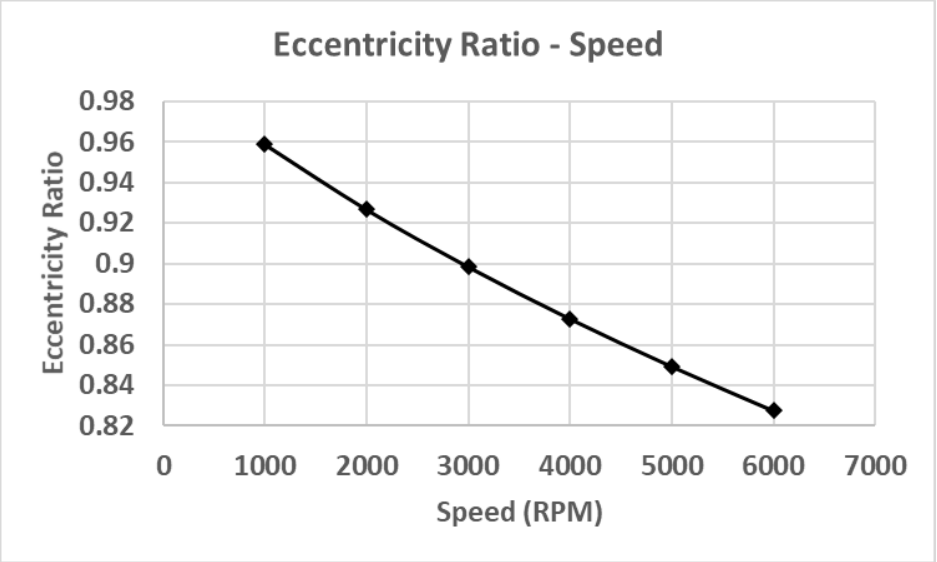

Figure 4.35 : Effect of rotational speed on eccentricity in EHD (oil)

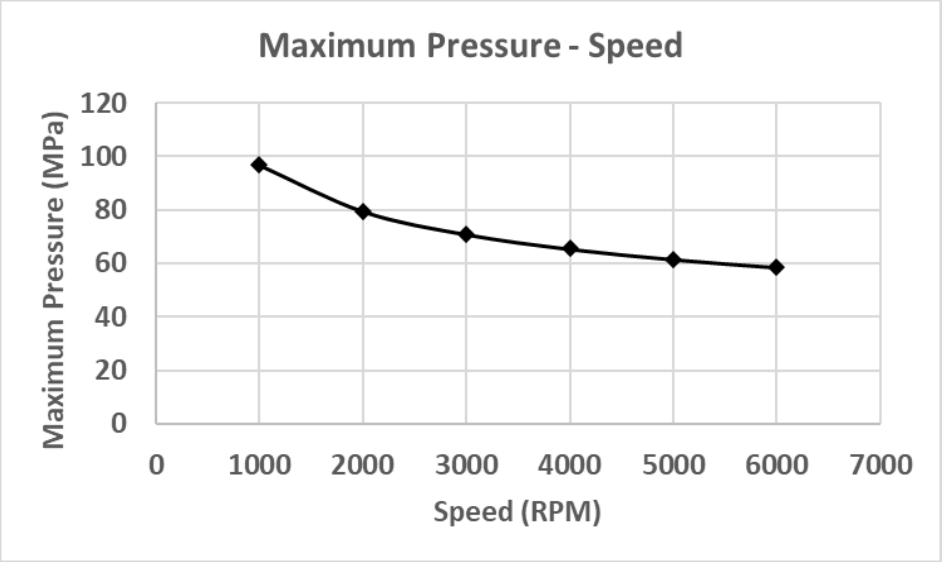

Figure 4.36 : Effect of rotational speed on Maximum Pressure in EHD (oil)

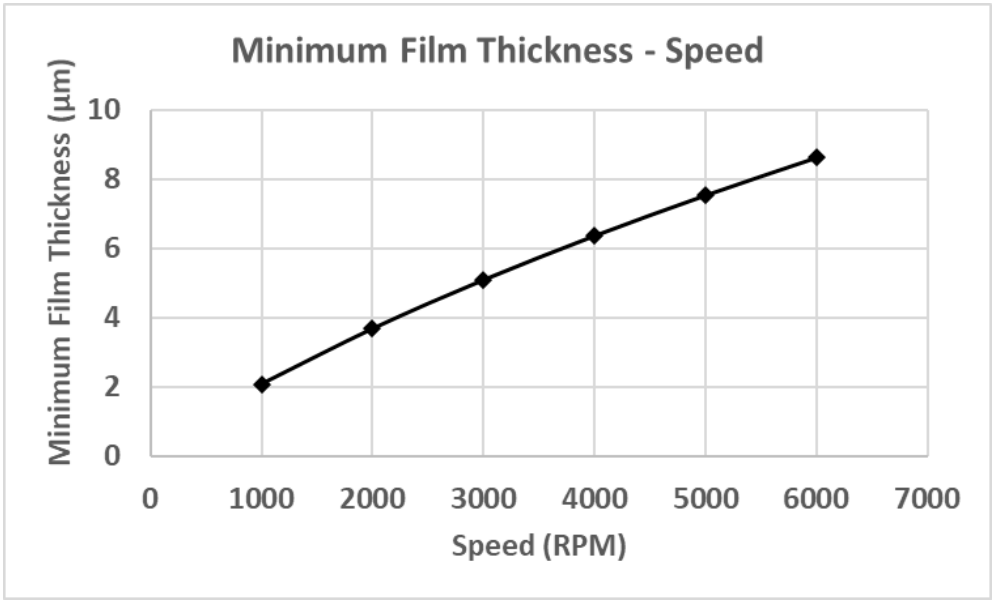

Figure 4.37 : Effect of rotational speed on minimum film thickness in EHD (oil)

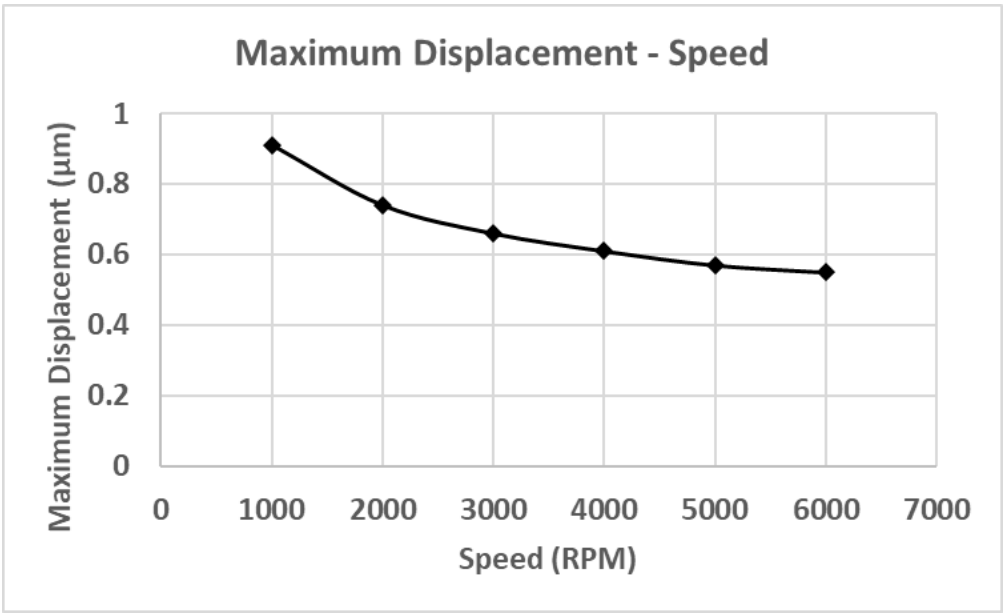

Figure 4.38 : Effect of rotational speed on maximum displacement in EHD (oil)

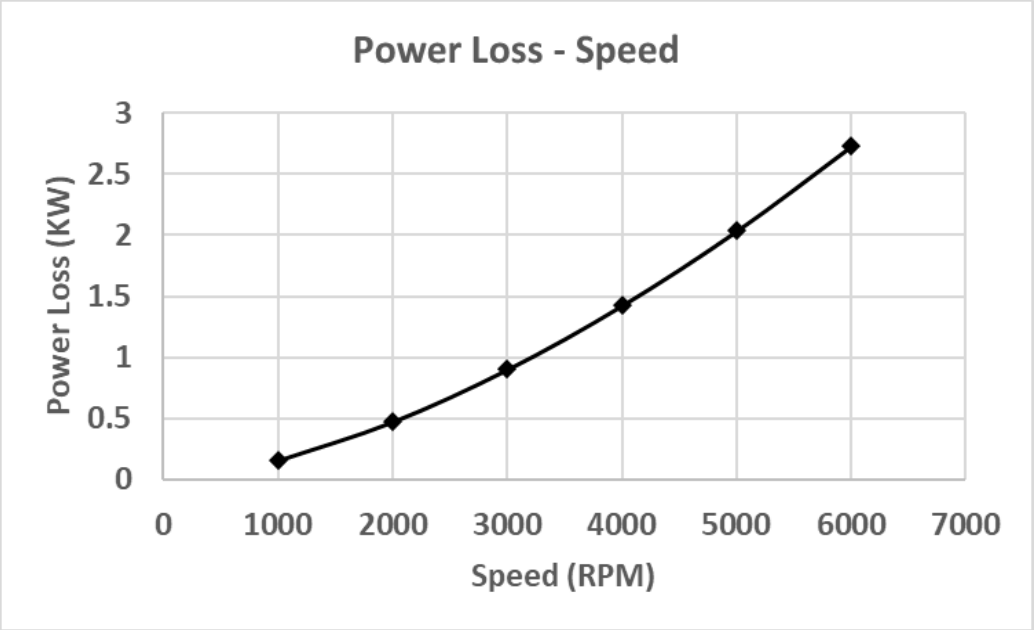

Figure 4.39 : Effect of rotational speed on Power loss in EHD (oil)

As we observe in the figures above, the increase of angular speed decreases eccentricity ratio, maximum pressure and bush maximum displacement, while increases the power losses and minimum film thickness for the same operating Load. As already known[20], in low load conditions the rotational speed has only a little influence on maximum pressure. The increase in speed tends to reduce the maximum pressure in high load applications because the hydrodynamic effect becomes more significant in higher eccentricities. In addition, in high speed conditions, the minimum film thickness becomes higher due to the increasing hydrodynamic effects. The higher the load, the more important are the hydrodynamic effects on the film thickness. As far as the displacements are concerned, they are dependent on the developed pressures; so reasonably, they decrease. The eccentricity is also reasonable to decrease as the minimum film thickness increases. The power losses mainly depend on the speed; An increase in speed affects the shearing of the lubricant, which in turn increases the power losses.

The same results will be presented in the case of a water lubricated bearing from chapter 4.22 under load 25 KN and bush thickness 40 mm with rotational speed varying from 100 rpm to 600 rpm:

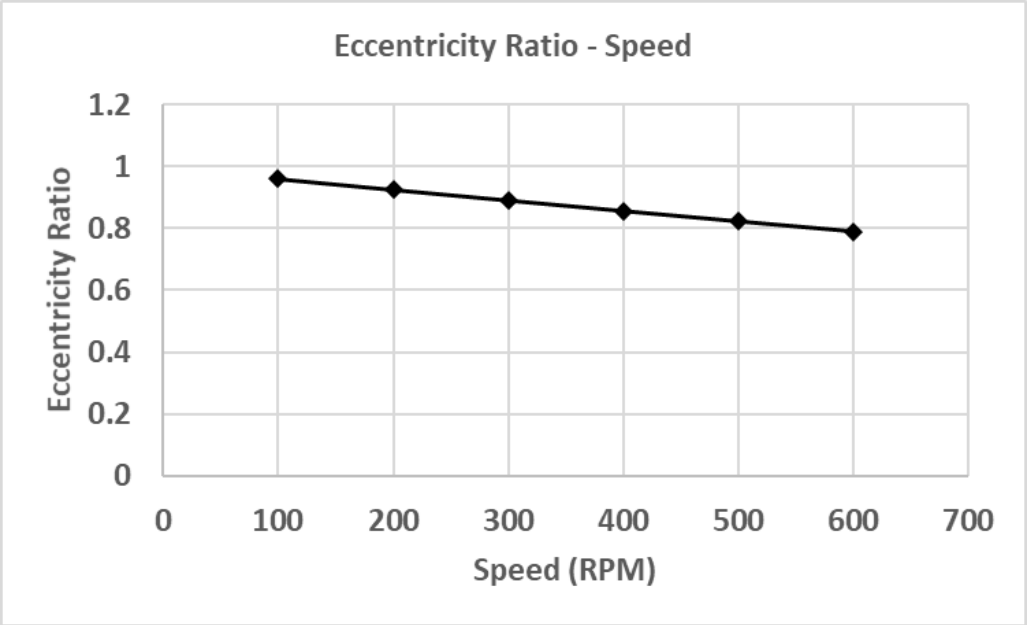

Figure 4.40 : Effect of rotational speed on eccentricity in EHD (water)

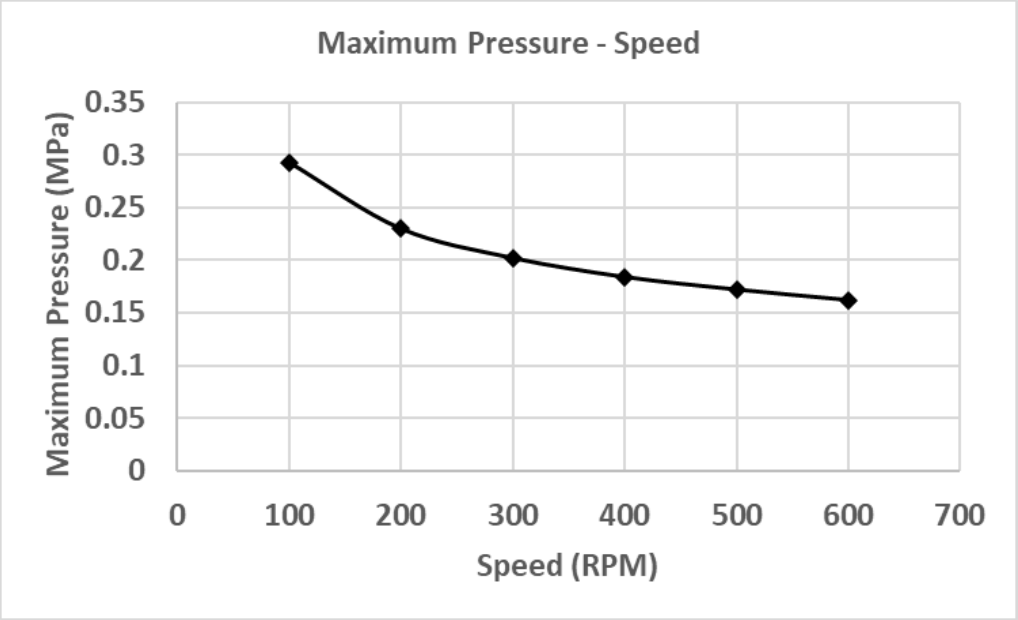

Figure 4.41 : Effect of rotational speed on Maximum Pressure in EHD (water)

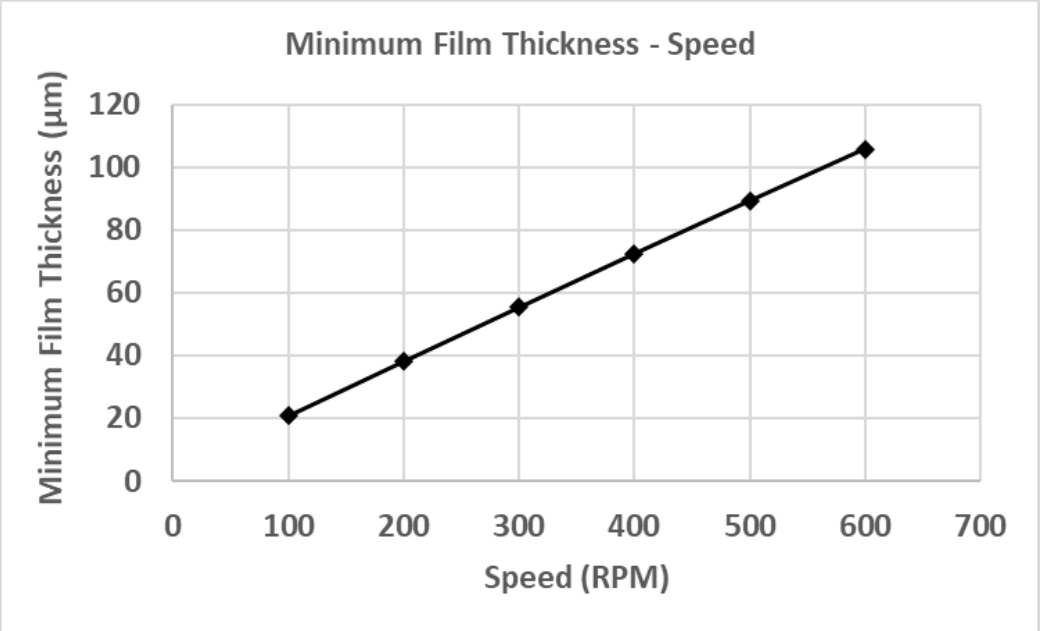

Figure 4.42 : Effect of rotational speed on minimum film thickness in EHD (water)

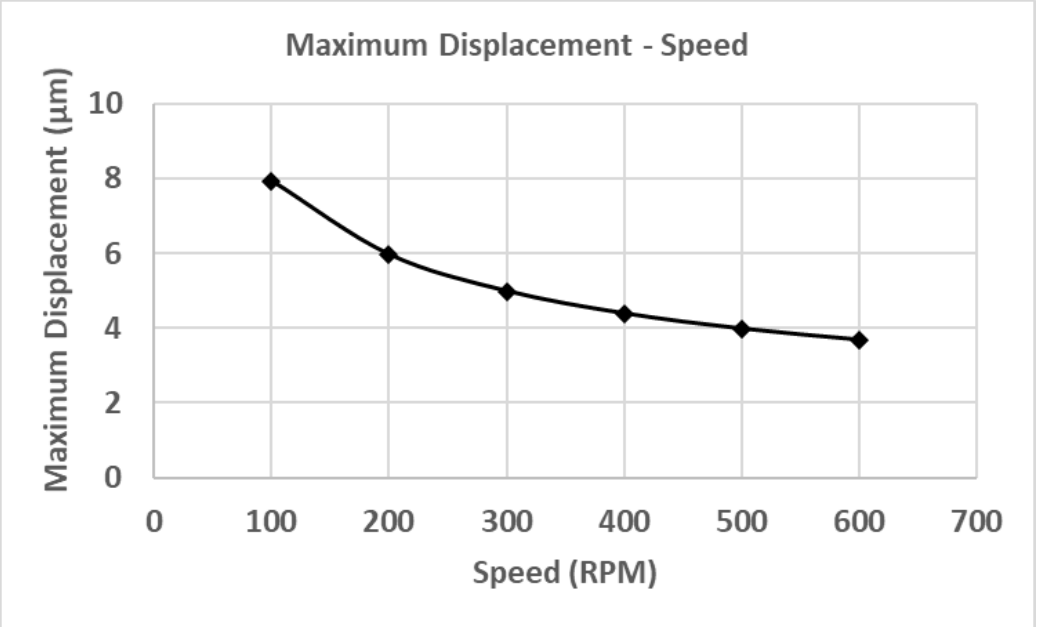

Figure 4.43 : Effect of rotational speed on maximum displacement in EHD (water)

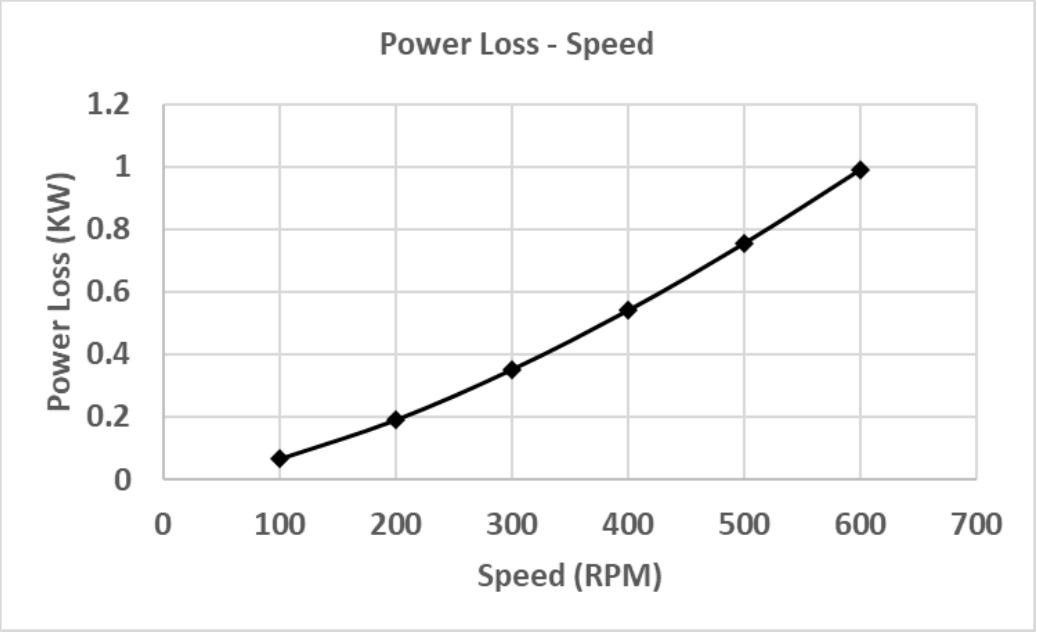

Figure 4.44 : Effect of rotational speed on Power loss in EHD (water)

5. Results And Discussion

In the present thesis, an EHD analysis was proposed using the Finite Element Method for predicting elastic displacements. The fluid - solid interaction was achieved using an in-house solver coupled with CalculiX software tool. At first, the proposed model was validated with available literature results and then compared to the Winkler Model. From this analysis we deduced that winkler can have high accuracy and even coincide with FEM when the bearing bush is thin, the displacements are small and poisson ratio close to 0.3. When the applied load or bush thickness increases, the Winkler Model can be used as only an approximation of the solution(and as input value to the FEM coupled model); But if accuracy is needed, a proper analysis is vital in order to capture the complex interaction of nodes inside the bearing bush.

Then, the influence of bearing bush thickness was investigated for an oil and a water lubricated bearing. We observed that, in the oil lubricated bearing analysis, even though the winkler model had a good accuracy at least at low loads, in the water lubricated bearing analysis the error between the two models was great, for almost every load. That is why water lubricated bearing materials demand highly accurate study, due to their low modulus of elasticity and high poisson ratio (incompressibility).

Another important parameter for the displacements is the modulus of elasticity. Its influence was investigated as far as maximum pressure, displacement and minimum film thickness are concerned. It was proved that as the elasticity modulus is increased, the maximum pressure increases (reduction of peak pressure of HD study is decreased as expected), while minimum film thickness and displacements are decreased because of the increase of bush stiffness.

The next step of this thesis was to check the proposed model under misalignment conditions. The misalignment angles used were 0.1 and 0.2. We conclude that as the misalignment angle increases we get an increase in maximum pressure and consequently in maximum displacement, while minimum film thickness and eccentricity ratio decrease.

Last but not least, we looked into the influence of rotational speed on bearing operational parameters of the proposed EHD model, such as eccentricity ratio, maximum pressure and displacement, minimum film thickness and power losses for rotational speed varying between 1000 - 6000 RPM for the oil lubricated bearing and 100-600 RPM for the water lubricated bearing .

In conclusion, elastic displacements are an important parameter in journal bearing operation, which modify the film thickness and pressure field. In low loads or/and in very stiff materials they may play a minor role in bearing performance, but in high loads or/and in more flexible bush materials such as polymers for water lubrication, it is vital to be taken into account in order to perform an accurate analysis.

6.Future Work

Future work, in continuation of the present, could include the following topics:

- Extension of the present model for high eccentricities (>1) by film thickness equation modification.
- Extension of the present model in order to take into account the elasticity of the shaft.
- Perform a full TEHD analysis of a journal bearing using CalculiX software.
- Extend this analysis in order to include in the coupled EHD solver geometrical modifications of bearing bush, such as grooves.
- Experimental validation of the proposed EHD study, with an experimental test - rig for journal bearings.
- Extension of the present model to account for transient loading of the bearing.
- Extension of the present model to study multilayer journal bearings with appropriate modification of the input file for CalculiX

7. Literature

[1] The Reynolds Centennial: A Brief History of the Theory of Hydrodynamic Lubrication, oscar Pinkus 1987
[2] Petroff, N. "Friction in Machines and the Effect of Lubricant,"(Russian)." *Eng. Journal, St. Petersburg, 1* 71 (1883): 2.
[3] Tower B. First Report on Friction Experiments. *Proceedings of the Institution of Mechanical Engineers*. 1883;34(1):632-659.
[4] Grubin, Alexandr Nikolaevich. "Investigation of the contact of machine components." *Central Scientific Research Inst. Tech. & Mech. Eng.* (1949).
[5] Lundberg, Gustaf. "Dynamic capacity of roller bearings." *Acta poly., Mech. Eng. Ser.* (1952).
[6] Dowson, Duncan, and Gordon Robert Higginson. *Elasto-hydrodynamic lubrication: international series on materials science and technology*. Elsevier, 2014.
[7] Hamrock, Bernard J., Bernard J. Schmid, and Bo O. Jacobson. *Fundamentals of fluid film lubrication*. Vol. 169. CRC press, 2004.
[8] Determining Proper Oil Flow to Journal Bearings (machinerylubrication.com)
[9]Dowson, Duncan, and Gordon Robert Higginson. *Elasto-hydrodynamic lubrication: international series on materials science and technology*. Elsevier, 2014..
[10] Stachowiak, Gwidon W., and Andrew W. Batchelor. *Engineering tribology*. Butterworth-heinemann, 2013.
[11] Density of Oil - About Tribology (tribonet.org)
[12]Cameron, Alastair. "Basic Lubrication Theory." *Ellis Horwood Ltd.,* (1981): 256.
[13] Georgios Nikitas Rossopoulos, "Tribological Study of the Stern Tube Bearing of Marine Vessels," National Technical University of Athens, Athens, 2018
[14]Gero, L. R., and C. M. McC. Ettles. "An evaluation of finite difference and finite element methods for the solution of the Reynolds equation." *ASLE transactions* 29.2 (1986): 166-172.
[15] Leonidas Raptis, "Software Development for the Solution of Hydrodynamic Lubrication Problems in main Bearings of marine Diesel Engines," National Technical University of Athens, Athens, 2014
[16]Yu, Rufei, Wei Chen, and Pei Li. "The analysis of elastohydrodynamic lubrication in the textured journal bearing." *Proceedings of the Institution of Mechanical Engineers, Part J: Journal of Engineering Tribology* 230.10 (2016): 1197-1208.
[17] CALCULIX: A Three-Dimensional Structural Finite Elemente Program
[18]Ren, Guojun Gary. "Hypo-elastohydrodynamic lubrication of journal bearings with deformable surface." *Tribology International* 175 (2022): 107787.
[19]Nikolakopoulos, Pantelis G., Christos I. Papadopoulos, and Lambros Kaiktsis. "Elastohydrodynamic analysis and Pareto optimization of intact, worn and misaligned journal bearings." *Meccanica* 46 (2011): 577-588.
[20]Pierre, I., and M. Fillon. "Influence of geometric parameters and operating conditions on the thermohydrodynamic behaviour of plain journal bearings." *Proceedings of the Institution of Mechanical Engineers, Part J: Journal of Engineering Tribology* 214.5 (2000): 445-457.
[21] Khonsari, M. M., and S. H. Wang. "On the fluid-solid interaction in reference to thermoelastohydrodynamic analysis of journal bearings." (1991): 398-404.

[22]Skaltsas, Dimitrios, Georgios N. Rossopoulos, and Christos I. Papadopoulos. "A comparative study of the Reynolds equation solution for slider and journal bearings with stochastic roughness on the stator and the rotor." *Tribology International* 167 (2022): 107410.
[23]Attia Hili, Molka, et al. "Hydrodynamic and elastohydrodynamic studies of a cylindrical journal bearing." *Journal of hydrodynamics* 22.2 (2010): 155-163.
[24]Litwin, Wojciech, and Artur Olszewski. "Water-lubricated sintered bronze journal bearings—theoretical and experimental research." *Tribology Transactions* 57.1 (2014): 114-122.
[25]Meng, Fanming, and Yuanpei Chen. "Analysis of elasto-hydrodynamic lubrication of journal bearing based on different numerical methods." *Industrial Lubrication and Tribology* (2015).
[26]Wodtke, Michał, and Wojciech Litwin. "Water-lubricated stern tube bearing-experimental and theoretical investigations of thermal effects." *Tribology International* 153 (2021): 106608.
[27]Bendaoud, N., et al. "An experimental and numerical investigation in elastohydrodynamic behaviour of a plain cylindrical journal bearing heavily loaded." *Proceedings of the Institution of Mechanical Engineers, Part J: Journal of Engineering Tribology* 226.10 (2012): 809-818.
[28]Wang, Yanzhen, et al. "Study of the lubrication performance of water-lubricated journal bearings with CFD and FSI method." *Industrial Lubrication and Tribology* (2016).
[29]Lahmar, Mustapha, Salah Ellagoune, and Benyebka Bou-Saïd. "Elastohydrodynamic lubrication analysis of a compliant journal bearing considering static and dynamic deformations of the bearing liner." *Tribology Transactions* 53.3 (2010): 349-368.
[30]Higginson, G. R. "Paper 1: The theoretical effects of elastic deformation of the bearing liner on journal bearing performance." *Proceedings of the Institution of Mechanical Engineers, Conference Proceedings*. Vol. 180. No. 2. Sage UK: London, England: SAGE Publications, 1965.
[31]Litwin, Wojciech. "Influence of local bush wear on water lubricated sliding bearing load carrying capacity." *Tribology International* 103 (2016): 352-358.
[32]Yang, Zhen, et al. "Study on elastohydrodynamic lubrication performance of double-layer composite water-lubricated bearings." *Mechanics & Industry* 24 (2023): 3.
[33]Ouyang, Wu, et al. "Lubrication Performance Distribution of Large Aspect Ratio Water-Lubricated Bearings Considering Deformation and Shaft Bending." *Tribology Transactions* 64.4 (2021): 730-743.
[34]Linjamaa, Aki, et al. "Modelling and analysis of elastic and thermal deformations of a hydrodynamic radial journal bearing." *Key Engineering Materials*. Vol. 674. Trans Tech Publications Ltd, 2016.
[35]Lahmar, M., and D. Nicolas. "Effets des déformations élastiques sur le comportement des paliers multi-couches." *Mécanique & industries* 1.5 (2000): 499-510.
[36]Cha, Matthew, Evgeny Kuznetsov, and Sergei Glavatskih. "A comparative linear and nonlinear dynamic analysis of compliant cylindrical journal bearings." *Mechanism and Machine Theory* 64 (2013): 80-92.
[37]Lahmar, M., A. Haddad, and D. Nicolas. "Elastohydrodynamic analysis of one-layered journal bearings." *Proceedings of the Institution of Mechanical Engineers, Part J: Journal of Engineering Tribology* 212.3 (1998): 193-205.

[38]Li, Hulin, et al. "Study on the performance of journal bearings in different lubricants by CFD and FSI method with thermal effect and cavitation." *MATEC Web of Conferences*. Vol. 249. EDP Sciences, 2018.
[39]Bulk modulus - HAWE Hydraulik
[40]Jacobson, Bo O., and Pascal Vinet. "A Model for the Influence of Pressure on the Bulk Modulus and the Influence of Temperature on the Solidification Pressure for Liquid Lubricants." (1987): 709-714.